Université catholique de Louvain
École Polytechnique de Louvain
Département d'ingénierie mathématique

Center for Systems Engineering and Applied Mechanics

On-line periodic scheduling of hybrid chemical plants with parallel production lines and shared resources

Iliyana Simeonova

To the memory of my Grandma Preslava

Acknowledgments

Firstly my gratitude goes to my principal adviser Georges Bastin. For me he was a major input of ideas, guidelines and indispensable criticism during my scientific development. I deeply appreciate that he gave me the opportunity and his confidence to start my doctoral studies with him.

I am grateful for the remarks and suggestions of each jury member. I would like to thank Françoise Lamnabhi-Lagarrigue for her proposition to transform the stability section in a chapter and for taking part of a selection board which accorded me the Marie-Curie CTS fellowship. This fellowship gave the beginning of my enjoyable Ph.D. adventure at CESAME/UCL. My thesis was a part of an industrial project funded by the Solvay-Group and having two mutually connected parts: scheduling and control. Consistently I am thankful to Yves Pochet for clarifying me the scheduling aspect and for his kindness. I am grateful for the comments of Guy Campion that expanded some points in the thesis. I would like to thank Paul Van Dooren for accepting to preside my jury. I am indebted to my co-adviser Denis Dochain for introducing me to the chemical process control subject by his lectures and comments.

I am particularly thankful to François Warichet, who made his thesis on the scheduling part of the Solvay-project at CORE/UCL. François thank you for your kindness, enthusiasm and for being always available for many helpful project discussion, especially by phone.

I benefited a lot from the nice international atmosphere of CESAME. During these years it has been very rewarding and stimulating to be in the same office with Laure Ninove. I am grateful to Laure for sharing some of her mathematical and Latex skills as well as for helping me in French. Laure thank you for the nice time that we have spent eating cookies and laughing. I also enjoyed the com-

pany of my short-term officemates: Hadyan Fibrianto, Isabelle Motte, Clementina Dellomonaco and Luciola Campestrini. I am thankful to all my friends who helped me during the thesis, either with advices or with occasional help or just with a friendship: thank you Pierre-François Matty (my French teacher) and Karmen; Jean Dezert (ONERA, France); Stephanie Lefèvre, Claire Mattelet and Colin (my DEA friends); Catherine Fraikin, Christobald de Kerchove, Gonzalo Robledo, Damien François, Jean-Baptiste Coulaud, Jean-Charles Delvenne, Julien Hendrickx, Manuel Betancur, Maxime Raison, Mariana Titica, Nadia Beniich, Valérie Dos Santos (all from CESAME) as well as Kerstin Graeser and Zenia. I am especially indebted to Rachel Dutrieue from TERM/UCL for her friendship and for the diverse invaluable advices she gave me throughout these years.

A really appreciate the kindness and assistance of all the administrative team of CESAME: thank you Lydia De Boeck, Michèle Termolle, Étienne Huens and Yannick Majoros. Spatial thanks and deepest gratitude go to Isabelle Hisette and Jean-Claude; Véro, Vincent and Basile; Lo, Sam and Mattis for accepting as a member of the family; for their unlimited helpfulness and for their friendship.

I would like to acknowledge my colleagues from the Institute For Parallel Information Processing (IPIP) of the Bulgarian Academy of Science: Tzvetan Semerdjiev, Pavlina Konstantinova, Albena Tchamova, Ludmil Bojilov, Boriana Vassileva, Violeta Bogdanova, Kiril Alexiev, Rayna Georgieva, Sofia Ivanovska and Mariya Durchova for their encouragements. Special thanks go to Donka Angelova. Donka thank you for your scientific advices and friendship since my first working-day at the IPIP. I am also grateful to Lyuba Petrounova and Lilyana Gerogieva, for always being here, despite the distance.

During my Ph.D. I was financed by the: UCL - "Fonds de Recherche Solvay", "HYCON Network of Excellence" and "Belgian Programme on Interuniversity Attraction Poles", initiated by the Belgian Federal Science Policy Office, for which I am especially grateful.

Last but not least Mummy and Daddy thank you for everything that I am.

Summary

This thesis deals with chemical plants constituted by parallel batch-continuous production lines with shared resources.

For such plants, it is highly desirable to have optimal operation schedules which determine the starting times of the various batch processes and the flow rates of the continuous processes in order to maximize the average plant productivity and to have a continuous production without interruptions. This optimization problem is constrained by the limitation of the resources that are shared by the reactors and by the capacities of the various devices that constitute the plant.

Such plants are "hybrid" by nature because they combine both continuous - time dynamics and discrete-event dynamics. The formalism of "Hybrid Automata" is therefore well suited for the design of plant models.

The first contribution of this thesis is the development of a hybrid automaton model of the chemical plant in the Matlab-Simulink-Stateflow environment and its use for the design of an optimal periodic schedule that maximises the plant productivity. Using a sensitivity analysis and the concept of Poincaré map, it is shown that the optimal schedule is a stable limit cycle of the hybrid system that attracts the system trajectories starting in a wide set of initial conditions.

The optimal periodic schedule is valid under the assumption that the hybrid model is an exact description of the plant. Under perturbations on the plant parameters, it is shown that two types of problems may arise. The first problem is a drift of the hybrid system trajectory which can either lead to a convergence to a new stable sub-optimal schedule or to a resource conflict. The second problem is a risk of overflow or underflow of the output buffer tank. The second contribution of the thesis is the analysis of feedback control strategies to

avoid these problems. For the first problem, a control policy based on a model predictive control (MPC) approach is proposed to avoid resource conflicts. The feedback control is run on-line with the hybrid Simulink-Stateflow simulator used as an internal model. For the solution of the second problem, a classical PI control is used. The goal is not only to avoid over- or under-filling of the tank but also to reduce the amplitude of outflow rate variations as much as possible. A methodological analysis for the PI controller tuning is presented in order to achieve an acceptable trade-off between these conflicting objectives.

A preview of the thesis

The chemical plants are widely used in the pharmaceutical, oil, PVC etc... industries. They are generally made up of several parallel working batch reactors "sharing" common resources. By "sharing" we mean that different reactors may simultaneously use the same resource. The reactors discharge their final product in a buffer tank used to transfer it continuously to the next plant devices (reactors, columns, buffers centrifuges, etc...). The particularity of the batch reactors is that their operation cyclically passes through a sequence of phases, namely loading of raw material, reaction, etc...

An overall description of the industrial *polyvinyl chloride* (PVC) chemical plant motivating the study as well as of the benchmark plant that shall be studied through the thesis are given in **Chapter 1**.

For such plants, it is highly desirable to have optimal operation schedules. These schedules determine the stand by times between the batch reactor phases, their flow and transfer rates as well as the flow rates between the different devices in order to maximize the average plant productivity and to have a continuous production without interruptions. The optimization problem is constrained by the limitation of the "shared" resources and by the capacities of the various plant units.

The main challenge for the solution of this problem comes from the "hybrid" nature of the plant.

From a process engineering viewpoint the plant is "hybrid" because it combines both batch and continuous processes. From a system the-

oretic viewpoint it is a "hybrid" system because it combines both continuous-time dynamics (e.g. the continuous time evolution of a reactor temperature) and discrete-event dynamics (e.g. the transitions between the reactor phases are driven by events occurring at discrete time instants).

For such "hybrid" chemical plants three main issues shall be concerned in the thesis: simulation modelling; design of off-line periodic schedules and their feedback control in the presence of disturbances.

Simulation modelling. Chapter 2 begins with the presentation of the hybrid automaton formalism which is one of the methods for hybrid systems modeling. Then we have applied this methodology for the benchmark hybrid chemical plant modeling. Based on the model a numerical simulator of the plant is developed in a *Matlab-Simulink-Sateflow* environment. This simulator is the **first contribution** of the thesis. The model and the simulator have been published in [Sim03] [SWB+05a] [SWB+05b].

Design of off-line periodic schedules. One of the main concerns in this thesis is the design of periodic schedules which achieve some performance optimization of the hybrid chemical plant. In **Chapter** 3 it is shown how the *Simulink-Stateflow* simulator can be a very useful tool for the design of periodic schedules. Three case studies are considered: a single reactor having resource rate restrictions; a two reactors plant with resource rate restrictions and finally a two-reactors buffer tank plant having not only resource rate restrictions but also tank capacity limitations. Indeed the second contribution of the thesis is the development of **optimal** off-line heuristic scheduling rules for these cases. Various simulation results are shown. The results from the stability analysis of a designed periodic schedule based on the hybrid trajectory sensitivity analysis is given in **Chapter** 4. During the analysis due to the non-linearity of the system all equations are solved numerically by means of the simulator. In **Chapter** 5 it is shown the use of the simulator for testing a sub-optimal schedule obtained by a mixed integer programing (MIP) formulation. Note that in the simulation design of

the periodic schedules no disturbances are considered.

Feedback control. In **Chapter** 6 we analyze the plant behaviour under periodic schedules in the case where there are constant (or piecewise constant) disturbances on the plant parameters. Under such perturbations it is shown that two types of problems may arise: a drift in the hybrid system trajectory which can either lead to a convergence to a new sub-optimal schedule or to a resource conflict; the second problem could be an overflow or a wash-out of the buffer tank. The main objective here is to assess the feasibility and efficiency of feedback strategies in order to avoid these problems. Consequently the **third contribution** of the thesis is the development of a control policy based on a model predictive control (MPC) approach to avoid resource conflicts. Its basic issues are the conflict prediction for the next reactor cycle; the computation and the allocation of the stand by times on appropriate reactor. Here once again is shown the utility of the plant simulator which is used as a model in this MPC and is run on-line. For the solution of the second problem a classical Proportional-Integral (PI) control is proposed. The use of such continuous control law is possible because as shown in **Chapter** 6 the hybrid buffer tank process can also be presented as a continuous time model. Here the aim is not only to avoid the over- or under-filling of the tank but also to reduce as much as possible the amplitude of the tank output flow rate in order to have a smooth product transfer to the downstream units. Consequently the **fourth thesis contribution** is the development of a methodological analysis for the PI controller tuning in order to achieve an acceptable trade-off between these conflicting objectives. Results of the PI feedback tank control are published in [SWB$^+$06b] and [SWB$^+$06a]. In [SWB$^+$05b] the feedback control problem is treated in terms of re-scheduling, where a new plant schedule is determined based on a MIP formulation.

Contents

List of Figures

List of Tables

Nomenclature

Abbreviations

PVC	polyvinyl chloride
PR	polymerization reactor
BR	batch reactor
ST	storage tank
DFT	drier feeding tank
HAM	hybrid automaton model
SF	stand by filling
SH	stand by heating
SD	stand by discharging
F	filling
H	heating
R (or TR)	reaction
C	cooling
D	discharging
M	maintenance and cleaning
FD	filling from a reactor/reactors and discharging
DO	discharging only
OUF	over/under filling
MPC	model predictive control
$HMPC$	hybrid model predictive control
TDE	time discrete event control

Chemical notations

V	batch reactor volume (m^3)
U	storage tank volume (m^3)
Δ_U	variation of the tank volume profile (m^3)
Δ_m	tank volume security margin (m^3)
T	batch reactor temperature (K)
T_h	hot steam temperature (K)
T_c	cold water temperature (K)
T_a	ambient temperature (K)
C	vector of the concentrations of reactor's chemical species (mol/l)
C_A	reactant A concentrations (mol/l)
C^{tr}	vector of the treshold concentrations of reactor's chemical species (mol/l)
P	vector of the product concentrations in the storage tank (mol/l)
C_B	product B concentration (mol/l)
δ	coefficient proportional to the reaction enthalpy $(l.K/mol)$
S	stoichiometric vector
$k(T)$	dependence of the reaction rate on the temperature
k_0	rate constant $(l/mol.h)$
R	gas constant $(J/mol.K)$
E	activation energy of the reaction (J/mol)
$r(C)$	dependence of the reaction rate on the concentration
F_{disch}	reactor's output flow rate (m^3/h)
F	total reactors output flow rate (m^3/h)
ΔF^m	magnitude of the step disturbance in F^m (m^3/h)
w	storage tank output flow rate (m^3/h)
α	relative amplitude attenuation of w
Q_h	hot steam transfer rate (h^{-1})
Q_c	cold water transfer rate (h^{-1})
$Q_{c,cooling}$	cold water transfer rate during the cooling phase (h^{-1})
$Q_{c,regulation}$	cold water transfer rate during the regulation phase (h^{-1})
$Q_{c,TOTAL}$	total cold water transfer rate of all reactors (h^{-1})

Mathematical notations

$\Re$	set of real numbers
$\Re_+$	set of positive real numbers
Σ	finite set of discrete states (phase)
σ	phase
E	finite set of admissible discrete transitions
X	continuous state-space
F	finite set of continuous vector functions
f	continuous vector function
I	"reset map" to each admissible discrete transition
G	set of transition guards
U	continuous input space
t	time variable
a_n, b_n	Fourier series coefficients of F
a_n^U, b_n^U	Fourier series coefficients of U
a_n^w, b_n^w	Fourier series coefficients of w
DP	differential of the Poincaré map
g	switching plane
∇g	gradient of the switching plane
h	reset map between the phases
Dh	gradient of the reset map between the phases
Φ_i	sensitivity matrix away from the events
$\Phi_{i,j}$	sensitivity matrix at the transition from phase i to j

Index

i	index of a reactor
N	maximal reactors number
in	inflow
opt	optimal
$subopt$	sub-optimal
$stoch$	stochastic
TOT	total
min	minimal
max	maximal
m	mean value
d	disturbances

Other notations

Lag_2 time lag before filling of the second reactor (h)
Δ_{SF} stand by before filling (h)
Δ_{SH} stand by before heating (h)
Δ_{SD} stand by before discharging (h)
T_p production period (h)
ω_p production frequency (rad/h)
T_d production period under disturbances(h)
ω_d production frequency under disturbances (rad/h)
K_p proportional parameter of the PI controller
K_I integral parameter of the PI controller (h^{-1})
U^* reference value for the tank content (m^3)
ξ dumping factor

Chapter 1

Introduction

This Chapter is the first stage of a research study concerned with the development of systematic approaches for the: modeling, simulation, optimization and stabilization of the operation of "hybrid" chemical plants. Its aim is:

 i. *to present a motivating example, namely a PVC production plant*

 ii. *and to define a benchmark chemical plant with a simpler structure than the PVC plant but having its main features. This benchmark-example shall be used throughout the thesis for the application of the above mentioned approaches.*

1.1 Motivation

The thesis is motivated by a current industrial project related to a *polyvinyl chloride* (PVC) production plant, entitled: "*PVC Line Predictive Inventory Control: A production Rate Optimization for a Hybrid System*" [Mel03]. The project was sponsored by the *Solvay* Research Funds at Université Catholique de Louvain. Solvay is one of the
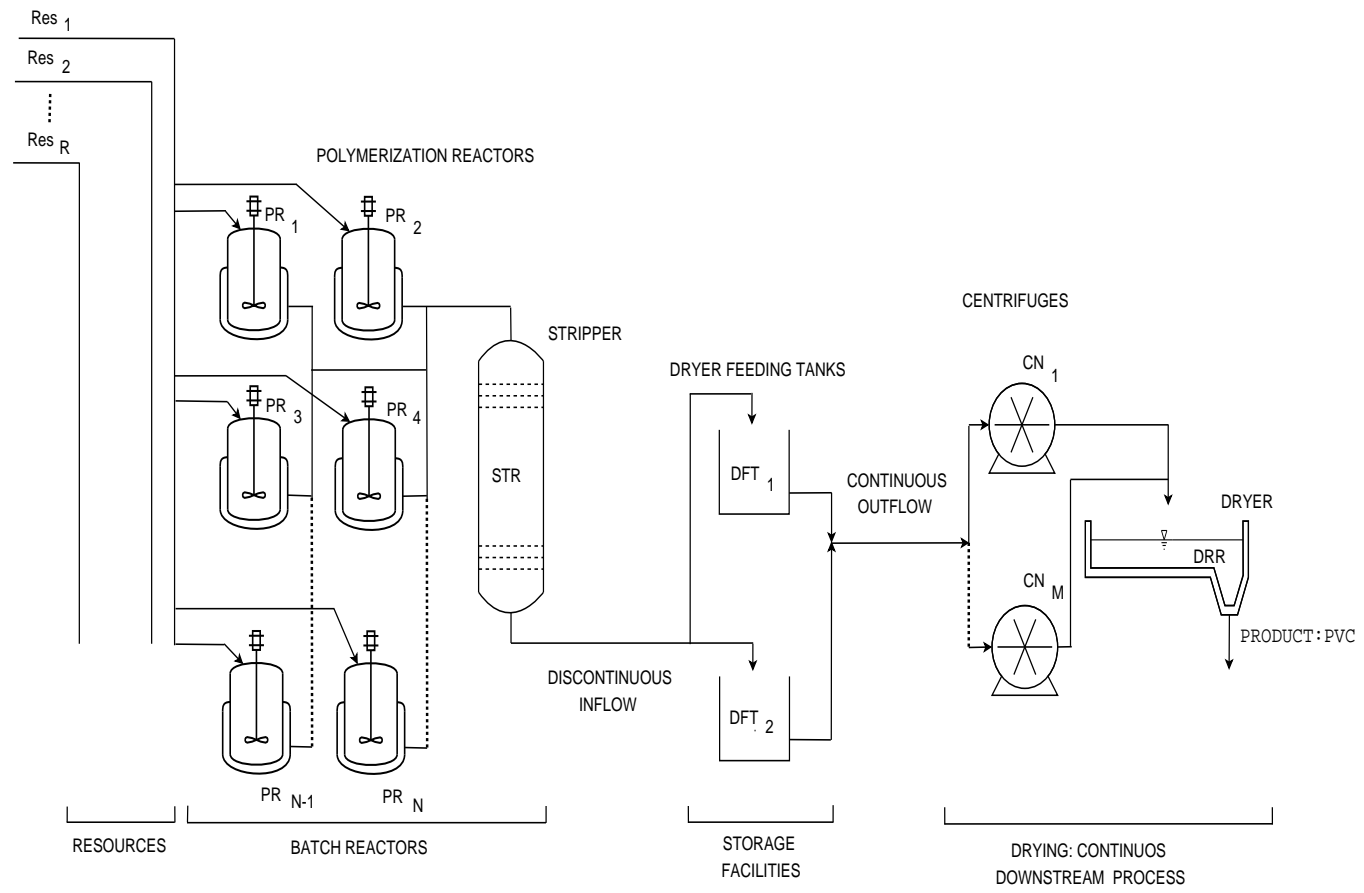
Fig. 1.1: A typical flowsheet of a PVC production line

biggest producers of PVC, ranking second in Europe (1.3 $Mt/year$) and third globally. The activities of the Group in PVC and other products of the vinyl chain span across Asia and Latin America, through the affiliates in Thailand, Argentina and Brazil [Tho07][Tes07]. In this section, according to the project information provided in [Mel03], we give a brief description of the processes carried out in the PVC plant, having a productivity of 350 $kt/year$.

A PVC plant is generally made up of several parallel production lines. A flow sheet of one such line is presented in Figure 1.1. A description of the involved processes is as follows:

i. The core of the plant is a set of parallel batch polymerization reactors (denoted PR_i in Figure 1.1) in which a PVC slurry is formed. The operation of each reactor cyclically passes through a succession of working phases, namely loading of raw material (e.g. monomers and precursors), polymerization, discharge of final products, cleaning etc... The polymerization reactors share several resources like the raw materials, as well as the heating and cooling fluids. By "sharing", we mean that different reactors may have simultaneous access to the same resource.

ii. When the polymerization is completed, the PVC slurry of each reactor is discharged into a single stripping column where the non-reacted monomers are separated from the polymer. This process is also discontinuous and operates in successive batches.

iii. The PVC extracted from the stripping column is then stored in two parallel buffering tanks (denoted DFT_i in Figure 1.1) which are fed *discontinuously* (after each operation cycle of the stripping column).

iv. The aim of the buffer tanks is to ensure a *continuous* and *almost constant* supply to the drying section of the plant which consists of several parallel centrifuges (where most of the water is mechanically removed) followed by a dryer where the remaining water is evaporated and the final dry PVC product is delivered.

For such plants, it is highly desirable to have optimal operation schedules which determine the starting times of the various batch processes

and the flow rates between the different processes in order to maximize the average plant productivity and to have a continuous production without interruptions. This optimization problem is constrained by the limitation of the resources that are shared by the reactors and by the capacities of the various devices (reactors, columns, buffers centrifuges) that constitute the plant.

1.2 A benchmark chemical plant

In this thesis, for the sake of clarity, we shall limit ourselves to consider a benchmark chemical plant with a simpler structure as represented by the flowsheet of Figure 1.2. The plant is constituted of a bunch of parallel batch chemical reactors followed by a single common buffer tank. The aim is to provide a downstream processing unit with a *constant* continuous flow of some chemical product which is made in a discontinuous manner in the batch reactors. As such, it is clear that the plant can be viewed as a kind of simplified representation of the general PVC plant of Figure 1.1, keeping the two main critical features that may limit the performance namely:

i. the plant combines both discontinuous (or batch) and continuous processes;
ii. the resources are shared by the batch units.

This plant will serve as a benchmark example throughout the thesis. In this section we shall give a discursive description of the plant operation. The mathematical modelling will be considered in Chapter 2, as well as the development of a *Matlab-Simulink-Stateflow* simulator.

The plant operation is as follows:

i. In each batch reactor, the product of interest is made by an exothermic chemical reaction from one or several reactants.

ii. The batch reactors share three kinds of resources : (1) the reactants that constitute the raw material of the process; (2) the hot steam used for the initial heating of the process; (3) the cold water which is used for temperature regulation (since the process is exothermic) and final cooling.
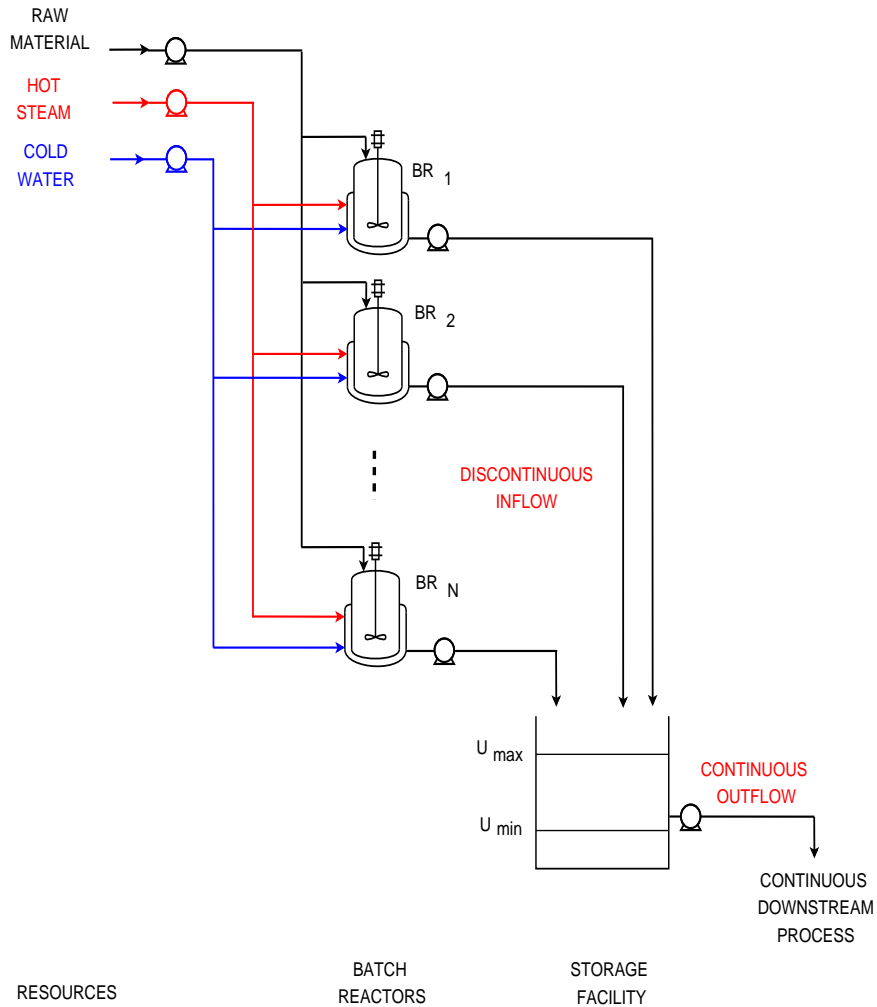
Fig. 1.2: Benchmark chemical plant

iii. During each production cycle, every batch reactor follows a sequence of 9 phases in a predefined order as presented in Figure 1.3 The successive phases are (1) Filling of the reactor with the reactants, (2) Standby before heating, (3) Heating, (4) Reaction at constant temperature, (5) Cooling, (6) Standby before discharging, (7) Discharge in the storage tank, (8) Cleaning and maintenance, (9) Standby until next cycle. The transitions between the succes-

```
        ┌──────────────────────────┐
        ↓                          │
   ┌─────────────────┐             │
   │  (1) FILLING    │             │
   └─────────────────┘             │
        ↓                          │
   ┌─────────────────┐             │
   │  (2) STAND BY    │            │
   │ (BEFORE HEATING) │            │
   └─────────────────┘             │
        ↓                          │
   ┌─────────────────┐             │
   │  (3) HEATING    │             │
   └─────────────────┘             │
        ↓                          │
   ┌─────────────────┐             │
   │  (4) REACTION   │             │
   └─────────────────┘             │
        ↓                          │
   ┌─────────────────┐             │
   │  (5) COOLING    │             │
   └─────────────────┘             │
        ↓                          │
   ┌─────────────────┐             │
   │  (6) STAND BY    │            │
   │ (BEFORE DISCH.)  │            │
   └─────────────────┘             │
        ↓                          │
   ┌─────────────────┐             │
   │ (7) DISCHARGING │             │
   └─────────────────┘             │
        ↓                          │
   ┌─────────────────┐             │
   │(8) CLEANING AND │             │
   │  MAINTENANCE    │             │
   └─────────────────┘             │
        ↓                          │
   ┌─────────────────┐             │
   │  (9) STAND BY    │            │
   │(BEFORE FILLING)  │            │
   └─────────────────┘             │
        ↓                          │
        └──────────────────────────┘
```
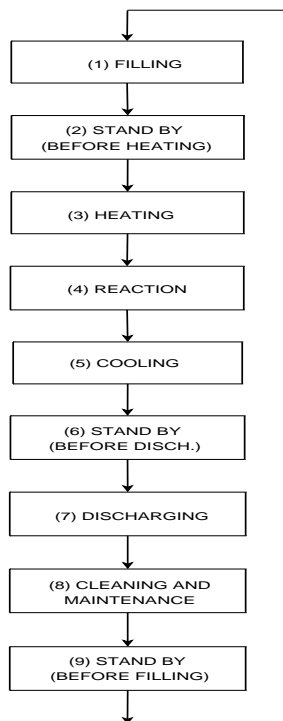
Fig. 1.3: Production cycle of a batch reactor

sive phases are triggered by logical rules that may depend either on the state of the process or on external decisions taken by the operators, as it will be described in detail in Chapter 2.

iv. The storage tank is fed discontinuously (when the batch reactions are finished) but it is discharged continuously. The continuous output flow rate corresponds to the rate at which the continuous downstream process operates.

1.3 Conclusion

In order to analyze the behaviour of the benchmark chemical plant and to be able to optimize and stabilize its operation, we shall develop a mathematical model, as well as a simulator in the next Chapter. As we have seen in this Chapter, the benchmark plant is "hybrid" by

nature. From a process engineering viewpoint it is a hybrid plant because it combines both batch and continuous processes. From a system theoretic viewpoint it is a hybrid system because it combines both continuous-time dynamics and discrete-event dynamics : indeed the state variables of chemical reactions and mass transfers occurring in the system are clearly continuous variables that depend continuously on time while the transitions between the various production phases are typically described by discrete states that are driven by events occurring at discrete time instants. As we shall see in the next Chapter, the formalism of "Hybrid Automata" is therefore well suited for this modelling purpose.

Chapter 2

An hybrid simulation model of the benchmark chemical plant

The purpose of this Chapter is:

i. *to describe the "Hybrid Automata" framework for hybrid process modelling;*

ii. *to apply this methodology on the modelling of the benchmark hybrid chemical plant presented in the previous Chapter;*

iii. *to develop a simulator of the plant in a Matlab-Simulink-Stateflow environment;*

2.1 Hybrid automaton modelling

In this Chapter, the operation of the benchmark chemical plant of Figure (1.2) will be described by an *Hybrid Automaton Model (HAM)* [SW03], [Wil03]. Hybrid Automata are mathematical models that are

able to describe systems that involve simultaneously continuous-time dynamics and discrete event dynamics. Traditionally, continuous-time dynamics are represented by differential equations while discrete-event dynamics may be represented by finite automata. Therefore, hybrid automata, as they are used in this thesis, will be represented by interconnected systems of both ordinary differential equations and discrete transition equations.

Mathematically speaking, the definition of a HAM requires to specify a collection of sets $H = (\Sigma, E, X, U, F, I, G)$ where:

i. $\Sigma = \{\sigma_1, \sigma_2, \ldots, \sigma_N\}$ is the finite set of discrete states (that will be most often called "modes" or "phases" in this thesis).

ii. $E \subseteq \Sigma \times \Sigma$ is the finite set of admissible discrete transitions. As we shall see hereafter, these transitions are usually represented by directed edges in the underlying directed graph of the HAM.

iii. $X \subseteq \mathbb{R}^n$ is the continuous state-space.

iv. $U \subseteq \mathbb{R}^m$ is the continuous input space.

v. $F = \{f_1, f_2, \ldots, f_N\}$ assigns a continuous vector function $f_i : X \times U \rightarrow \mathbb{R}^n$ to each discrete state $\sigma_i \in \Sigma$. This is interpreted as follows: while the hybrid system stays in discrete state σ_i, the continuous-time dynamics (i.e. the evolution of the continuous variables) are governed by the differential equation $\dot{x} = f_i(x, u)$, $x \in X, u \in U$.

vi. $I = \{I_{ij} : X \rightarrow X, (\sigma_i, \sigma_j) \in E\}$ assigns a "reset map" to each admissible discrete transition. When a transition occurs from mode σ_i to mode σ_j, the continuous state is reset to a new value according to I_{ij}. This new value is the initial condition for the evolution of the continuous state in mode σ_j according to f_j. In this thesis, we shall restrict ourselves to two specific situations:

   a) either I_{ij} is an identity map, which means that there is no state reset and the initial state for mode σ_j is just the final state of

the previous mode σ_i;

b) or there is a reset to an a-priori fixed value x_0 when the system enters the new mode σ_j independently of the final value of the state in the previous mode.

vii. $G = \{G_{ij} : X \times \mathbb{R}_+ \to \mathbb{R}, (\sigma_i, \sigma_j) \in E\}$ is the set of transition guards that define the conditions for the transition occurencies between the discrete states. Each transition guard is formulated under the form of a rule expressed as : "If $G_{ij}(x(t), t) \geq 0$ then the transition $\sigma_i \to \sigma_j$ occurs". In this thesis, two types of transition guards are considered:

a) *state event guards:* where the switching between the discrete states is provoked by the dynamics of the system itself (when a certain boundary in the continuous state space X is crossed).

b) *time event guards:* where the switching between the discrete states is an external time constraint.

For a particular application, the set-up of a model then essentially consists in deriving explicit and complete definitions of these sets. We shall first present separate HAMs for each batch reactor and the buffer tank. Then the overall HAM for the complete system involving all the batch reactors and the buffer tank together will be presented. In the course of this presentation, we shall also introduce additional modelling assumptions which are necessary for the model consistency and have not yet been mentioned.

2.1.1 Hybrid Automaton Model of a batch reactor

Discrete states and transitions. According to the description given in Chapter 1, during the production cycle, each batch reactor follows a sequence of 9 phases in a predefined order as shown in the directed graph of Figure (2.1) (with the notations defined in Table (2.1)). This graph is a typical example of the graphs that are commonly used in the literature to represent graphically, in a compact way, the behaviour of HAMs. In this graph, the vertices represent
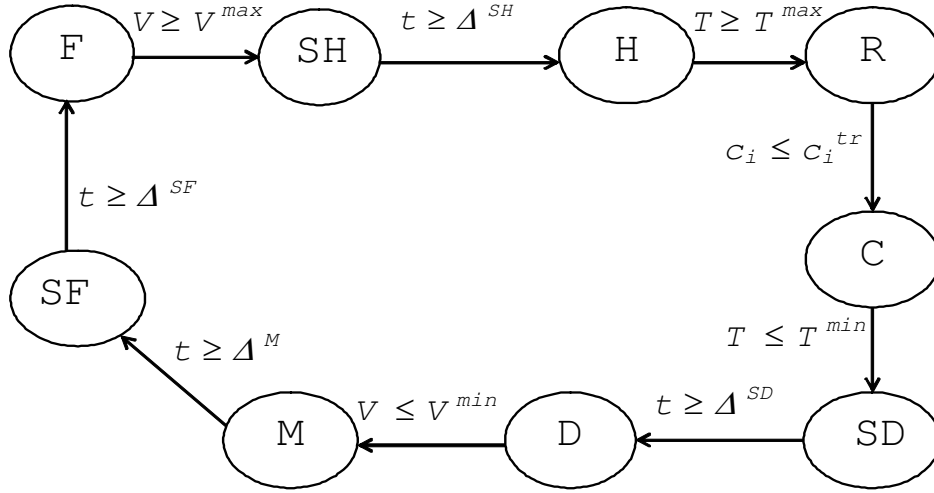
Fig. 2.1: HAM of a batch reactor

abbreviation	phase name
F	Filling
SH	Stand by (before heating)
H	Heating
R	Reaction
C	Cooling
SD	Stand by (before discharging)
D	Discharging
M	Cleaning and maintenance
SF	Stand by (before filling)

Table 2.1: Phases in a batch reactor

the discrete states (or modes) and the edges represent the admissible transitions. The elements of the set Σ of discrete states is then naturally defined as the set of process phases:

$$\Sigma = \{F, SH, H, R, C, SD, D, M, SF\}$$

The set E of transitions between the discrete states is:

$$E = \{(SF, F), (F, SH), (SH, H), (H, R), (R, C),$$
$$(C, SD), (SD, D), (D, M), (M, SF)\}$$

Continuous states. As we have mentioned in Chapter 1, it is assumed that the product of interest is made, in batch stirred tank reactors, by an exothermic chemical reaction from one or several reactants. Therefore, in accordance with the classical modelling of stirred tank reactors, the continuous state variables are: V [m^3] the **volume** of the reactor, T [K] the reactor **temperature** and $C = (c_1, c_2, \ldots, c_p)$ [mol/l] the vector of the **concentrations** of the chemical species in the reactor. Since these variables are physically non-negative, we have $X \triangleq \mathbb{R}_+^{p+2}$.

In the next paragraphs, we shall present a detailed description of the successive modes (or phases) of the reactor. This description will include all the elements necessary for an (implicit) definition of the sets F, I, G, U that are needed to complete the HAM.

Continuous-time dynamics, discrete-time dynamics and input variables. The process behaviour may then be described, in each phase, by a set of continuous differential equations (mass and energy balances). The successive phases are described as follows.

F : Filling. During this phase, the reactor is progressively fed with a reactant flow. For simplicity, it is assumed that the reaction is not initiated at this stage and consequently that the reactant concentrations and the temperature in the reactor remain constant at their values C_{in} and T_{in} in the feed flow. The volumetric inflow rate is denoted F_{in}. Then the balance equations are:

$$\begin{cases} \dfrac{dV}{dt} = F_{in} \\[2mm] \dfrac{dC}{dt} = 0 \\[2mm] \dfrac{dT}{dt} = 0 \end{cases} \quad or \quad \begin{cases} V(t) = \int_{t_0}^{t} F_{in}(\tau)d\tau \\[2mm] C(t) = C_{in} \\[2mm] T(t) = T_{in} \end{cases}$$

In these equations, t is the independent (continuous) time variable and t_0 denotes the initial time instant of the current filling phase. The reactor filling lasts until the volume V reaches a given maximum value V^{max} (a state event guard). The initial conditions are reset to $V(t_0) = 0, C(t_0) = C_{in}, T(t_0) = T_{in}$.

SH : Standby before heating. During this phase, it is assumed that the state remains constant (i.e. there is no heat or mass losses and no initiation of the reaction). The balance equations are trivially as follows:

$$
\begin{cases}
\dfrac{dV}{dt} = 0 \\[2mm]
\dfrac{dC}{dt} = 0 \\[2mm]
\dfrac{dT}{dt} = 0
\end{cases}
\quad or \quad
\begin{cases}
V(t) = V^{max} \\[2mm]
C(t) = C_{in} \\[2mm]
T(t) = T_{in}
\end{cases}
$$

The transition to the next phase (Heating) is triggered when a certain time period Δ_{SH} [h], fixed by the plant scheduler (a time event guard) has elapsed.

H : Heating. During this phase, the reactor is heated with hot steam circulating in a heat exchanger. The balance equations are:

$$
\begin{cases}
\dfrac{dV}{dt} = 0 \\[2mm]
\dfrac{dC}{dt} = Sk(T)r(C) \\[2mm]
\dfrac{dT}{dt} = -\delta k(T)r(C) + Q_h(T_h - T)
\end{cases}
$$

In these equations $k(T)r(C)$ denotes the reaction rate. The first term $k(T)$ represents the dependence of the reaction rate on the temperature T and the second term $r(C)$ represents the dependence on the concentrations in the reactor. Typical examples of such functions are the *Arrhenius law* for $k(T)$ and the *law of mass action* for $r(C)$ (see the next section of this Chapter for a concrete example). The vector S in the second equation is the stoichiometric vector. In the third equation, the first term $-\delta k(T)r(C)$ represents the heat produced by the reaction with the constant coefficient $\delta < 0$ being proportional to the reaction enthalpy. The last term $Q_h(T_h - T)$ represents the exchange of heat between the reactor and the heating coil, with T_h the steam temperature and Q_h the specific heat transfer rate (proportional to the steam flow rate). The heating phase lasts until the temperature T reaches a given maximum value T^{max} (a state event guard).

R : Reaction or Temperature regulation. During this phase, the temperature is regulated at the set-point T^{max}. The regulation is achieved by a cooling coil fed with cold water. Here we assume that the regulation is perfect (i.e. $T(t) = T^{max}\ \forall t$) and therefore that the cooling rate exactly compensates for the exothermicity. Hence the balance equations are:

$$\begin{cases} \dfrac{dV}{dt} = 0 \\[2ex] \dfrac{dC}{dt} = Sk(T^{max})r(C) \\[2ex] \dfrac{dT}{dt} = 0 \quad \Leftrightarrow \quad \delta k(T^{max})r(C) = Q_c(T_c - T^{max}) \end{cases}$$

In the last equation, T_c is the coolant temperature and Q_c the specific heat transfer rate (proportional to the coolant flow rate). The regulation phase stops when the reactants are almost

depleted, for instance when the concentration of one key reactant, c_i $i \in \{1, ..., p\}$ is under a given threshold value c_i^{tr} (a state event guard).

C: Cooling. Here cold water is added into the cooling device of the reactor in order to stop the reaction quickly. The balance equations are:

$$
\begin{cases}
\dfrac{dV}{dt} = 0 \\[2ex]
\dfrac{dC}{dt} = Sk(T)r(C) \\[2ex]
\dfrac{dT}{dt} = -\delta k(T)r(C) + Q_c(T_c - T)
\end{cases}
$$

The cooling phase lasts until the reactor temperature achieves a given minimal temperature T^{min} (a state event guard).

SD : Standby before discharge. During this phase, it is assumed that the state remains constant and the balance equations are:

$$
\begin{cases}
\dfrac{dV}{dt} = 0 \\[2ex]
\dfrac{dC}{dt} = 0 \\[2ex]
\dfrac{dT}{dt} = 0
\end{cases}
\quad or \quad
\begin{cases}
V(t) = V^{max} \\[2ex]
C(t) = C^{tr} \\[2ex]
T(t) = T^{min}
\end{cases}
$$

Here the phase transition is triggered by the elapse of a certain time period Δ_{SD} [h], fixed by the plant scheduler (a time event guard).

D : Discharging During this phase the obtained product of interest is progressively discharged in the storage tank. The volumetric outflow rate is denoted F_{disch}. Consequently the balance equations are:

$$
\begin{cases}
\dfrac{dV}{dt} = -F_{disch} \\[2ex]
\dfrac{dC}{dt} = 0 \\[2ex]
\dfrac{dT}{dt} = 0
\end{cases}
\quad \text{or} \quad
\begin{cases}
V(t) = V^{max} - \int_{t_0}^{t} F_{disch}(\tau)d\tau \\[2ex]
C(t) = C^{tr} \\[2ex]
T(t) = T^{min}
\end{cases}
$$

Reactor discharging lasts until the volume V reaches a certain minimal value V^{min} (a state event guard).

M : Cleaning and maintenance. During this phase, the reactor is cleaned and prepared for new production cycle. For simplicity, this is modeled as:

$$
\begin{cases}
V(t) = 0 \\[2ex]
C(t) = 0 \\[2ex]
T(t) = T_a
\end{cases}
$$

with T_a the ambient temperature. The maintenance phase lasts for a certain fixed time duration, Δ_M a priory known.

SF : Standby before filling. During this phase, it is assumed that the state remains constant and the balance equations are simply:

$$
\begin{cases}
\dfrac{dV}{dt} = 0 \\[2mm]
\dfrac{dC}{dt} = 0 \\[2mm]
\dfrac{dT}{dt} = 0
\end{cases}
\quad or \quad
\begin{cases}
V(t) = 0 \\[2mm]
C(t) = 0 \\[2mm]
T(t) = T_a
\end{cases}
$$

Here the phase transition is triggered when a certain time period Δ_{SF} [h], fixed by the plant scheduler (a time event guard) has elapsed.

In accordance with the general concepts of chemical process modelling the input flow rates of the reactors during the phases: filling, heating, temperature regulation and cooling can be classified as input variables and grouped in the vector $u = (F_{in}, F_{disch}, Q_h, Q_c)$. Since these variables are physically non-negative, $U \triangleq \mathbb{R}_+^4$. The constraints on these input variables will be defined in the next Chapter. Moreover, as was defined, the stand by times are coming from the scheduler (an external unit) consequently they are also classified as input variables for the plant and grouped in the vector $\Delta_{SB} = (\Delta_{SF}, \Delta_{SH}, \Delta_{SD})$.

2.1.2 Hybrid Automaton Model of the storage tank

Discrete states and transitions. According to the description given in Chapter 1, during the production cycle the tank is fed discontinuously (when a BR_i $i \in \{1, ..., N\}$ is discharged) but is discharged continuously. This process is modeled by the directed graph in Figure (2.2) (with the notations defined in Table (2.2)). The phase OUF is undesirable and the tank enters in it only if its volume is over its maximal or under minimal allowed values. The elements of the set Σ^{ST} of discrete states is then naturally defined as the set of process phases:

$$
\Sigma^{ST} = \left\{
\begin{array}{l}
F_1 D, \ F_2 D, \ ... \ , \ F_N D, \ F_{12} D, \ ... \ , \ F_{(N-1)N} D, \\
F_{123} D, \ ... \ , \ F_{(N-2)(N-1)N} D, \ ... \ , \ F_{12...N} D, \ DO, \ OUF
\end{array}
\right\}
$$
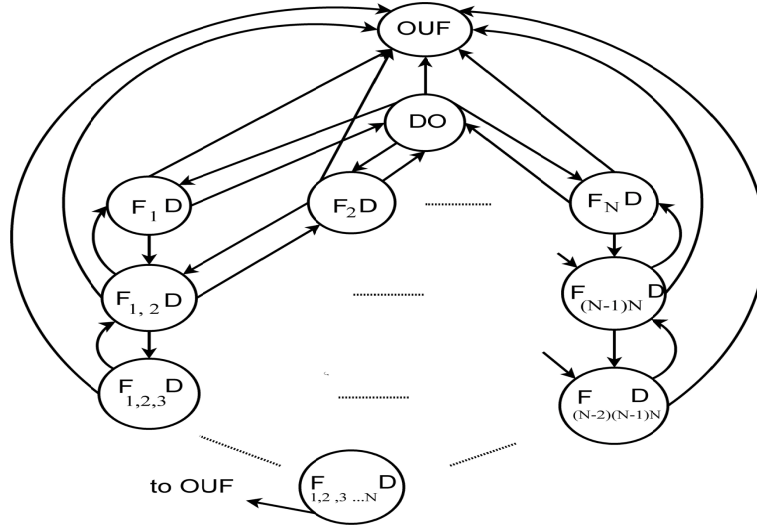
Fig. 2.2: HAM of a storage tank

abbreviation	phase name
$F_i D$	Filling from BR_i $i \in \{1, ..., N\}$ and discharging
$F_{ij} D$	Filling from BR_i and BR_j
	$i, j \in \{1, ..., N\}$ $i \neq j$ and discharging
$F_{i...k} D$	Filling from BR_i ... BR_k
	$i, k \in \{1, ..., N\}$ $i \neq k$ and discharging
$F_{12...N} D$	Filling from all reactors and discharging
DO	Discharging only
OUF	Over/under filling

Table 2.2: Phases in the storage facility

Note that at time t only one reactor can start discharging in the tank and consequently the initial phase of the tank is $F_i D$ $i \in \{1, ..., N\}$. The set E^{ST} of **transitions** between the discrete states is:

$$
E^{ST} = \begin{cases}
(DO, F_1D), \ \dots \ , \ (DO, F_ND), \\
(F_1D, DO), \ \dots \ , \ (F_ND, DO), \\
(F_1D, F_{12}D), \ \dots \ , \ (F_{N-1}D, F_{(N-1)N}D), \\
(F_{12}D, F_1D), \ \dots \ , \ (F_{(N-1)N}D, F_{N-1}D), \\
(F_{12}D, F_{123}D), \ \dots \ , \ (F_{(N-1)N}D, F_{(N-2)(N-1)N}D), \\
(DF_{12}, DF_{123}), \ \dots \ , \ (DF_{(N-1)N}, DF_{(N-2)(N-1)N}), \dots \\
(DO, OUF), (F_1D, OUF) \dots (F_ND, OUF), \\
, (F_{12}D, OUF) \dots (F_{(N-2)(N-1)N}D, OUF)
\end{cases}
$$

Continuous states. As it was described in Chapter 1, there is no chemical reaction taking place in the tank but only a transfer of material and consequently, in accordance with the classical modelling of such chemical vessels, the continuous state variables are simply: U [m^3] the **volume** of the storage facility, and P [mol/l] the **concentration** of the chemical product in it. Since these variables are physically non-negative, we have $X^{ST} \triangleq \mathbb{R}^2_+$.

Note that except otherwise mentioned, there is no reset of the values of the continuous state variables at the transition from one phase to another.

Continuous-time dynamics, discrete-time dynamics and input variables. The process behaviour may then be described, in each phase, by a set of continuous differential equations (mass balances only):

$$
\begin{cases}
\dfrac{dU}{dt} = \sum_{i=1}^{N} \varphi(\sigma^i(t)) F^i_{disch} - w \\[2ex]
\dfrac{dPU}{dt} = \sum_{i=1}^{N} \varphi(\sigma^i(t)) F^i_{disch} P^i_{in} - wP
\end{cases}
\tag{2.1}
$$

with $\sigma^i : \Re \to \Sigma^i$, where $\sigma^i(t)$ is the working phase of the ith reactor at time t such that,

$$
\begin{aligned}
\varphi(\sigma^i(t)) &= 1 \ \ \text{if} \ \ \sigma^i(t) = D \\
&= 0 \ \ \text{if} \ \ \sigma^i(t) \neq D
\end{aligned}
$$

and P^i_{in} [mol/l] is the concentration of the product coming from each reactor, F^i_{disch} [m^3/h] and w [m^3/h] are the volumetric output

flow rates of product going out from BR_i and from the tank, respectively. It should be noted that during the **DO** phase the tank is not fed with a product but it is only discharged with an outflow rate w.

Let us now describe the transition conditions between some of the phases of the storage facility. The definition of the other phases is similar.

DO: Discharging only. Tank discharging lasts

- either until any of the batch reactors i enters its discharging phase, D (an input event guard). At that moment the storage tank, goes to the phase F_iD.

- or until the volume of the storage facility U reaches its minimal allowed value U^{min} (a state event guard) and consequently the tank process goes to the over/under filling phase, OUF.

F_iD: Filling from BR_i and discharging. This phase stops

- either when BR_i is completely discharged and enters the maintenance and cleaning phase, M (an input event guard). In this case the storage facility goes to the discharging only phase, DO.

- or when another reactor BR_j enters the discharging phase, D (an input event guard). In this case the storage tank, goes to the phase of filling from reactor i and reactor j and discharging, $F_{ij}D$.

- or when its volume U reaches a given maximal value U^{max} (a state event guard). In this case the tank goes to the *over/under filling* phase, OUF.

F$_{ij}$D: Filling from both reactors and discharging. This phase proceeds

- either until BR_i is completely discharged and enters the maintenance and cleaning phase, M (an input event guard). In this case the tank goes to the phase of filling from reactor j and discharging, F_jD.

- or until BR_j is completely discharged and it enters the maintenance and cleaning hase, M (an input event guard). In this case the tank goes to the phase of filling from reactor i and discharging, F_iD.

- or until its volume U reaches a given maximal value U^{max} (a state event guard). In this case the storage tank goes to the *over/under filling* phase, OUF.

OUF : Over/under filling The plant cannot go out of this phase unless a new production scheduling is made.

The input and output flow rates of the tank during all of the phases are classified as input variables and grouped in the vector: $u^{ST} = (F_{disch}^1, ..., F_{disch}^N, w)$. Since these variables are physically non-negative, $U^{ST} \triangleq \mathbb{R}_+^{N+1}$. The existing constraints on these input variables will be defined in the next Chapter.

2.1.3 Hybrid Automaton Model of the entire benchmark plant

The overall hybrid automaton model of the plant is made as a combination of the models of its units, namely the N automata of the batch reactor processes and the automata of the storage facility process. The directed graph of the plant is given in Figure (2.3) where a possible combination of active phases of the plant processes is emphasized with bold circles, namely:

*BR_1 and BR_j are in the phase **Discharging** and respectively the storage tank is in the phase **Filling from** BR_1 **and** BR_j **and discharging**. At this time BR_N is in the **Stand by before filling phase**.*
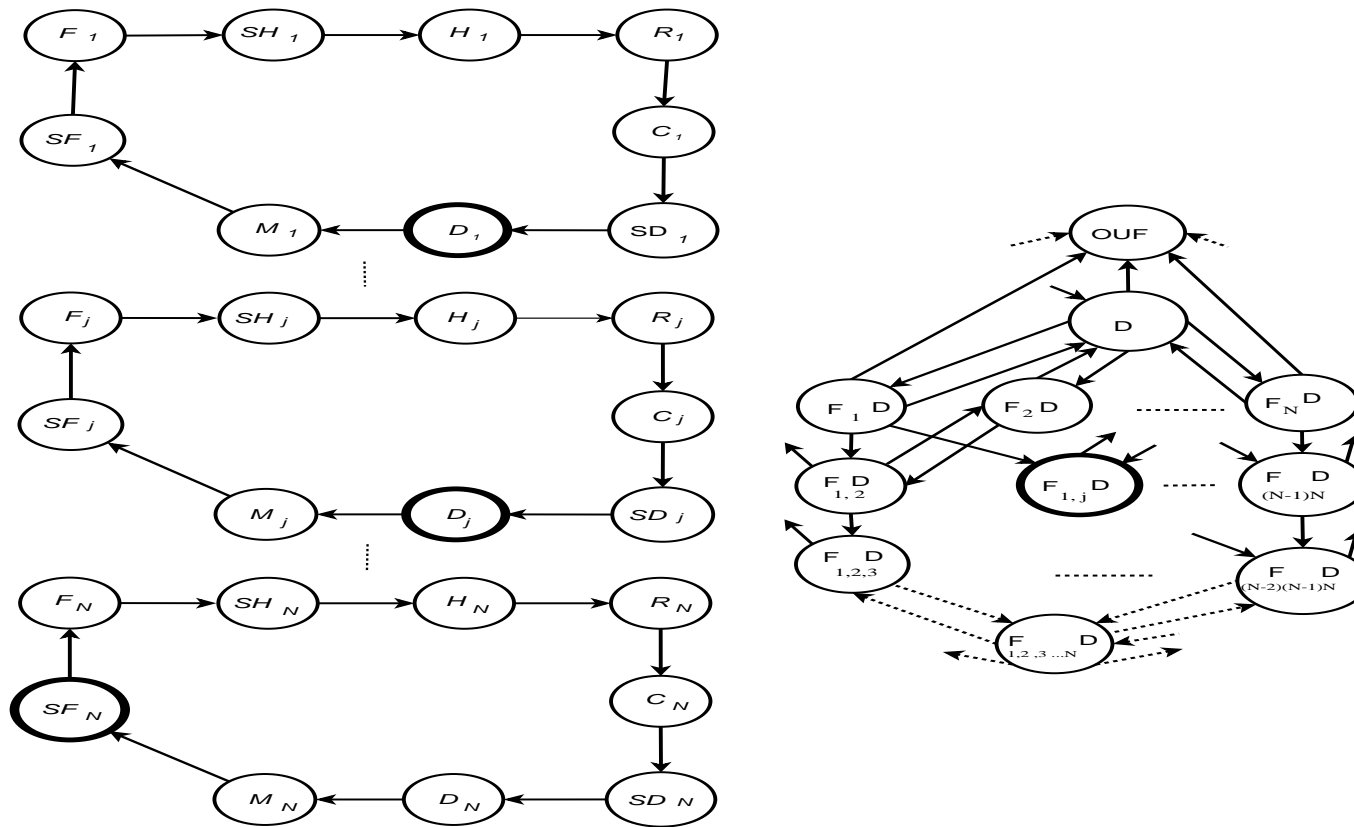
Fig. 2.3: Combined HAM of a benchmark chemical plant

Mathematically the collection of sets of the hybrid plant automaton is defined hereafter.

Discrete states and transitions. The plant has a combined discrete set of states and a combined discrete transition set, namely:

- the plant discrete set is a subset of the Cartesian product of the discrete sets of its $N + 1$ units:

$$\Sigma^{TOT} \subset \{\Sigma^1 \times \Sigma^2 \times ... \times \Sigma^N \times \Sigma^{ST}\}$$

  An active phase of the overall plant at time t is a combination of all $N + 1$ simultaneously active phases of its units (Figure (2.3), bold circles).

- Similarly the plant admissible discrete transition set is a subset of the Cartesian product of the sets of discrete transitions of its $N + 1$ units:

$$E^{TOT} \subset \{E^1 \times E^2 \times ... \times E^N \times E^{ST}\}$$

Continuous states. The plant continuous state combines all state variables of its $N + 1$ units:

$$x^{TOT} = \left(V^1 \ \ T^1 \ \ C^1 ... V^N \ \ T^N \ \ C^N \ \ U \ \ P\right)'$$

Continuous-time, discrete-time dynamics and input variables.

- The plant continuous-time dynamics is a subset of the Cartesian product of the sets of continuous time dynamics of its $N + 1$ units:

$$F^{TOT} \subset \{F^1 \times F^2 \times ... \times F^N \times F^{ST}\}$$

  respectively, continuous dynamics of the plant process at time t is a combination of all $(N + 1)$ simultaneously active continuous dynamics of its units (Figure (2.3), bold circles).

- The definition of the set of transition guards is similar:

$$G^{TOT} \subset \{G^1 \times G^2 \times ... \times G^N \times G^{ST}\}$$

- The plant input variables namely the flow and transfer rates as well as the stand by times coming from the plant scheduled are grouped as follows:

  – Plant input flow/transfer rates:

$$u^{TOT} = \left(F_{in}^1 \; Q_c^1 \; Q_h^1 \; F_{disch}^1 \quad F_{in}^2 \; Q_c^2 \; Q_h^2 \; F_{disch}^2 \; ... \right.$$
$$\left. F_{in}^N \; Q_c^N \; Q_h^N \; F_{disch}^N, w \right)'$$

  – Plant input stand by times coming from the scheduler:

$$\Delta^{TOT} = \left(\Delta_{SF}^1 \; \Delta_{SH}^1 \; \Delta_{SD}^1 \; \Delta_{SF}^2 \; \Delta_{SH}^2 \; \Delta_{SD}^2 \; ... \Delta_{SF}^N \; \Delta_{SH}^N \; \Delta_{SD}^N \right)'$$

Note that taking into account the number of reactors N, that in each of them 9 phases are performed, as well as the number of phases performed in the storage facility, it is obvious that the number of possible combination of simultaneously active phases (and continuous dynamics respectively) is very high. The same is valid for the number of simultaneously active transition conditions between the phases of the different units.

Consequently, the main advantage of a separate modeling of the hybrid processes performed in the plant units as presented in this thesis, is that it avoids the enumeration over all elements of the discrete set of phases, the set of continuous-time and discrete-time dynamics, needed to model the plant behaviour at any time.

In order to observe and analyze the behaviour of the benchmark chemical plant and to be able to optimize and stabilize its operation, we shall develop a simulator in the next section.
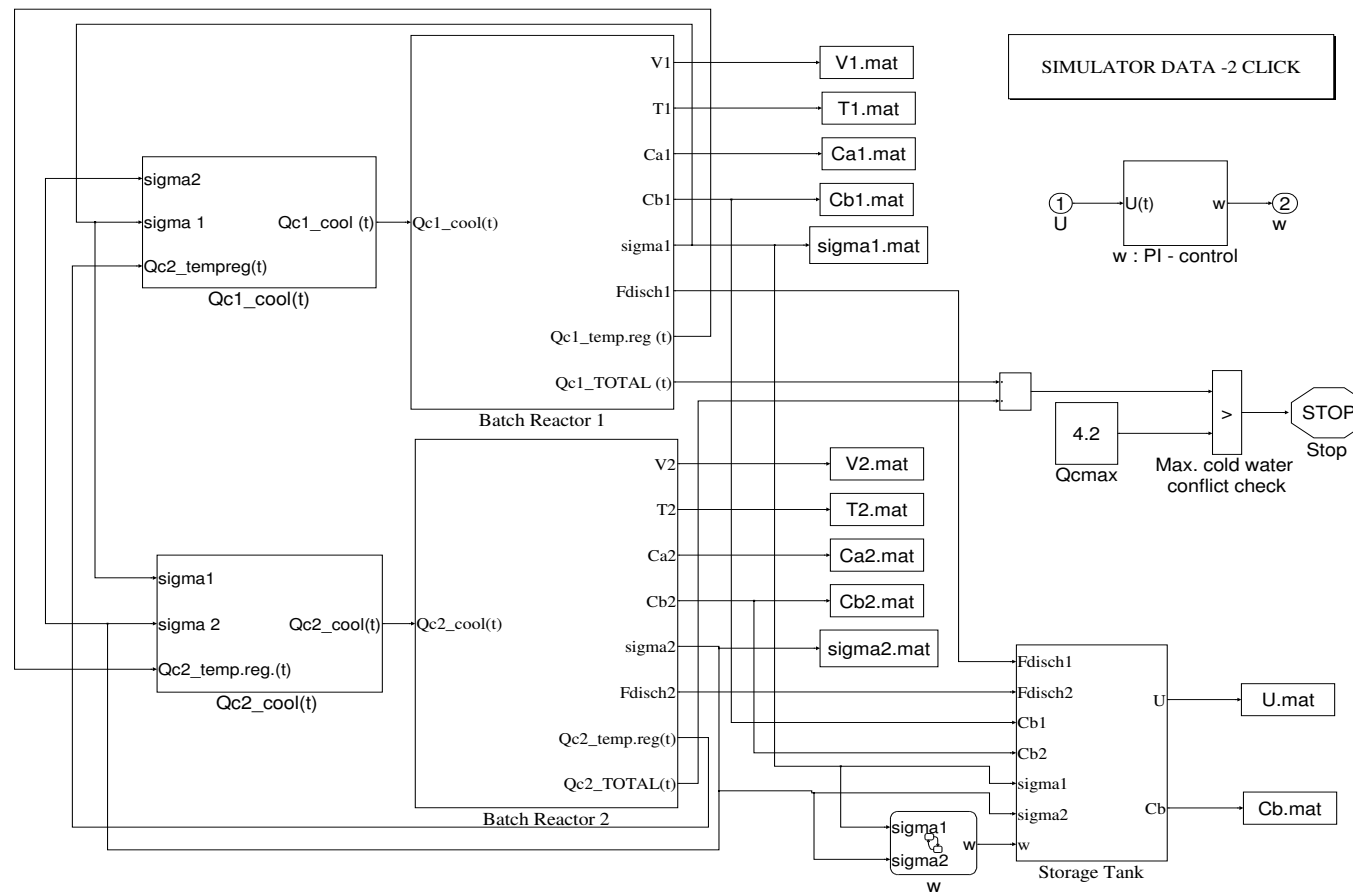
Fig. 2.4: Plant simulator

2.2 A Matlab-Simulink-Stateflow simulator of the plant

The hybrid automaton framework presented in the previous Section is used to build a simulator for the considered hybrid chemical plant. It is developped in a *Matlab* environment by the combination of the *Stateflow* and *Simulink* tools. A more detailed presentation of the simulator is given in Appendix A. The main features of the simulator are as follows:

- *Stateflow* is an interactive graphical design tool that works with *Simulink* to model and simulate mostly *discrete-event dynamics*. It is based on the *Statechart* formalism of Harnel [Har87]. *A Stateflow chart* is build by using *Stateflow* graphical objects. Likewise the directed graph of an hybrid system it has phases called `states` and transition conditions (presented as: `[condition]`) between them, representing a Boolean expression that must be true for a transition to occur from one `state` to another. Consequently *Stateflow* is well appropriate for the simulation of the *discrete-time dynamics* of a hybrid system. During the simulation when a `state` or a transition is active they are highlighted.

- *Simulink* is an interactive graphical design tool that models and simulates mostly *continuous-time dynamics*. Actually *Stateflow* associates with each `state` a set of equations which are modeled and simulated using various *Simulink* blocks. The synchronization between `states` activation and equations solving is accomplished by so a called `entry` function available in each mode of the *Stateflow chart*. Consequently *Simulink* is used to simulate the *continuous-time dynamics* of a hybrid system.

A presentation of some other features of the *Stateflow* and *Simulink* tools of *Matlab* are given hearafter during the simulator description.

The global *Simulink* model of the chemical plant simulator is shown in Figure (2.4). Similarly to the plant presented in Figure (1.2) it has:

i. Two subsystems: *Batch Reactor* 1 and *Batch Reactor* 2 to simulate the hybrid automaton model of each batch reactor (here it is

assumed that we have only two reactors);

ii. The subsystem: *Storage Tank* to simulate the hybrid automaton
model of the storage facility;

moreover there are:

iii. Two subsystems: *Qc1_cool(t)* and *Qc2_cool(t)*, to calculate during
the cooling phase of each reactor BR_i, $i \in \{1, 2\}$, the cooling
water rate Q_c^i as a function of the cooling water used in the other
reactor BR_j, $j \in \{1, 2\}$ $i \neq j$ (See for details Chapter 3, Section
3.3 and Appendix A);

iv. Two subsystems: *w* and *w : PI - control*, the former is use to set
output flow rate of the tank to its scheduled value and the latter to
compute it based on a *PI* control law as given by Equation (6.13)
(See for details Chapter 6, Section 6.3 and Appendix A).

On the other hand:

i. the block "SIMULATOR DATA - 2 CLICK" is used to load the
plant parameters via a *Matlab* code in the *Matlab* work space;

ii. the blocks "NAME.mat" are used to save the time evolutions of
the reactor and the tank continuous state variables.

Based on the mathematical model developed in this Chapter the
Simulink blocks are interconnected by arrows which represent the in-
teractions between the plant units. Now some of the various building
modules of the simulator shall be described in more details.

2.2.1 Matlab-Simulink-Stateflow model of the batch reactor

The *Simulik-Stateflow* model of BR_1 is depicted in Figure (2.5). This
model is obtained after a double click on the *Batch Reactor* 1 block of
Figure (2.4). The model of BR_2 is identical (See Appendix A). As seen
it consists of two mutually connected subsystems: a *Stateflow* and a
Simulink diagrams.

It is assumed that there is a simple second order exothermic reaction performed in the reactors, namely:

$$2A \overset{k(T)}{\rightarrow} B$$

Fig. 2.5: Simulink-Stateflow diagram of BR_1

- The continuous state variables of the plant are the concentrations of the reactant A and of the product B. The corresponding state vector is denoted: $C = (C_A \quad C_B)'$

- It is assumed that the dependence of the reaction rate on the temperature, $k(T)$ obeys an *Arrhenius law* and consequently it is expressed as follows: $k(T) = k_0 exp^{-\frac{E}{RT}}$, where k_0 $[l/mol.h]$ is the rate constant, R $[J/mol.K]$ is the gas constant and E $[J/mol]$ is the activation energy of the reaction.

- The dependence of the reaction rate on the concentration, $r(C)$ obeys the *law of mass action*. Because the reaction is second order the dependence has the form, $r(C_A, \quad C_B) = C_A^2$

Fig. 2.6: Stateflow diagram of BR_1

- The stoichiometric vector has the form: S = (-2   1)

- The discrete states and transitions shall be defined during the description of BR_1 Stateflow diagram of the plant simulator.

Assumption: The **cleaning and maintenance phase** and the **stand by (before filling phases)** are aggregated into a single phase. Referring to the *Stateflow* diagram of BR_1 in Figure (2.6) it is seen that in this case there are 8 phases (instead of 9) namely: stand by (before filling): SF_1, filling: F_1, stand by (before heating): SH_1, heating: H_1, temperature regulation: TR_1, cooling: C_1, stand by (before discharging): SD_1 and discharging: D_1. The *code*(on the arrow between the states: D_1 and SF_1):
`{Tin1=288;Treset;Cain1=0;Careset;Cbin1=0;Cbreset;Vin1=0;Vreset;}`
is used to reset the values of the reactant and product concentrations, the temperature and the volume in the reactor to their values just before the **stand by (before filling) phase**.

The *Stateflow* realization of the HAM of the reactor process is given hereafter.

In Figure (2.6) it is seen that there is an arrow which enters the phase F_1 and is not connected with the other phases. In the *Stateflow* language it is used to set up that this phase becomes active first when the simulation is run.

- the phase changes from stand by (before filling) SF_1 to filling F_1, when the time duration, $SF1$ [h] fixed by the plant scheduler has elapsed. In *Stateflow code* this is defined though the so called `after` function: `[after(SF1/st,wakeup)]`. The *code*:
  `{Tin1=300;Treset;Cain1=10;Careset;Cbin1=0;Cbreset;Vin1=0;Vreset;}`
  is used to reset the values of the reactant and product concentrations and the temperature in the reactor to their inflow value.

- the phase changes from filling F_1 to stand by (before heating) SH_1, when the reactor volume, V1 reaches its maximal value, Vmax $[m^3]$. In *Stateflow code* this is expressed as: `[V1>=Vmax]`.

- the phase changes from stand by (before heating) SH_1 to heating H_1, when the time duration, $SH1$ $[h]$ fixed by the plant scheduler has elapsed. In *Stateflow code* this is defined as: `[after(SH1/st,wakeup)]`.

- the phase changes from heating H_1 to temperature regulation TR_1, when the reactor temperature, T1 reaches its maximal value, Tmax $[K]$. In *Stateflow code* this is expressed as: `[T1>=Tmax]`.

- the phase changes from temperature regulation TR_1 to cooling C1, when the reactant concentration, C_1 reaches its threshold value, Catr $[K]$. In *Stateflow code* this is expressed as: `[C1<=Catr]`.

- the phase changes from cooling C_1 to stand by (before discharging) SD_1, when the reactor temperature, T1 reaches its minimal value, Tmin $[K]$. In *Stateflow code* this is denoted as: `[T1<=Tmin]`.

- the phase changes from stand by (before discharging) SD_1 to discharging D_1, after the stand by time $SD1$ $[h]$ defined by the scheduler has elapsed. In *Stateflow code* this is expressed as: `[after(SD1/st,wakeup)]`.

- finally the phase changes from discharging D_1 to stand by (before filling) SF_1 , when the reactor volume, V1 reaches its minimal value, Vmin $[m^3]$. In *Stateflow code* this is defined as: `[V1<=Vmin]`.

Here the variable `sigma1` is used for the graphical representation of the working phase of reactor one. Because the used version of *Stateflow* does not have a possibility for symbolic data they are replaced by numbers (Table (2.3)); `k1,k2,k3,k4,k5` (See Figure (2.7)) are variables used to connect the *Stateflow* diagram of the tank with the *Simulink* blocks where the continuous time equations of the volume and product concentration of the storage facility are solved; `Fin1`, `Fdisch1` and `Qh1` are used to denote the rates of filling, discharging and heating, respectively. Note that because the cooling flow rate `Qc1cooling(t)` is time dependent it is computed outside the *Stateflow* diagram (See Figure (2.4)).

sigmai	1	2	3	4	5	6	7	8
σ^i	SF	F	SH	H	TR	C	SD	D

Table 2.3: Correspondence between the HAM and the simulator discrete state variables for BR_i $i \in \{1, 2\}$

The *Simulink* realization of the continuous dynamics of the hybrid automaton model of BR_1 is given in Figure (2.7). It consists of a set of blocks which solves volume, concentration and energy balances equations, respectively. As a result it produces the time evolution of the state variables: *V1, Ca1, Cb1, T1.*

The content of the volume balance block is depicted in Figure (2.8). It is used to solve (though the integrator block $1/s$) the differential equation of the volume during each phase. The value of the flow rate $F1$ switches between 8 values (for each phase): $\{Fin1, 0, 0, 0, 0, Fdisch1, 0\}$. The switching is governed by the *Stateflow* diagram of BR_1 via the `Switch` $k4$ (Figure (2.7)).

Now we shall present the state flow diagram of the storage facility. The realization of the continuous dynamics *Simulink*-blocks for the solution of the continuous dynamics equations of the tank is straightforward (See Appendix A).

2.2.2 Matlab-Simulink-Stateflow model of the storage facility

As seen from Figure (2.9) the *Stateflow* diagram of the storge tank has five phases: filling from BR_1 and discharging $F1D$, filling from BR_2 and discharging $F2D$, filling from BR_1 and BR_2 and discharging $F12D$, discharging only DO and over/under filling OUF. The single arrow entering the phase DO and not connected with the other phases defines that the storage facility operation starts with it. Here the variable `sigmaST` is used for the graphical representation of the working phase of the tank.

The transitions between the modes are described as follows:
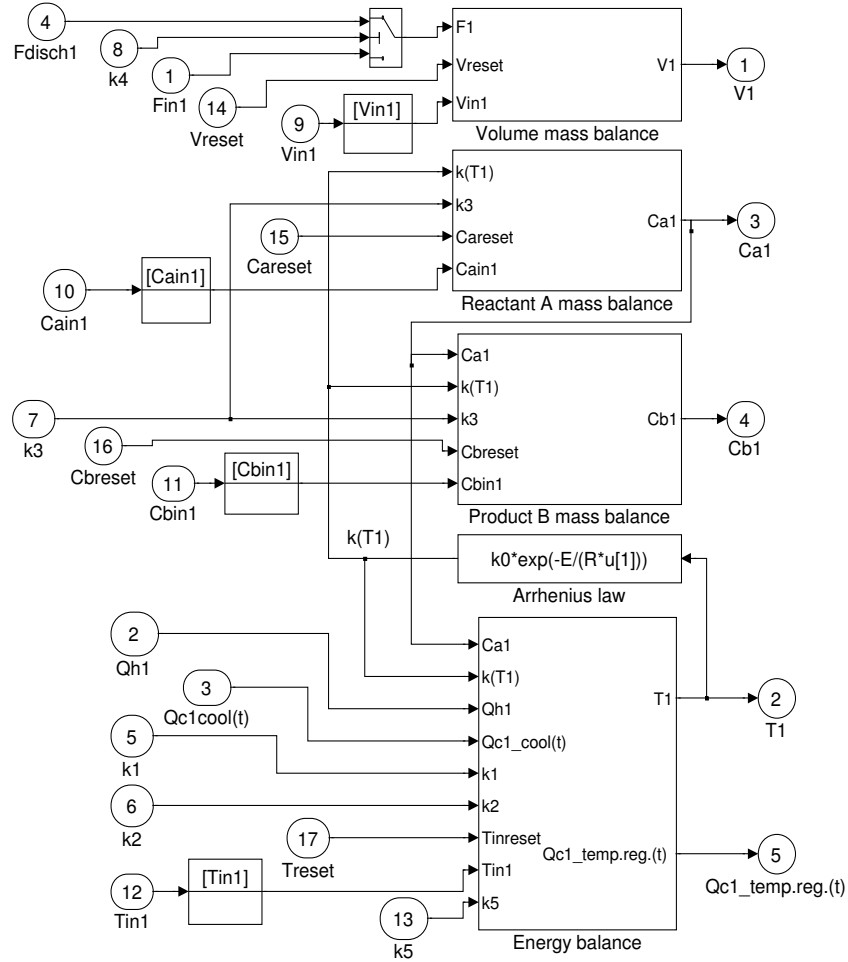
Fig. 2.7: Simulink blocks of the BR_1
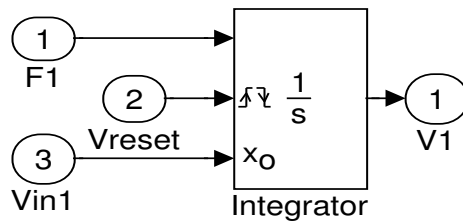
Fig. 2.8: Simulink model of the BR_1 volume balance

OUF

stp = 1;

sigmaST = 5;

[U>=Umax]

[U>=Umax]

[U>=Umax]

[U<=Umin]

F1D

s1=2;
s2=1;
s3=1;

sigmaST = 2;

[sigma1==8]

[sigma1==1]

DO

s1=1;
s2=0;
s3=1;

sigmaST = 1;

[sigma2==8]

[sigma2==1]

F2D

s1=3;
s2=1;
s3=1;

sigmaST = 3;

[sigma2==1]

F12D

s1=4;
s2=1;
s3=1;

sigmaST = 4;

[sigma1==1]

[sigma2==8]

[sigma1==8]
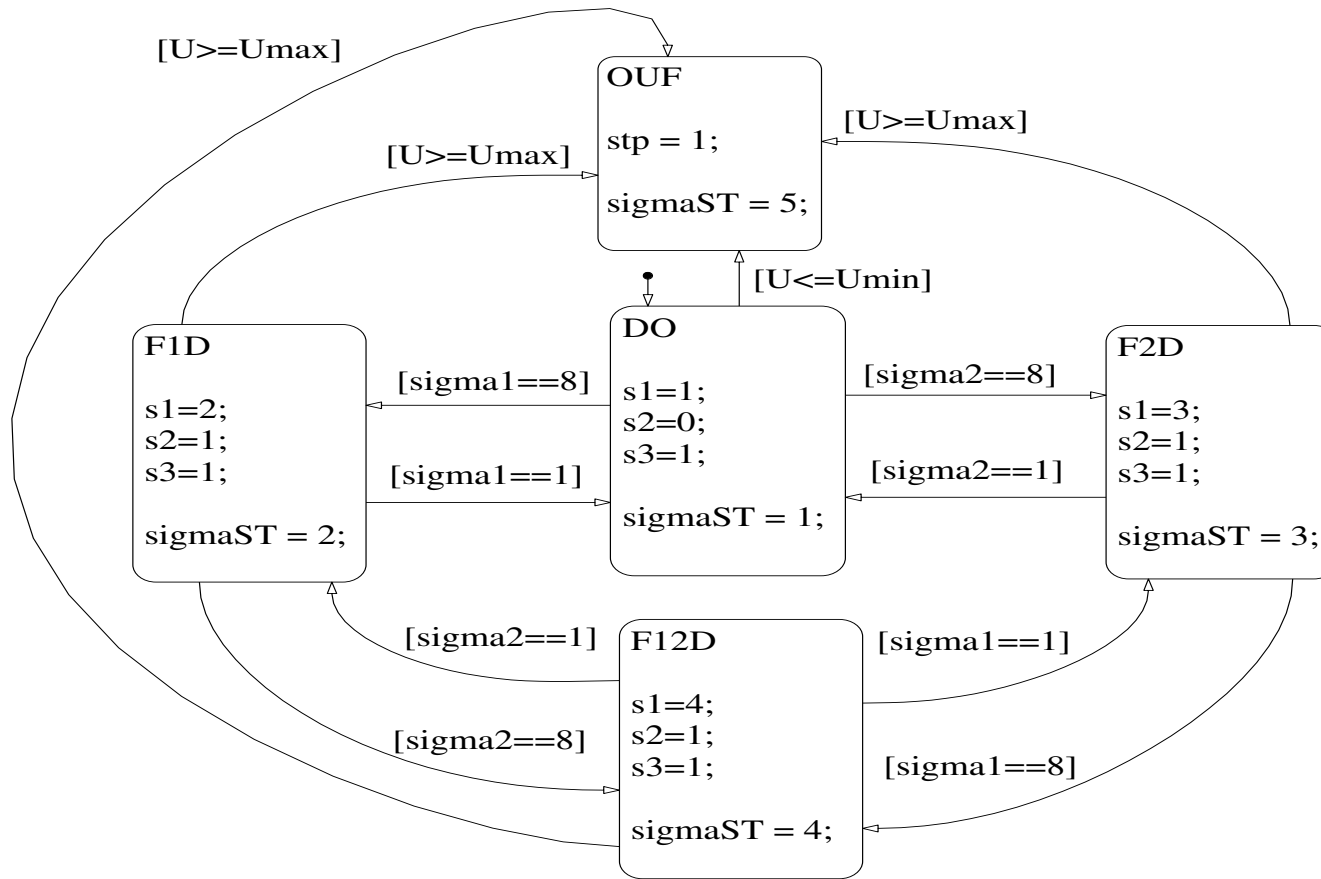
Fig. 2.9: Stateflow diagram of ST

sigmaST	1	2	3	4	5
σ^{ST}	DO	F_1D	F_2D	$F_{12}D$	OUF

Table 2.4: Correspondence between the HAM and simulator discrete state variables for the ST

- The phase changes from DO to $F1D$, when BR_1 enters its discharging phase. In *Stateflow code* this is expressed as: `[sigma1==8]`.

- The phase changes from DO to $F2D$, when BR_2 enters its discharging phase. In *Stateflow code* this is expressed as: `[sigma2==8]`.

- The phase changes from $F1D$ to DO, when BR_1 enters its stand by (before filling) phase. In *Stateflow code* this is expressed as: `[sigma1==1]`.

- The phase changes from $F2D$ to DO, when BR_2 enters its stand by (before filling) phase. In *Stateflow code* this is expressed as: `[sigma2==1]`.

- The phase changes from $F1D$ to $F12D$, when BR_2 enters its discharging phase. In *Stateflow code* this is expressed as: `[sigma2==8]`.

- The phase changes from $FD2$ to $F12D$, when BR_1 enters its discharging phase. In *Stateflow code* this is expressed as: `[sigma1==8]`.

- The phase changes from $F12D$ to $F1D$, when BR_2 enters its stand by (before filling) phase. In *Stateflow code* this is expressed as: `[sigma2==1]`.

- The phase changes from $F12D$ to $F2D$, when BR_1 enters its stand by (before filling) phase. In *Stateflow code* this is expressed as: `[sigma1==1]`.

- The phase changes from one of the phases: $F1D$ or $F2D$ or $F12D$ to OUF, when the maximal volume of the tank is reached. In *Stateflow code* this is expressed as: `[U>=Umax]`.

- The phase changes from *DO* to *OUF*, when the minimal volume of the tank is reached. In *Stateflow code* this is expressed as: `[U<=Umin]`.

Here the variable `s1`,`s2`, `s3` are variables used to connect the *Stateflow* diagram of the tank with the *Simulink* blocks where the continuous time equations of the volume and product concentration of the storage facility are solved.

2.3 Conclusions

In this Chapter we have presented and applied the hybrid automaton formalism for the modeling of the benchmark hybrid chemical plant. The process performed in each vessel is modeled by a hybrid automaton and the overall model is obtained as a combination of the hybrid automata models of the plant units. The main advantage of the proposed separate modeling of the hybrid processes is that it avoids the enumeration, over all elements of the $N+1$ discrete set of phase, $N+1$ set of continuous-time and discrete-time dynamics, needed to model the plant behaviour at any time. Note that a complete enumeration over all possible states of the tank automaton is needed. Based on the model a simulator of the plant is implemented in a Matlab-Simulink-Sateflow environment. Next Chapter presents the use of the simulator for optimal scheduling of a simple two reactors-storage tank plant under resources and tank capacity limitations.

Chapter 3

Design of periodic schedules: case studies

The purpose of this Chapter is:

i. *to define the problem of the optimal periodic scheduling for the benchmark plant with two reactors and a storage tank.*

ii. *to present an heuristic rule to solve this scheduling problem.*

iii. *to show how the Simulink-Stateflow simulator can be a very useful tool for the design of periodic schedules for the plant.*

Three case studies shall be presented: a single reactor having resource rate restrictions; a two reactors plant with resource rate restrictions and finally a two-reactors buffer tank plant having not only resource rate restrictions but also tank capacity limitations.

3.1 Case studies

In this thesis, an important concern is the design of **periodic** schedules which achieve some performance optimization of the hybrid chemical plant. In the present Chapter, we shall investigate how the simulator can be a useful tool for the design of such periodic schedules.

Three case studies will be considered. They are summarized in Figure 3.1. In all cases the aim is to operate the plant as fast as possible under some restrictions. The number of vessels (reactors and storage tank) and the type of restrictions are indicated in each box of Figure 3.1.

```
┌─────────────────────────┐  ┌─────────────────────────┐
│ 3.2. CASE 1             │  │ 3.3.  CASE  2           │
│                         │  │                         │
│ Single reactor          │  │ Two reactors            │
│                         │  │                         │
│   • Resource rate       │  │   • Resource rate       │
│     restrictions        │  │     restrictions        │
└─────────────────────────┘  └─────────────────────────┘
      ┌──────────────────────────────────────┐
      │ 3.4. CASE  3                         │
      │ (details in Chapter 5)               │
      │                                      │
      │ Two reactors and a storage tank      │
      │                                      │
      │   • Resource rate restrictions       │
      │   • Tank capacity restriction        │
      └──────────────────────────────────────┘
```
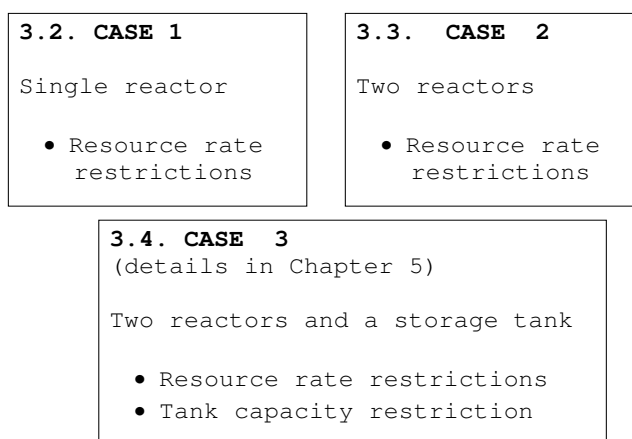
Fig. 3.1: Summary of the three case studies

The numerical values of the main model parameters used in the simulations are given in Table 3.1 (Reaction parameters) and Table 3.2 (Switching parameters). The values of the reaction parameters are chosen in a way to obtain phase durations (filling, heating, etc...) which are in accordance with the *Solvay project* description [Mel03]. The various resources (raw material, hot steam for heating and cold water for cooling and regulation) are shared by the two batch reactors under the following constraints and limitations:

k_0	reaction rate constant	10000	$l/mol.h$
E	activation energy	40200	J/mol
R	gas constant	8.3143	$J/mol.K$
δ	constant proportional to the reaction enthalpy	-100	$l.K/mol$
T_A^{in}	inlet reactant (A) temperature	288	K
C_A^{in}	inlet reactant (A) concentration	10	mol/l
C_B^{in}	inlet product (B) concentration	0	mol/l
T_h	hot steam temperature	380	K
T_c	cold water temperature	280	K

Table 3.1: Reaction parameters

V^{max}	maximal volume	27 (stop filling)	m^3
T^{max}	maximal temperature	400 (stop heating)	K
C_A^{tr}	threshold concentration	2 (stop regulation)	mol/l
T^{min}	minimal temperature	300 (stop cooling)	K
V^{min}	minimal volume	0 (stop discharging)	m^3

Table 3.2: Switching parameters

F_{in}^{max}	maximal reactant (A) feed flow rate	162	m^3/h
$F_{disch}^1 = F_{disch}^2$	discharging flow rate	162	m^3/h
Q_h^{max}	maximal hot steam transfer rate	3	h^{-1}
Q_c^{max}	maximal cooling water transfer rate	4.2	h^{-1}
Q_c^{min}	minimal cooling water transfer rate	2	h^{-1}

Table 3.3: Limitations of the resource rates

i. There is a physical constraint on the maximum value of the total filling flow rate $F_{in} = F_{in}^1 + F_{in}^2 \leq F_{in}^{max}$ $[m^3/h]$, of the total heating transfer rate $Q_h = Q_h^1 + Q_h^2 \leq Q_h^{max}$ $[h^{-1}]$ and of the total cooling transfer rate $Q_c = Q_c^1 + Q_c^2 \leq Q_c^{max}$ $[h^{-1}]$ when the two reactors are operated separately or simultaneously. The maximal values are given in Table 3.3.

ii. Under the conditions of Tables 3.1 - 3.2 and referring to the set of differential equations for the **reaction phase** of the reactor HAM given in Chapter 2 the cooling transfer rate Q_c^i ($i = 1, 2$) for performing the temperature regulation is:

$$Q_c(t) = \frac{\delta \overbrace{\left(k_0 exp^{-\frac{E}{T^{max}R}}\right)}^{\text{Arrhenius law}} \overbrace{C_A^2(t)}^{\text{law of mass action}}}{T_c - T^{max}} \quad with \qquad (3.1)$$

$$C_A(t) = \frac{C_A(0)}{1 - 2(k_0 exp^{-\frac{E}{T^{max}R}})C_A(0)(t - t_0)}$$

where $C_A(0)$ is the reactant A concentration at the end of the
heating phase. As a result the cooling profile is graphically represented in Figure 3.2. Remark that the transfer rate Q_c^i can reach
the value 3.6 $[h^{-1}]$ which is close to the maximal admissible value
$Q_c^{max} = 4.2 \ [h^{-1}]$.

iii. During the cooling phase, in order to have a sufficiently fast cooling,
the cooling transfer rate must be large enough $Q_c^i \geq Q_c^{min}$ $(i = 1, 2)$.
The numerical value is given in Table 3.3.

From these conditions, we observe that the limitation in terms of cooling transfer rate Q_c may induce two kinds of conflict for this resource:

i. either the total demand may exceed the maximum Q_c^{max} value when
both reactors are simultaneously in regulation phases

ii. or the cold water transfer rate for cooling must be larger than
Q_c^{min} when a reactor is in cooling phase and the other reactor in
regulation phase.

Furthermore, the discharge flow rates are supposed to be constant and
identical for both reactors $F_{disch}^1 = F_{disch}^2$ (see Table 3.3).

3.2 CASE 1: A single batch reactor

We first consider the case when a **single** batch reactor is repeatedly
operated. In order to operate the reactor as fast as possible (or in other
terms to obtain an optimally scheduled operation) the successive tasks
(filling, heating, reaction, cooling, discharging) are immediately performed without delay and the stand-by times Δ_{SF} (before filling), Δ_{SH}
(before heating), Δ_{SD} (before discharging) are set to zero. The filling,
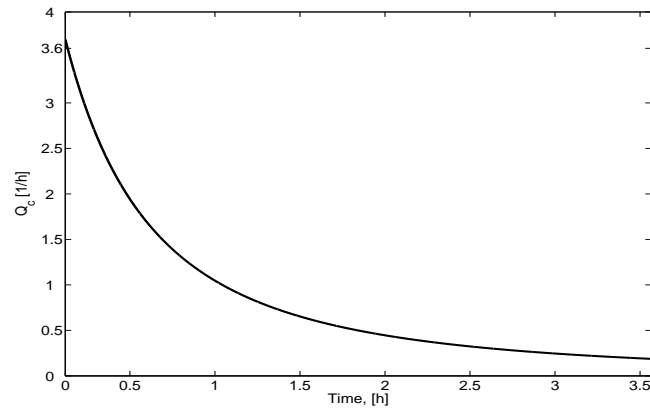heating and cooling tasks are obviously performed with maximal rates

Fig. 3.2: Quantity of cold water used by BR_1 (BR_2) to perform the temperature regulation during the reaction phase, Equation (3.1)
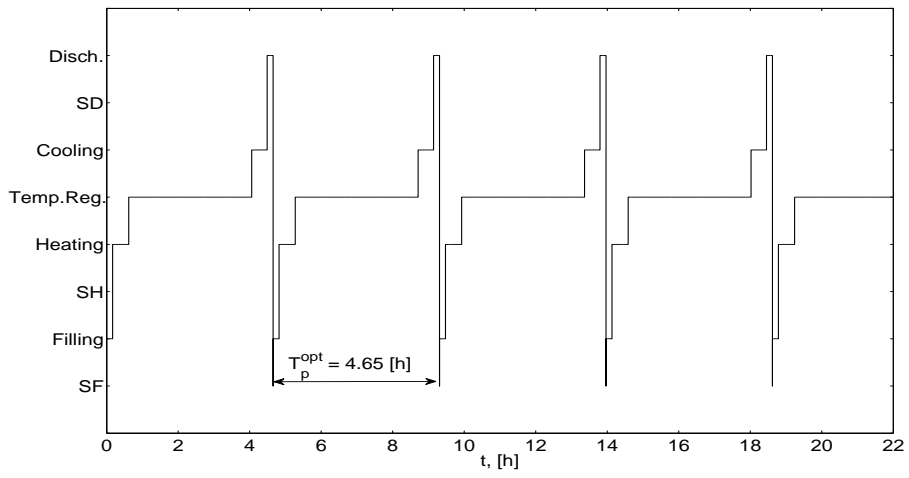

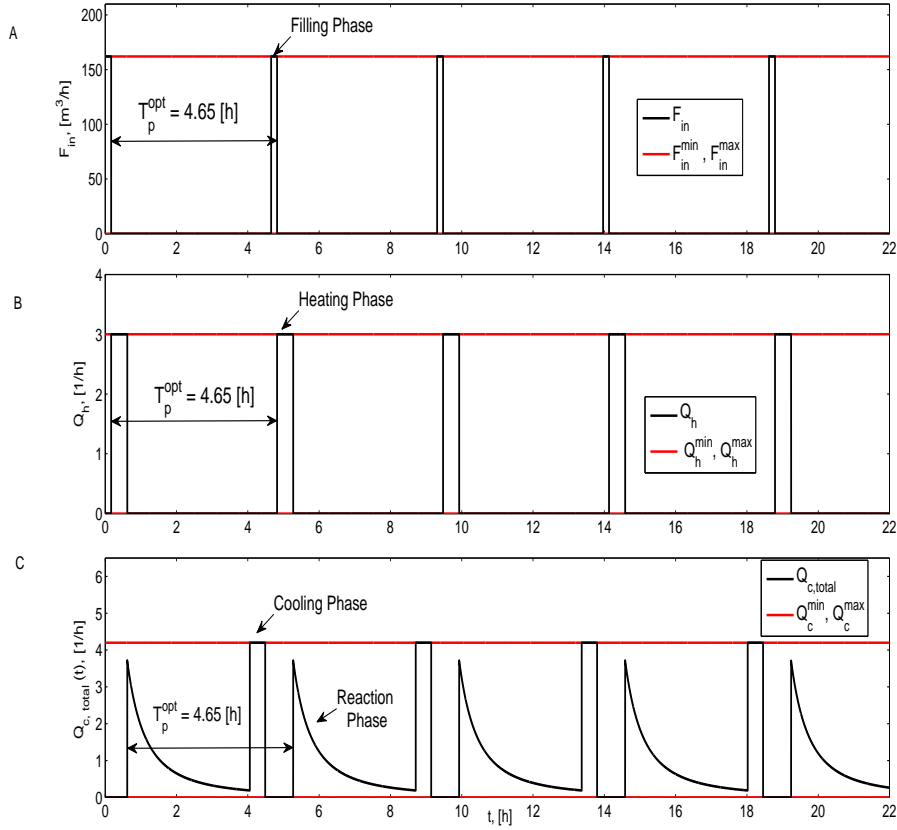Fig. 3.3: CASE 1: Schedule of a batch reactor

Fig. 3.4: CASE 1: Scheduled flow rates of a batch reactor

F_{in}^{max}, Q_h^{max}, Q_c^{max}.

Scheduling

In Figure 3.3 we give the chart of the plant schedule. It is seen that as was described in Subsection 2.2.1 the reactor cycle passes through the phases: filling, heating, reaction, cooling and discharging. When the discharging is done a new production cycle starts. It is important to observe that the reactor is automatically **periodically** operated with an optimal period $T_p^{opt} = 4.65$ [h].
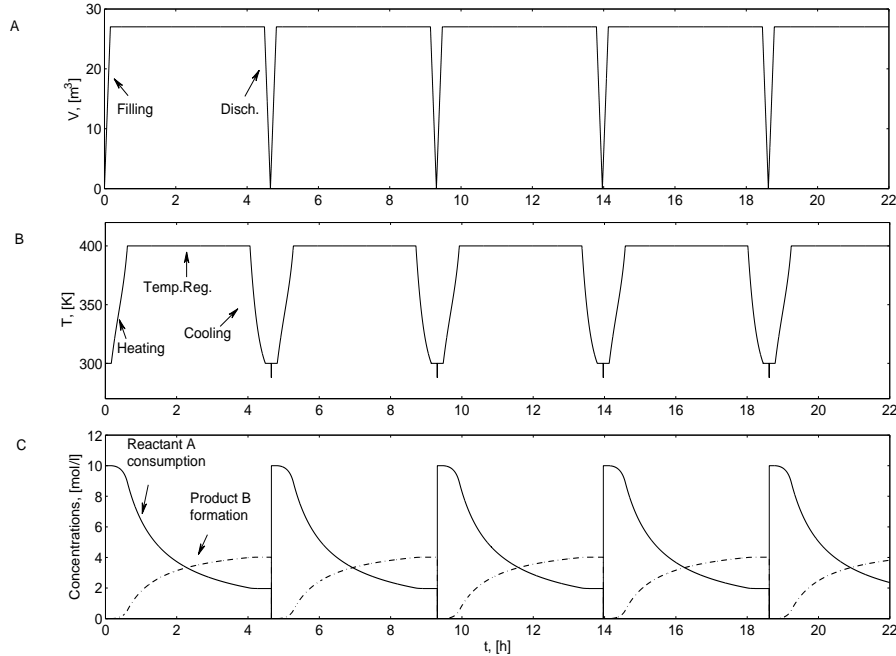
Fig. 3.5: CASE 1: Continuous state variables of a batch reactor

Flow rates evolution

The periodic character of the flow rates of raw material F_{in} and hot steam Q_h is observed in Figure 3.4 A and B, respectively. As seen during the corresponding phases they operate at maximal rates. The total cooling water transfer rate, used during the reactor operation, is presented in Figure 3.4 C. Its value is zero when the reactor is in the phases: filling, heating and discharging; it is a constant equal to the maximal value: 4.2 $[h^{-1}]$ when the reactor is in the cooling phase (Table 3.3) and it is exponentially decreasing when the reactor is in the reaction phase (Figure 3.2).

State variables evolution

The periodic volume and the temperature profiles of the reactor are given in Figure 3.5 A and B, respectively where the different phases of

the reactor operation are clearly seen. The profiles of the concentration of the raw material A and product B are presented in Figure 3.5 C.

3.3 CASE 2: Two batch reactors

Let us now consider a plant having two reactors operated in parallel. In order to operate the plant as fast as possible the first reactor is supposed to be started right from the beginning, with a maximal filling rate F_{in}^{max} and a maximal heating rate Q_h^{max}. Obviously the second reactor has to be started with a certain time lag with respect to the first one because the filling and heating resources are no longer available. There is another more important reason for delaying the second reactor. The reason is that there is a risk of conflict for the use of cooling water during the reaction phase if the two reactions are performed simultaneously. Furthermore in order to have a maximal utilization of the cold water, **during the cooling phase of each reactor** BR_i, $i \in \{1, 2\}$, **the cooling rate** Q_c^i is calculated as a function of the cooling water used in the other reactor BR_j, $j \in \{1, 2\}$ $i \neq j$. This is expressed as follows:

i. if

   a) $\sigma^i(t) = C$ and $\sigma^j(t) \neq TR$ or
   b) $\sigma^i(t) = C$ and $\sigma^j(t) \neq C$

   then $Q_{c,cooling}^i(t) = Q_c^{max}$;

ii. if $\sigma^i(t) = C$ and $\sigma^j(t) = TR$ then $Q_{c,cooling}^i(t) = Q_c^{max} - Q_{c,regulation}^j(t)$;

   where $Q_{c,regulation}^j(t) = \frac{\delta k_0 \exp^{-E/RT^{max}} C_j^2}{T_c - T^{max}}$ (See Figure 3.2)

iii. and finally if $\sigma^i(t) \neq C$ then $Q_{c,cooling}^i(t) = 0$.

Note that the chemical reaction is such that the duration of the reaction phase is larger than the duration of the cooling phase. Therefore both reactors can not be together in the cooling phase. We assume that these rules for determining $Q_c(t)$ during the cooling phase are added as constraints to the reactor continuous time dynamics in the

HAM and consequently in the *Simulik-Stateflow* simulator (See Figure 2.4 and Appendix A).

Finally, in order to operate the reactors as fast as possible, we impose that **all** stand by times are set to zero, namely $\Delta_{SF}^i = 0, \Delta_{SH}^i = 0, \Delta_{SD}^i = 0$ for $i \in \{1, 2\}$.

3.3.1 Convergence to a periodic operation

In order to avoid a conflict for the cold water utilization the second reactor must start with time lag of at least, 1.76 $[h]$. Otherwise as illustrated in Figure 3.6 the total cold water capacity is exceeded.
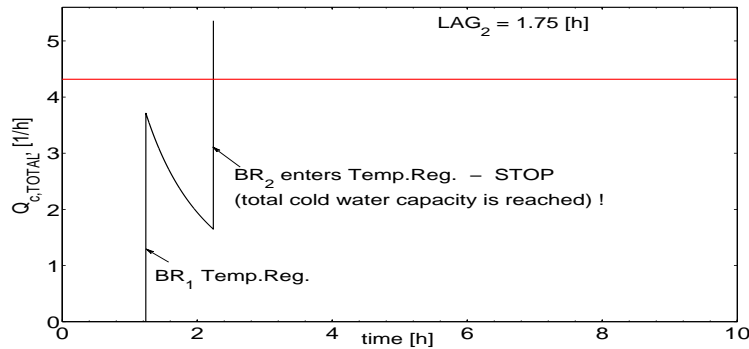

Fig. 3.6: Total cold water conflict: $Lag_2 = 1.75[h]$

The plant operation is illustrated in Figure 3.7, A where the profile of the total cold water flow rate $Q_{c,TOTAL}(t) = Q_c^1(t) + Q_c^2(t)$ is represented. In this Figure, an important feature can be observed: the hybrid plant trajectory automatically **converges** to a periodic operation with a period equal to 4.74 $[h]$ which is reached after approximately 80 hours. Note that this convergence has been discovered through the use of the simulator.

It turns out that the cold water conflict is alleviated for all time lags in the interval $[1.76 \quad 3.13]$ $[h]$. For instance, if the second reactor is started with a lag time of 2.6 $[h]$, the process behaviour is shown in Figure 3.7, B. Here also, it can be observed that the plant trajectory
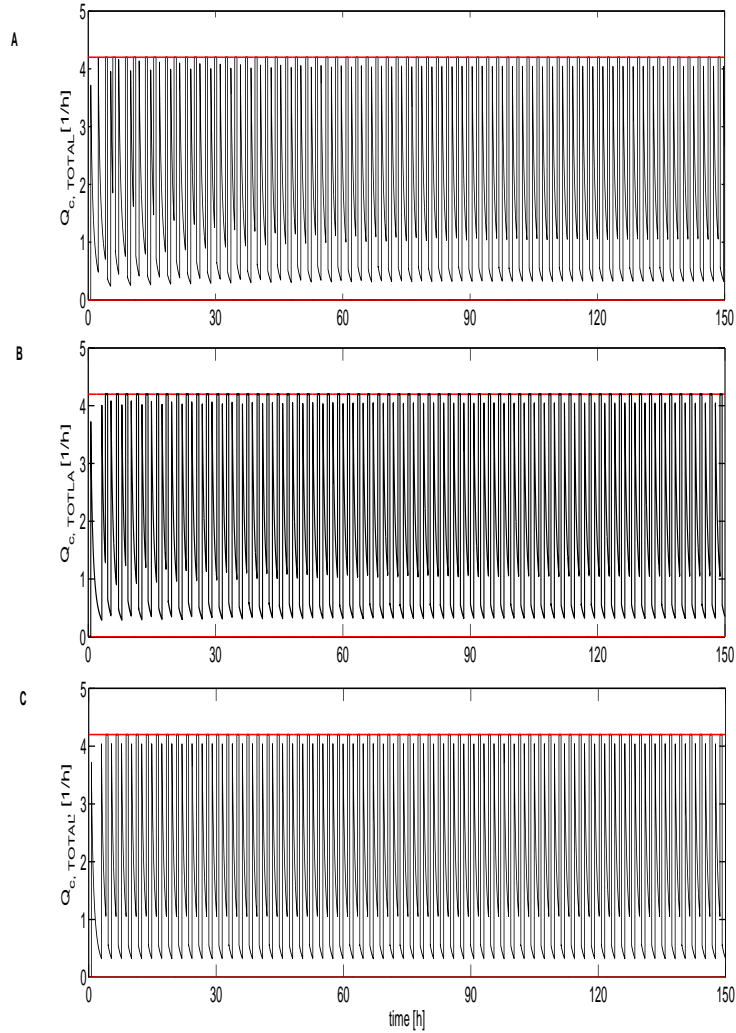
Fig. 3.7: CASE 2: Convergence at a periodic operation, A: $Lag_2 = 1.76[h]$, B: $Lag_2 = 2.6[h]$, C: $Lag_2 = 2.37[h]$

converges to exactly the **same** periodic operation with the same period of $T_p = 4.74$ $[h]$. The convergence time is here approximately equal to 40 hours.

In fact a set of simulations shows that for all initial time lags in the interval $[1.76\ \ 3.13]$ $[h]$, the overall plant behaviour always converges to the same periodic trajectory which appears clearly to be an **at-**

tracting limit cycle of the hybrid chemical plant.

In the special case when the time lag is 2.37 $[h]$, the plant is initialised on the limit cycle and the operation is periodic right from the beginning. This case is presented in Figure 3.7, C.

Another representation of the convergence to the periodic limit cycle for different initial conditions is given in Figure 3.8 A-B. In these Figures it is seen that cycle duration of each reactor T_p $[h]$ converges after a certain number of batches to the limit cycle period $T_p = 4.74$ $[h]$.

In Figure 3.8 C, we represent the number of successive batches that are performed before to reach the periodic operation: the closer is the initial time lag to the optimal one (= 2.37 $[h]$), the faster is the convergence to the periodic schedule.

Finally, Figure 3.9 is another way to summarize our observations: the interval $[1.76 \ 3.13]$ $[h]$ is the only admissible set of values for the time lag between the starting times of the to reactors. All other values outside this interval will lead the process to a blocking, either because the total cold water capacity is exceeded or because the minimal cold water capacity is reached. Figure 3.9 represents the time instants where the blocking occurs in function of the time lag.

3.3.2 Optimal periodic schedule

The analysis that we have done here above shows that the limit cycle is the only possible **periodic** operation of the plant with zero stand-by times $\Delta_{SF}^i = \Delta_{SH}^i = \Delta_{SD}^i = 0$ $[h]$. Hence, by using the *Simulink-Stateflow* simulator, we have been able to discover the **optimal periodic schedule** of the plant. This schedule is optimal in the sense that there is no other periodic schedule that could be faster and perform more batches per unit of time. Indeed at every time instant each reactor is using when necessary all available quantity of the corresponding resource. In other terms, it is the periodic schedule that gives the highest possible plant productivity. The behaviour of the hybrid plant under this optimal schedule is illustrated in Figures 3.10, C, E, F. As seen in these Figures there is no conflict of cooling water sharing. Moreover the cold water used during the cooling phases
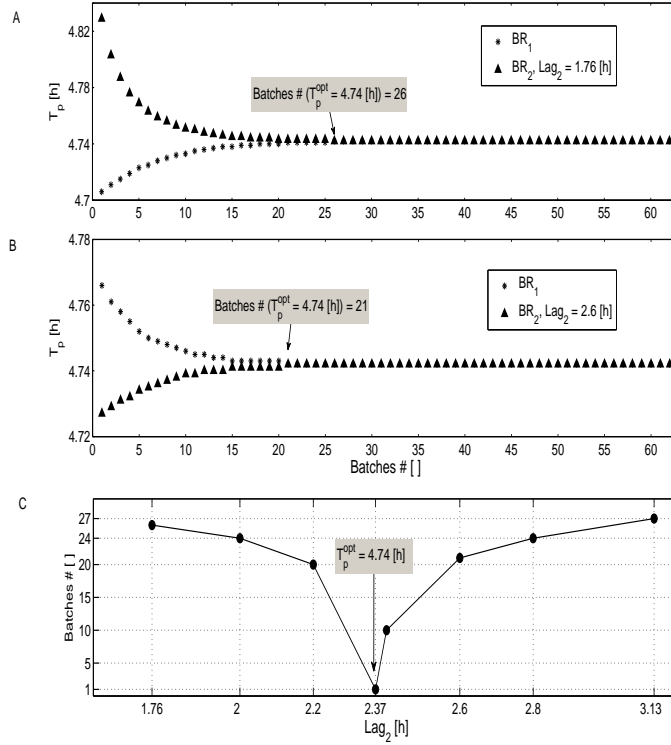
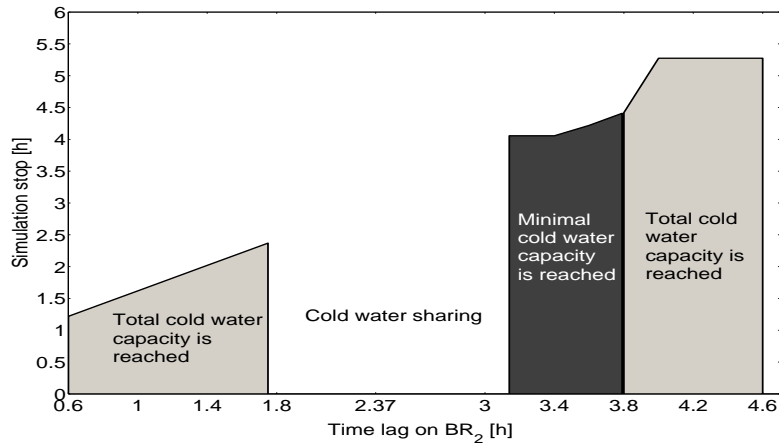Fig. 3.8: CASE 2: Summary of the convergence to a periodic limit cycle

Fig. 3.9: CASE 2: Zones of cooling water sharing

is not constant but is obtained based on the available cooling water quantity used in the other reactor (see Figure 3.10 C and E).
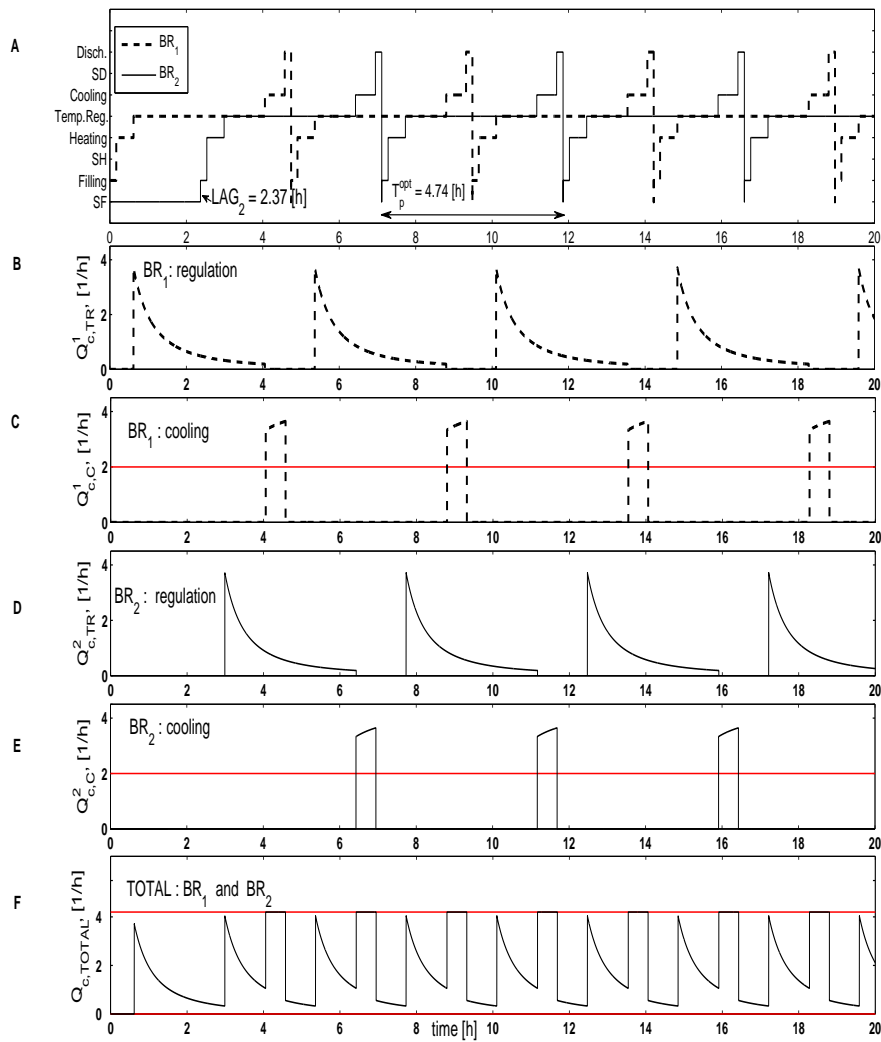

Fig. 3.10: CASE 2: The optimal periodic solution with zero stand by times

3.3.3 Other sub-optimal periodic schedules

As we have seen above, the optimal schedule is carried on with zero stand-by times. In order to robustify the periodic plant operation with respect to disturbances and model inaccuracies, it may however be interesting to define sub-optimal periodic schedules with non-zero stand-by times. Indeed, this can give some robustness margin to the process operation by adjusting the stand-by times on-line possibly with a feedback control strategy. This control issue will be discussed in Chapter 6.

Let us first consider the case when the plant is operated with the smallest time lag $Lag_2 = 1.76 \ [h]$ between the starting of reactors BR_1 and BR_2. The aim is to see, if thanks to the introduction of stand-by times, we could operate the plant periodically right from the beginning. In order to solve this problem we refer to Figure 3.8 A where we can see that, at the initial instant, there is a difference in the cycle durations of the two reactors: $T_{p1} < T_{p2}$. The idea is therefore to introduce stand by times in the cycle of reactor BR_1. It can be shown that with the following values $\Delta_{SF}^1 = 0.18 \ [h]$ (where $\Delta_{SF}^1 \approx |T_{p2} - T_{p1}|$), $\Delta_{SH}^1 = \Delta_{SD}^1 = 0 \ [h]$, it is indeed possible to have, right from the beginning, a periodic operation with a period $T_p = 4.88 \ [h]$ which is obviously larger than the optimal period $T_p = 4.74 \ [h]$. Actually the real difference of $0.14 \ [h]$ is smaller than the used stand by time Δ_{SF}^1 due to fact that during the cold water sharing the initial time lag is partially compensated. With this sub-optimal periodic schedule, the non-conflicting operation of the plant is illustrated in Figures 3.11 A-F.

The same approach can be followed with different time lags of BR_2 in the feasible "cold water sharing interval" of Figure 3.9. It is found that the plant can operate periodically in all the domain by adding appropriate stand by times. The results are summarized in Figure 3.12. As it can be seen the minimum of the resulting graph corresponds to the time lag of $2.37 \ [h]$ where the stand by times are zero and the period is minimal: $T_p^{opt} = 4.74 \ [h]$.
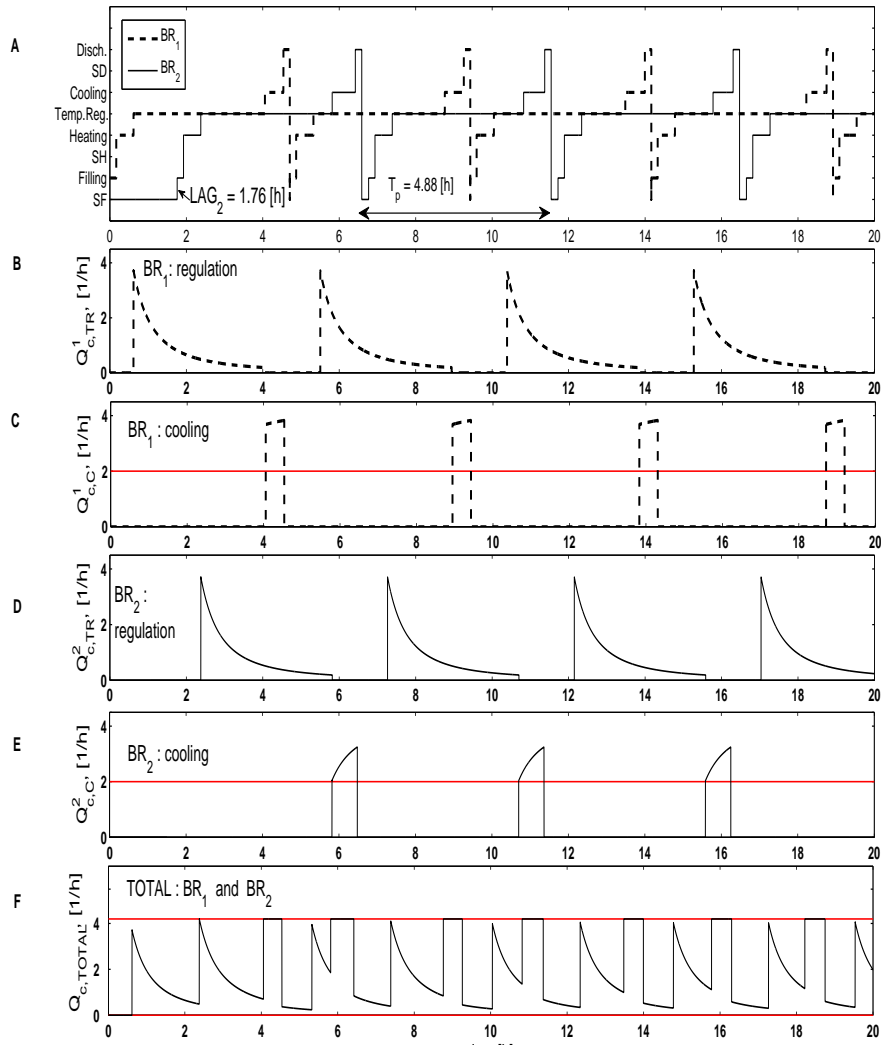
Fig. 3.11: CASE 2: A periodic solution with non-zero stand by times

3.4 CASE 3: Two batch reactors and the storage tank

In the analysis of CASE 2 we have considered a plant with two reactors but we have ignored the presence of the storage tank (or equivalently we have assumed that the capacity of the storage tank is not a limi-
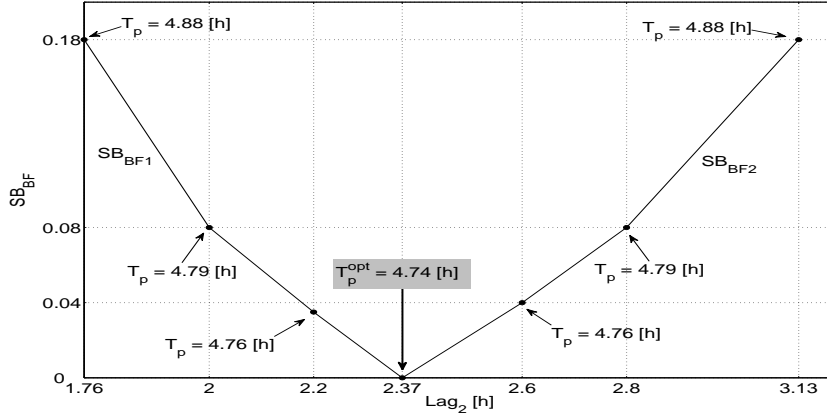
Fig. 3.12: CASE 2: Minimal stand by times for sub-optimal periodic solutions

tation).

In this section we shall discuss the behaviour of the full plant with the two reactors and the storage tank. Consider the plant operating under the optimal schedule given in Figure 3.10. Let us now assume that the capacity of the storage tank is also a resource limitation. From the optimal scheduling chart (Figure 3.10 A) it is seen that both reactors are **not** discharged at the same time. Consequently we can set the tank maximal capacity to $U_{max} = 35 \ [m^3]$, with $U_{max} \geq (V_{max} - V_{min})$ and the minimal capacity to zero, $U_{min} = 0 \ [m^3]$.

In order to have a periodic operation of the tank the constant output flow rate w is taken equal to the mean value of total input flow rate, $F(t) = F_{disch}^1 + F_{disch}^2$. Consequently based on the input flow rate profile given in Figure 3.13 we have that $w = F^m = 11.39 \ [m^3/h]$. This flow rate is applied as soon as BR_1 starts discharging in the tank.

Note that initially the tank is not empty but for safety reasons there is some product in it, $U_0 > 0 \ [m^3]$. Naturally to avoid overfilling of the tank from the very beginning U_0 must be smaller than $(U_{max} - (V_{max} - V_{min}))$. Here we have chosen, $U_0 = 5 \ [m^3]$.

As seen in Figure 3.14 the tank volume profile is periodic as soon as the discharging starts. But this periodic behaviour is obviously not robust at all. First, it is obvious that if the tank output flow rate is smaller or bigger than the optimal one the tank can be under- or overfed.
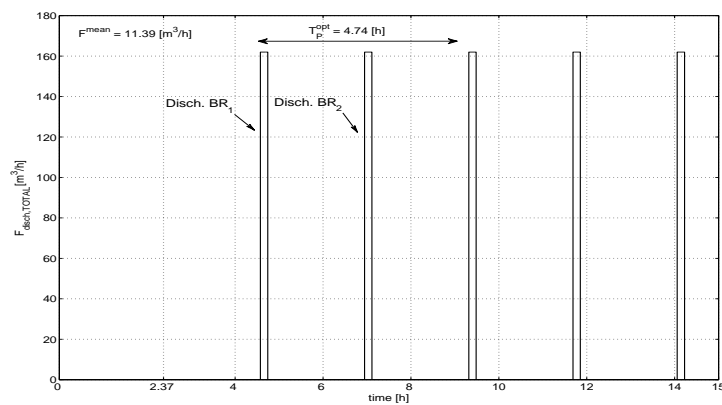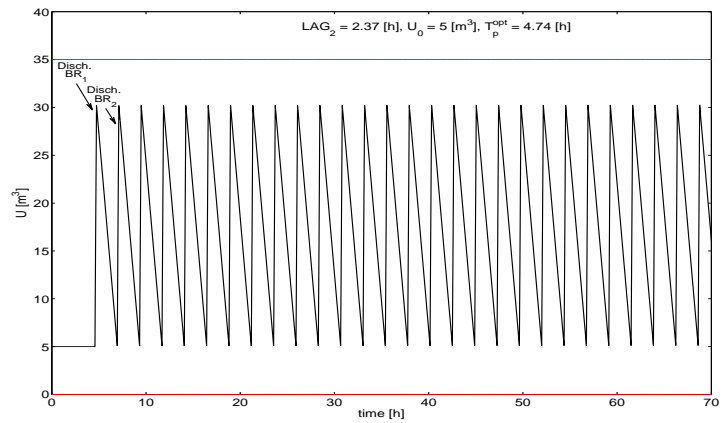

Fig. 3.13: CASE 3: Input flow rate of the tank
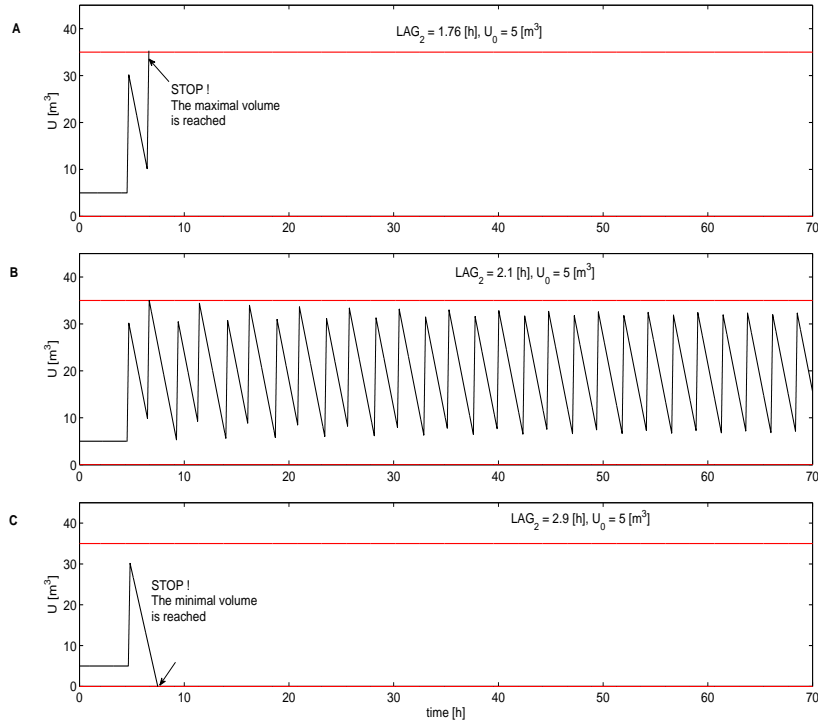

Fig. 3.14: CASE 3: Tank volume profile

Fig. 3.15: CASE 3: Volume profile under different time lags of BR_2

Moreover the behaviour is also sensitive to the value of the time lag between the two reactors as we shall now illustrate it. Let us apply the optimal output flow rate $w = 11.39\ [m^3/h]$ to the case when the second reactor starts working with a time lag of 1.76 $[h]$ and zero stand by times (Figure 3.7 A). It is seen in Figure 3.15 A, that at $time \approx 9\ [h]$ the maximal volume constraints are reached and the plant is blocked. On the other hand if the time lag of BR_2 is 2.1 $[h]$ it is seen that after some time the tank volume profile converges to a periodic profile which is however different from the optimal one (Figure 3.15, B). Referring to Figures 3.15 C it is seen that when the time lag of BR_2 is equal to 2.9 $[h]$ the minimal volume constraints are reached at $time \approx 8\ [h]$. This shows the complexity of the scheduling optimization problem and the need of an efficient algorithm for controlling the tank volume even in the case when there are no disturbances. This control issue will be addressed in Chapter 6.

3.5 Conclusions

In this Chapter we have shown the use of the plant simulator for optimal scheduling of a simple two reactors-storage tank plant. The simulation results for three case studies are presented and discussed. The aim of the case-studies is to give an idea of the complexity of the scheduling problem for productivity maximization in presence of resource limitations and capacity constraints of the tank. Moreover the need of an efficient algorithm for control of the tank volume even in the case when there are no disturbances is shown.

Chapter 4

Stability analysis of the hybrid plant limit cycle

This Chapter is concerned with the stability analysis of the limit cycle corresponding to the optimally scheduled plant operation. It uses the extension of trajectory sensitivity analysis presented in [His00] and [His05] to obtain the characteristic multipliers of nonsmooth limit cycles. The limit cycle is stable if its characteristic multipliers belong to the unit circle in the complex plane.

The hybrid system considered in this chapter is more complicated than the examples presented in the literature and consequently all computations are made numerically through the simulator.

4.1 Introduction

In Chapter 3 it was shown, through the simulations, that if BR_2 starts its operation with an initial time lag in the interval $[1.76 \quad 3.13]$ $[h]$, the overall plant behaviour always converges to the same periodic trajectory which appears to be an **attracting limit cycle**. Here we con-

sider the optimally scheduled plant operation, namely when BR_2 is initialized exactly on the limit cycle (see Figure 3.10). We shall make a stability analysis of this periodic trajectory, using the trajectory sensitivity, to prove analytically that it is really an **attracting limit cycle**.

The trajectory sensitivity is concerned with linearizing the system trajectory around a nominal trajectory, rather than an equilibrium point. It characterizes the influence of the parameters and/or the initial conditions on the dynamic behaviour of the system. The sensitivity of the system flow is defined through the sensitivity transition matrix. As shown in [His00] for a hybrid system with a single event, this matrix is composed of two terms describing the sensitivity evolution away from the switching event and at the event, respectively. A subsequent extension to a set of events is given in [His05]. The developed method is illustrated using a two tank system and power systems in [His05] and [His01] [His02], respectively. Actually the simple linear two tank system which illustrates the existence of a limit cycle in hybrid systems was initially given in [RLP98]. Its stability analysis is also discussed in [Gir03] where the main contribution lies in the computations of the limit cycle as well as in [RL00] by using discrete time Lyapunov techniques.

The stability analysis is done by using Poincaré maps [Kha96]. The Poincaré map samples the flow of a periodic system each period and its concept is shown in Figure 4.1.

Here x is a continuous state; Γ is a T_p-periodic limit cycle; $\phi(x)$ is the flow of x; Σ is a hyperplane transversal to Γ. The Poincaré map $P : \Sigma \to \Sigma$ is defined as the system flow after one cycle T_p i.e. $P(x_0) := \phi_{T_p}(x_0)$. Actually a limit cycle corresponds to a fixed point of a Poincaré map. A fixed point is defined as:

$$x_{i,i+1} = P(x_{i,i+1}) := \phi_{T_p}(x_{i,i+1})$$

meaning that a trajectory starting from $x_{i,i+1}$ will cross again Σ at $x_{i,i+1}$ after the period T_p. The stability of the Poincaré map at the fixed point $x_{i,i+1}$ is determined by linearizing P at the fixed point $x_{i,i+1}$ and studying its differential, $DP_{i,i+1}(T_p)$. It was show in [PC89] that:
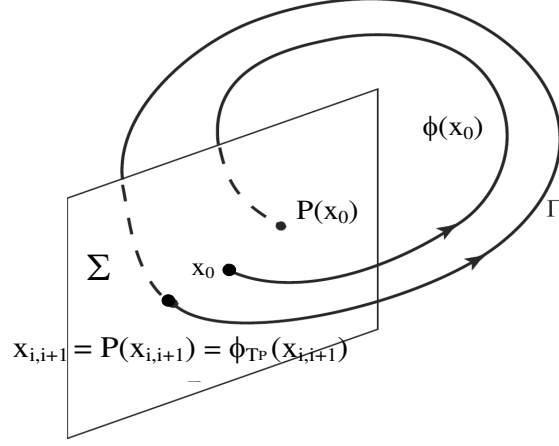
Fig. 4.1: Poincaré map - Hybrid trajectory sensitivity

$$DP_{i,i+1}(T_p) = \left(I - \frac{f_{i+1}(x_{i,i+1})\nabla g_{i,i+1}^t}{f_{i+1}^t(x_{i,i+1})\nabla g_{i,i+1}} \right)\Phi_{i,i+1}(T_p)$$
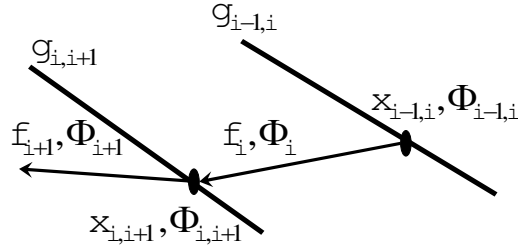
Fig. 4.2: $g_{i-1,i}$ switching plan, $x_{i-1,i}$ fixed point, f_i phases dynamics

Let us consider this expression from the hybrid systems viewpoint and refer to Figure 4.2. As stated in [His01] the eigenvalues are independent of the cross-section Σ and therefore for the hybrid system the section is usually chosen as the triggering hyper surface (or in other terms as the switching condition), $g_{i,i+1}$ corresponding to a switching from one phase to another along the periodic solution.

i. The matrix $\Phi_{i,i+1}(T_p)$ is the sensitivity transition matrix (or the **Monodromy matrix** [His01] [PC89]) after one period T_p of the limit cycle i.e. starting at the point $x_{i,i+1}$ which is laying on the switching surface and coming back in $x_{i,i+1}$. For hybrid systems the switching point can be considered as a fixed point. The two terms of the matrix are computed as follows:

a) **Away from the events:** During the phase i the system dynamics is governed by the equation $\dot{x} = f_i(x, u)$ with a solution $x_i(t)$. The trajectory sensitivity matrix, Φ_i is simply given by the solution of the equation:

$$\dot{\Phi}_i = Df_i(t)\Phi_i, \quad \Phi(t_i) = I$$

in the time interval $[t_i \ \ t_{i+1}]$ when the phase i is active and this time interval defines the so called duty time, Δ_i of the phase i; $Df_i(t) = \frac{\partial f_i(x)}{\partial x}$ is the gradient of f_i with respect to x over $\Re^n$ computed along the trajectory $x_i(t)$ and I is the $n \times n$ identity matrix.

b) **At events:** The trajectory sensitivity matrix at the transition from phase i to phase $i + 1$ is given by:

$$\Phi_{i,i+1} =$$
$$Dh_{i,i+1} + \left(f_{i+1}(x_{i,i+1}) - Dh_{i,i+1}f_i(x_{i,i+1}) \right) \frac{\nabla^t g_{i,i+1}}{\nabla^t g_{i,i+1}f_i(x_{i,i+1})}$$

note that it is assumed that the dynamics f_i crosses the hyper plane $g_{i,i+1}$ transversally i.e. $\nabla^t g_{i,i+1}f_i(x_{i,i+1}) \neq 0$; $f_i(x_{i,i+1})$ is the value of the continuous dynamics of the system during the phase i calculated at the point $x_{i,i+1}$; $Dh_{i,i+1} = \frac{\partial h_{i,i+1}(x)}{\partial x}$ is the gradient of the reset map, $h_{i,i+1}(x)$ of the discrete transition from phase i to phase $i + 1$ with respect to x. Here we restrict ourselves to two specific situations:

- $h_{i,i+1}(x) = x$ i.e. there is no state reset of initial conditions during the transition and in this case $Dh_{i,i+1} = I$;

- or there is a reset to an a-priori fixed value $\bar{x}$ when the system enters the new phase $i+1$ **independently** of the final value of the state in the previous phase i.e. $h_{i,i+1}(x) = 0$ and in this case $Dh_{i,i+1} = 0$.

  The Monodromy matrix after one period T_p of the limit cycle i.e. starting, for instance, at the fixed point x_{12} and coming back in x_{12} is:

$$\Phi_{12}(T_p) = \Phi_{N1}\Phi_N \ ... \ \Phi_{12}\Phi_1$$

ii. $f_{i+1}(x_{i,i+1})$ is the value of the continuous dynamics of the system during the phase $i+1$ calculated at the point $x_{i,i+1}$; $\nabla g_{i,i+1}$ is the gradient of the switching plane $g_{i,i+1}$ with respect to x; the plane $g_{i,i+1}$ is **transversal** to f_{i+1} i.e. $f_{i+1}^t(x_{i,i+1})\nabla g_{i,i+1} \neq 0$. Note that the last condition is **not** satisfied if after the switching occurs the system trajectory remains on the switching plane i.e. it is longitudinal to the plane. Such a hybrid system is called not unique in reverse time [His05]. In this case in order to perform a stability analysis we just have **not** to choose a switching point $\tilde{x}_{i,i+1}$ corresponding to this transition as a fixed point, otherwise $f_{i+1}^t(\tilde{x}_{i,i+1})\nabla g_{i,i+1} = 0$. For a specific example, refer to Section 4.2.

The periodic solution is stable if all the eigenvalues of $DP_{i,i+1}(T_p)$ (called also characteristic multipliers) are inside the unit circle of the complex plane.

4.2 Example: CASE 2

Referring to the above method description it is evident that in order to perform the stability analysis of the hybrid limit cycle of CASE 2, we have to determine the switching planes and their corresponding gradients; the switching points as well as the duty times that are needed for the computation of the sensitivity matrix away from the events. Note that due to the system non-linearity all the computations are based on numerical simulations performed on the plant simulator.

i. **The system:** Consider the plant operating under the optimal schedule discovered by the simulator. Due to the fact that the cold

water flow rate of BR_i during the cooling phase is a function of the cold water of BR_j during the reaction phase, the reactor state variables are interconnected. The joint dynamic profiles of the two vessels is given in Figure (4.3). It is seen that the combined model passes through ten successive phases. For instance during phase one: BR_1 is discharging and BR_2 is in regulation. The resulting joint HAM is given in Figure (4.4).
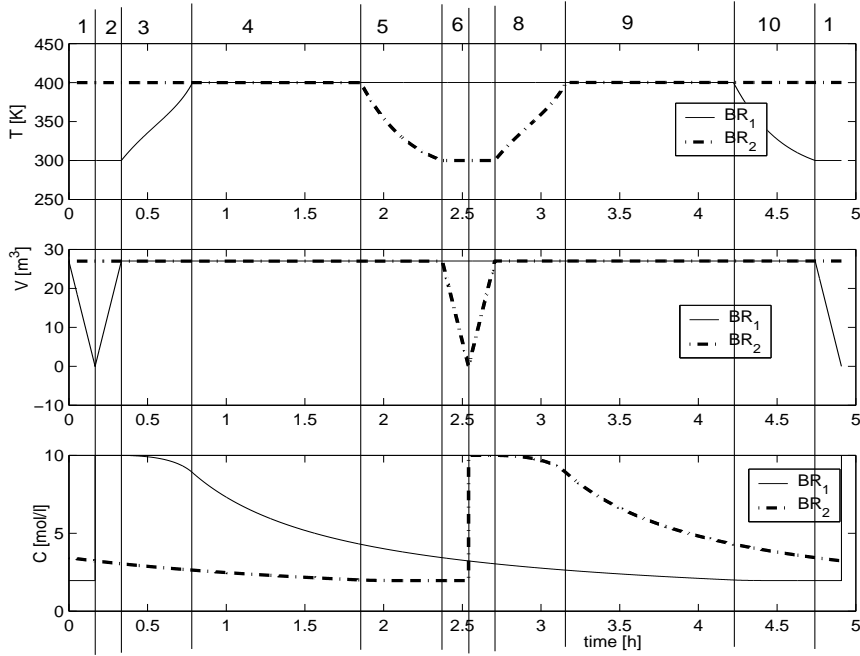

Fig. 4.3: Combined dynamics of both reactors

ii. **Define the combined automaton:** It is seen that the hybrid system has the form: $\dot{x} = f_i(x, u)$, where $i \in \{1, ..., 10\}$. Here: $x = [V_1 \ T_1 \ C_1 \ V_2 \ C_2 \ T_2]^t \in \Re^6$. For instance during the phase 5 namely when BR_1 is in regulation and BR_2 is cooling phase the joint dynamics, f_5 are:
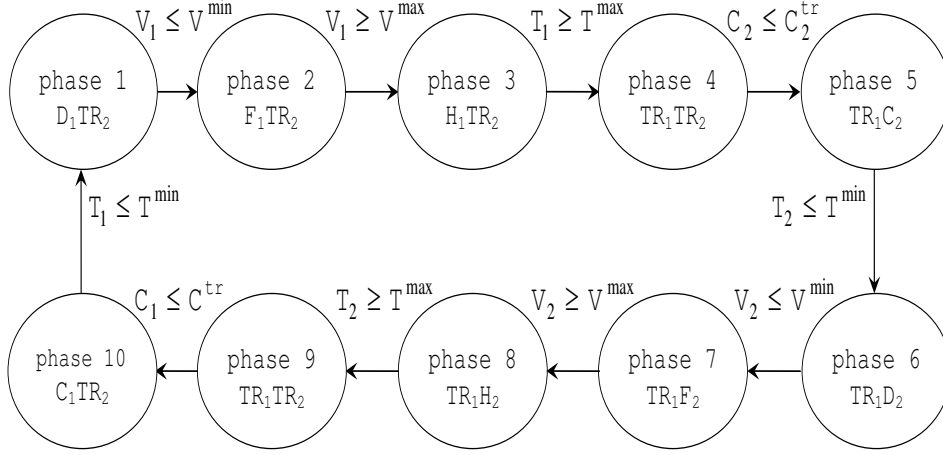
Fig. 4.4: Combined automaton for both reactors

$$\dot{V}_1 = 0$$

$$\dot{T}_1 = 0$$

$$\dot{C}_1 = -2\,k_0\,e^{-\frac{E}{RT^{max}}}\,C_1^2$$

$$\dot{V}_2 = 0$$

$$\dot{T}_2 = -\delta\,k_0\,e^{-\frac{E}{RT_2}}\,C_2^2 + \underbrace{\left(Q^{max} - \frac{\delta k_0 C_1^2 e^{-\frac{E}{RT^{max}}}}{(T_c - T^{max})}\right)(T_c - T_2)}_{Q_c^2(t)}$$

$$\dot{C}_2 = -2\,k_0\,e^{-\frac{E}{RT_2}}\,C_2^2$$

Referring to equation 5 i.e. $\dot{T}_2 = f(C_1, T_2, C_2)$ it is clearly seen that the dynamics of BR_2 depends on the one of BR_1.

iii. **Determine the switching planes:** The transition condition between the phases in terms of switching planes are summarized in Table 4.1.

iv. **Find the fixed points and the duty times:** The fixed points can be determined from the volume, temperature and concentration

phases	condition	switching plane
1 to 2	$V_1 \leq V_1^{min}$	$g_{12} : [1\ 0\ 0\ 0\ 0\ 0]x - V^{min} = 0$
2 to 3	$V_1 \geq V^{max}$	$g_{12} : [1\ 0\ 0\ 0\ 0\ 0]x - V^{max} = 0$
3 to 4	$T_1 \geq T^{max}$	$g_{34} : [0\ 1\ 0\ 0\ 0\ 0]x - T_{max} = 0$
4 to 5	$C_2 \leq C^{tr}$	$g_{45} : [0\ 0\ 0\ 0\ 0\ 1]x - C^{tr} = 0$
5 to 6	$T_2 \leq T^{min}$	$g_{56} : [0\ 1\ 0\ 0\ 0\ 0]x - T^{min} = 0$
6 to 7	$V_2 \leq V^{min}$	$g_{67} : [0\ 0\ 0\ 1\ 0\ 0]x - V^{min} = 0$
7 to 8	$V_2 \geq V^{max}$	$g_{78} : [0\ 0\ 0\ 1\ 0\ 0]x - V^{max} = 0$
8 to 9	$T_2 \geq T^{max}$	$g_{89} : [0\ 0\ 0\ 0\ 1\ 0]x - T^{max} = 0$
9 to 10	$C_1 \leq C^{tr}$	$g_{910} : [0\ 0\ 1\ 0\ 0\ 0]x - C^{tr} = 0$
10 to 1	$T_1 \leq T^{min}$	$g_{101} : [0\ 1\ 0\ 0\ 0\ 0]x - T^{min} = 0$

Table 4.1: Switching plans

phases	switching point	duty time, Δ_i [h]
1 to 2	$x_{12} = [27\ 300\ 1.95\ 27\ 400\ 3.43]^t$	0.16
2 to 3	$x_{23} = [0\ 300\ 1.95\ 27\ 400\ 3.22]^t$	0.16
3 to 4	$x_{34} = [27\ 300\ 10\ 27\ 400\ 3.04]^t$	0.45
4 to 5	$x_{45} = [27\ 400\ 8.88\ 27\ 400\ 2.63]^t$	1.06
5 to 6	$x_{56} = [27\ 400\ 4.29\ 27\ 400\ 2]^t$	0.51
6 to 7	$x_{67} = [27\ 400\ 3.43\ 27\ 300\ 1.95]^t$	0.16
7 to 8	$x_{78} = [27\ 400\ 3.22\ 0\ 300\ 1.95]^t$	1.95
8 to 9	$x_{89} = [27\ 400\ 3.04\ 27\ 300\ 10]^t$	0.45
9 to 10	$x_{910} = [27\ 400\ 2.63\ 27\ 400\ 8.88]^t$	1.06
10 to 1	$x_{101} = [27\ 400\ 2\ 27\ 400\ 4.29]^t$	0.51

Table 4.2: Switching points and duty times

profiles given in Figure (4.3) as well as the duty times. All the numerical values are given in Table 4.2.

Let us now apply the above described method. The switching hyper plane g_{12} (Table 4.1) is chosen for defining a Poincaré map and its corresponding normal vector is $\nabla g_{12} = [1\ 0\ 0\ 0\ 0\ 0]^t$. Consider the point x_{12} on g_{12} (Table 4.2). Note that in this system $f_3^t \nabla g_{23} = 0$, $f_4^t \nabla g_{34} = 0$, $f_6^t \nabla g_{56} = 0$, $f_8^t \nabla g_{78} = 0$, $f_9^t \nabla g_{89} = 0$ and $f_1^t \nabla g_{101} = 0$ because the reactors trajectory after the switch remains on the corresponding switching plane. For instance $f_4^t \nabla g_{34} = 0$ corresponds to the phase when both reactors are in regulation. Consequently because each of these terms can be in the denominator of the differential of the Poincaré map it is not convenient to compute the differential with respect to none of them. Based on our choice:

i. **The Monodromy matrix** after one cycle, $T_p = 4.74$ [h] starting from the phase 2 and coming back to it, $\Phi_{12}(T_p) = \Phi_{12}\Phi_1 ... \Phi_3\Phi_{23}\Phi_2$:

$$\Phi_{12}(T_p) =$$

$$
\begin{bmatrix}
0.9190 & 0.5890 & -9.1350 & -0.0870 & -0.0330 & -10.9660 \\
0.0 & 0.0 & 0.0 & 0.0 & 0.0 & 0.0 \\
0.0 & 0.0 & 0.0010 & 0.0 & 0.0 & -0.0070 \\
0.0 & 0.0 & 0.0 & 0.0 & 0.0 & 0.0 \\
0.0 & 0.0 & 0.0 & 0.0 & 0.0 & 0.0 \\
-0.0010 & 0.0 & 0.0060 & 0.0070 & 0.0030 & 0.9130
\end{bmatrix}
$$

having eigenvalues:

$$eig_{\Phi_{12}(T_p)} = \begin{bmatrix} 1.0204\ 0.8116\ 0.0010\ 0.0\ 0.0\ 0.0 \end{bmatrix}^t$$

Note that according to the reactors dynamics during the transition between the phases 1 and 2 as well as the phases 6 and 7 the concentration is reset from C^{tr} to a new value C_{in} and as a result the corresponding partial derivatives in the matrix Dh_{12} and Dh_{67}, respectively are zero. During the other transitions there is no state reset of the initial conditions and $Dh_{i,i+1} = I$.

ii. Finally the corresponding differential of the Poincaré map, $DP_{12}(T_p) = \left(I - \frac{f_2(x_{12})\nabla g_{12}^t}{f_2^t(x_{12})\nabla g_{12}}\right)\Phi_{12}(T_p)$
with $f_2(x_{12}) = \begin{bmatrix} 162.0\ 0.0\ 0.0\ 0.0\ 0.0\ -1.172 \end{bmatrix}^t$ is:

$$DP_{12}(T_p) =$$

$$
\begin{bmatrix}
0.0 & 0.0 & 0.0 & 0.0 & 0.0 & 0.0 \\
0.0 & 0.0 & 0.0 & 0.0 & 0.0 & 0.0 \\
0.0 & 0.0 & 0.0010 & 0.0 & 0.0 & -0.0070 \\
0.0 & 0.0 & 0.0 & 0.0 & 0.0 & 0.0 \\
0.0 & 0.0 & 0.0 & 0.0 & 0.0 & 0.0 \\
0.0060 & 0.0040 & -0.0600 & 0.0060 & 0.0030 & 0.8340
\end{bmatrix}
$$

having eigenvalues:

$$eig_{DP_{12}} = \begin{bmatrix} 0.0005 \ 0.8345 \ 0.0 \ 0.0 \ 0.0 \ 0.0 \end{bmatrix}^t$$

They are in the complex unit circle meaning that the hybrid limit cycle of the two-reactors system is attracting.

From the practical viewpoint the fact that the hybrid limit cycle is stable means that if the second reactor is started in the numerically found interval [1.76 3.13] [h], the plant operation will always converge to the optimally scheduled operation.

4.3 Conclusions

In this Chapter we have presented a method based on the hybrid trajectory sensitivity analysis for the stability analysis of the hybrid limit cycle corresponding to the optimally scheduled plant operation. The obtained analytical results correspond to the simulation observations, given in Chapter 3, Section 3.3 i.e. the plant hybrid limit cycle is attracting. However as shall be seen in the next Chapter due to disturbances in the plant parameters (e.g. the hot steam transfer rate) the periodic hybrid trajectory may be affected: it can either converge to a new sub-optimal schedule or a conflict for the resources arises. Consequently an algorithm based on the model predictive control is proposed to prevent the plant from a shut-down.

Chapter 5

On the optimal periodic scheduling of the hybrid chemical plant

The purpose of this Chapter is:

i. *to formulate the optimal scheduling of the hybrid chemical plant as an optimal control problem;*

ii. *to present the assumptions and simplifications added in three algorithms yielding suboptimal solutions of the problem namely: a continuous time periodic mixed integer linear programming (MILP) [PW07]; an hybrid model predictive control (HMPC) [RSdP06] and a time discrete event control [GGR06];*

iii. *to apply the obtained $MILP$ suboptimal solution on the plant simulator developed in Section 2.2 and to compare it with the solution of the optimal control problem given in Sections 3.3 and 3.4.*

5.1 Optimal periodic scheduling of the hybrid chemical plant formulated as an optimal control problem

We consider an hybrid chemical plant with N parallel batch reactors, a storage tank and limited shared resources, represented by an hybrid automaton model as described in Chapter 2.

As we have illustrated with the simulations in Sections 3.3 and 3.4, the objective is to find a periodic schedule which maximizes the plant productivity. Maximizing the productivity means that the product outflow rate wP must be constant and as large as possible. We consider the special case where the HAM of all batch reactors are identical and governed by the same transition guards. In such a case, it is clear that the product concentration P in the storage tank is a constant parameter independent of the plant schedule. Hence maximizing wP is equivalent to maximizing w. Note that the scheduling (production) period, T_p is reciprocal to the plant output flow rate w that is $T_p = \frac{N(V^{max}-V^{min})}{w}$. In this section, we shall formulate this problem as a general optimal control problem.

As we have just mentioned, the objective is simply stated as:

$$\text{Max } w.$$

The maximization must be performed with respect to the following decision variables

i. the continuous input functions of the continuous-time dynamics $F_{in}^i(t)$, $Q_h^i(t)$, $Q_c^i(t)$, $F_{disch}^i(t)$, $(i = 1, \ldots, N)$, $(0 \leqslant t \leqslant T_p)$;

ii. the discrete inputs which are the stand-by times Δ_{SF}^i, Δ_{SH}^i, Δ_{SD}^i, $(i = 1, \ldots, N)$.

Obviously the optimization must be performed **under the constraint of the hybrid dynamics** as they have been defined in Chapter 2. In addition, the maximization problem is also subject to a set of equality and inequality constraints which essentially express that the resource limitations must not be exceeded and that the continuous and discrete inputs are positive quantities. Moreover there are capacity constraints

on the buffer tank.

Limitations on the resources flow and transfer rates

Equality constraints As it was defined previously, when a reactor i is not in the *filling or discharging* phases there is no inflow or outflow of material and the values of the input variables $F_{in}^i(t)$ or $F_{disch}^i(t)$ are zero. This is expressed, as follows:

$$F_{in}^i(t) = 0 \ \text{ if } \ \sigma^i(t) \neq F$$

$$F_{disch}^i(t) = 0 \ \text{ if } \ \sigma^i(t) \neq D$$

The same is valid for the *transfer rate of the hot steam* which is zero if the reactor is not in the *phase heating* and for the *transfer rate of the cold water* which is zero if the reactor is not in the phases *reaction or cooling*, respectively. This is defined in the following way:

$$Q_h^i(t) = 0 \ \text{ if } \ \sigma^i(t) \neq H$$

$$Q_c^i(t) = 0 \ \text{ if } \ \sigma^i(t) \neq (C \ \text{ or } \ TR)$$

Moreover, during the *temperature regulation phase*, the reactor must use a specific quantity of cold water in order to compensate the exothermic heat of the reaction. This quantity is defined through the following equation:

$$Q_c^i(t) = \frac{\delta k(T^{max})r(C)}{(T_c - T^{max})} \ \text{ if } \ \sigma^i(t) = TR$$

In case of a simple second order exothermic reaction the required cold water profile is given in Figure (3.2).

Inequality constraints In addition to equality constraints, there are also inequality constraints on the plant input variables that are

stated as follows.

The various flow rates must be larger than zero during the corresponding phases, namely:

$$0 < F^i_{in}(t) \ \ \text{if} \ \ \sigma^i(t) = F$$

$$0 < F^i_{disch}(t) \leq F^{max}_{disch} \ \ \text{if} \ \ \sigma^i(t) = D$$

$$0 < Q^i_h(t) \ \ \text{if} \ \ \sigma^i(t) = H$$

$$Q^{min}_c \leq Q^i_c(t) \ \ \text{if} \ \ \sigma^i(t) = C$$

where F^{max}_{disch} is the maximal allowed outflow rate of product during the *discharging phase* and Q^{min}_c is the required minimal cooling water rate in order to have a sufficiently fast cooling during the *cooling phase*. The inequality constraints are also used to express the limitation on the resources sharing. For the input flow rate of raw material this is defined in the following way:

$$\sum_{i=1}^{N} F^i_{in}(t) \leq F^{max}_{in}$$

where F^{max}_{in} is the maximal allowed inflow rate of raw material during the *filling phase*. The inequality constraints are also used to define the limitation on the sharing of the hot steam and cold water transfer rates.

$$\sum_{i=1}^{N} Q^i_h(t) \leq Q^{max}_h$$

$$\sum_{i=1}^{N} Q^i_c(t) \leq Q^{max}_c$$

where Q^{max}_h is the maximal allowed transfer rate of hot steam during the *heating phase* and finally Q^{max}_c is the maximal allowed transfer rate of cold water for the *temperature regulation and cooling phases*.

The optimization problem is also constrained by the capacity constraints of the storage facility defined hereafter.

Capacity of the storage facility

Inequality constraints It is assumed that the volume of the storage facility, U $[m^3]$ is limited between some minimal U^{min} and maximal U^{max} level of the product in it. This constraint is expressed as follows:

$$U^{min} \leq U(t) \leq U^{max}$$

Periodicity of the plant operation

Equality constraint In addition, it is required that the resources flow rates must be periodic with a period, T_p $[h]$, namely:

$$F_{in}^i(t) = F_{in}^i(t + T_p)$$

$$Q_h^i(t) = Q_h^i(t + T_p)$$

$$Q_c^i(t) = Q_c^i(t + T_p)$$

$$F_{disch}^i(t) = F_{disch}^i(t + T_p)$$

Respectively the discrete inputs namely, the stand by times before: filling, heating and discharging of the reactor process shall also be periodic.

For the benchmark simulator with two batch reactors described in Chapter 3, we have intuitively discovered the solution of this optimal control problem. This solution was presented in Sections 3.3 and 3.4. But for more general plants with a large number of batch reactors, the optimal control problem described above is clearly a nonlinear optimization problem which is complicated. It is probably hopeless to try to design computer algorithms able to exactly solve this problem with a reasonable computational burden and within a reasonable time. Efforts have therefore been recently made to state tractable algorithms yielding suboptimal solutions obtained under additional simplifying assumptions. Three of these methods based on references [PW07], [RSdP06] and [GGR06] are briefly reviewed in the next sections.

5.2 Suboptimal continuous time periodic *MILP* scheduling solution

The first method is based on a mixed integer linear programming (MILP) [PW07], [War07], i.e. on the optimization of a mixed integer program defined by linear constraints and both continuous and discrete variables.

In the continuous time *MILP* formulation two main notions are used: the "event" and the "time slot" (Figure 5.1):
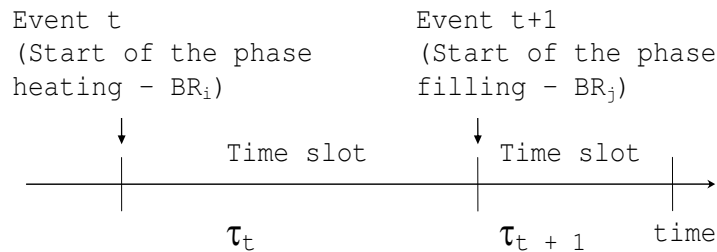
```
Event t                      Event t+1
(Start of the phase          (Start of the phase
heating - BRᵢ)               filling - BRⱼ)
```


Fig. 5.1

- An *Event* is defined as the beginning or the end of a phase of a batch reactor process. For instance: *Event t* denotes the start of the phase heating on one reactor, while *Event t + 1* denotes the start of the phase filling on another reactor.

- A *Time slot* is the time between two events.

The events and time slots are fixed and finite and are numbered from 1 up to T where T is a parameter of the scheduling formulation. The decomposition of time is the same for both reactors and for the tank. Because the schedule is cyclic, the event occurring at the end of time slot T coincides with the event occurring at the beginning of time slot 1 and is numbered as event 1 [PW07].

5.2.1 Assumptions and simplifications for the MILP approach

In the MILP approach of [PW07], [War07] the following assumptions and simplifications are considered.

i. During the filling phases, the input flow rates F_{in}^i are constant and set at their maximal values : $F_{in}^i(t) = F_{in}^{max}$ when $\sigma^i(t) = F$.

ii. During the heating phases, the heating flow rates Q_h^i are constant and set at their maximal values: $Q_h^i(t) = Q_h^{max}$ when $\sigma^i(t) = H$.

iii. During the cooling phases, the cooling flow rates Q_c^i are constant and set at their minimal values : $Q_c^i(t) = Q_c^{min}$ when $\sigma^i(t) = C$.

iv. During the discharging phases, the discharging flow rates F_{disch}^i are constant and set at their maximal values : $F_{disch}^i(t) = F_{disch}^{max}$ when $\sigma^i(t) = D$.

v. The cooling profile is approximated by a piecewise constant function as shown in Figure 5.2. This implies that the reaction phase is decomposed and replaced by a set of successive partial reaction phases (four in the benchmark simulator case) with decreasing values of the cooling flow rate denoted $Q_{cr,k}^i$ for the k_{th} phase during the reaction in the i_{th} reactor. Moreover as seen in Figure 5.2 the approximation is based on an over evaluation of the available cooling water rate which is needed in order to avoid resource shortage. Note that a finer decomposition of the reaction phase will lead to more a precise approximation but will decrease the feasibility of the formulation by increasing the computation time.

vi. The product outflow rate w is allowed to be time-varying inside a specified interval : $w^{min} \leq w(t) \leq w^{max}$.

Some consequences of these assumptions are :

i. The most important consequence of these assumptions is that each phase of the plant has now a fixed processing duration (Table 5.1) which can be computed in advance with the plant simulator. This means that the optimal scheduling problem is no longer under the
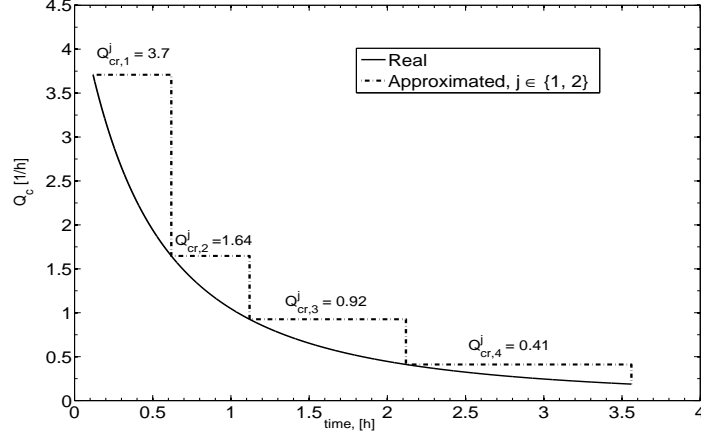
Fig. 5.2: Approximated and real cooling water rate

constraint of the hybrid plant dynamics which can just be replaced by the set of numbers corresponding to the phase processing times that are supposed to be given in advance.

p_1	filling	0.166	$[h]$
p_2	heating	0.4522	$[h]$
p_3	reaction 1	0.5	$[h]$
p_4	reaction 2	0.5	$[h]$
p_5	reaction 3	1	$[h]$
p_6	reaction 4	1.4412	$[h]$
p_7	cooling	0.919	$[h]$
p_8	discharging	0.166	$[h]$

Table 5.1: Fixed processing duration used in MILP

ii. Another consequence is that the decision variables reduce now to the scheduling period T_p and the stand-by times Δ^i_{SF}, Δ^i_{SH}, Δ^i_{SD}. The continuous input functions $F^i_{in}(t)$, $Q^i_h(t)$, $Q^i_c(t)$, $F^i_{disch}(t)$ **are no longer decision variables for the optimization** but simply constant parameters *a priori* fixed by the user.

iii. A third consequence is that two or more filling or heating phases cannot be performed at the same time and

iv. only the reaction and cooling phases can be simultaneous to some extent.

v. Moreover due to the piecewise constant function approximation the available cooling water capacity may not be fully used.

vi. And finally the solution is obtained off line and does not consider the presence of disturbances.

The suboptimal periodic scheduling solution and the simulation results obtained from its application on the plant simulator are presented here. The scheduling solution is obtained through a *MOSEL* optimization software.

5.2.2 Simulation results

Consider again CASE 3 from Section 3.4. The periodic suboptimal scheduling solution found though the algorithm given in [PW07], [War07] is discussed as follows.

The maximized **average** productivity is found to be: $w^m = 10.49$ $[m^3/h]$. It can be noted that this is smaller than the optimal one $w = 11.39$ $[m^3/h]$ found in Section 5.4 through simulations (Figure 3.13).

The other decision variables, namely the stand by times are found to be zero similarly to the ones in Section 3.3.2.

It should be noted that the scheduling decision variables [PW07], [War07] are obtained in terms of *Time slots durations, Events indicators (0 or 1), Quantity of product in the tank* and can not be applied directly as inputs to the plant simulator. They are further transformed in terms of stand by times and a tank output flow rate.

On the other hand in the statement of the scheduling optimization problem it was defined that the output flow rate of the tank must

be constant. Knowing that the $MILP$ scheduled output flow rate, $w(t) = w(t + T_p)$ is not constant but periodic and varies in large bounds, one can take its maximized average value w^m and apply it on the simulator. However, the direct application of w^m instead of $w(t)$ can lead to infeasible operation of the tank meaning that its minimal and the maximal volume bounds can be exceeded. A possible procedure to cope with this problem is to reduce the variations as follows:
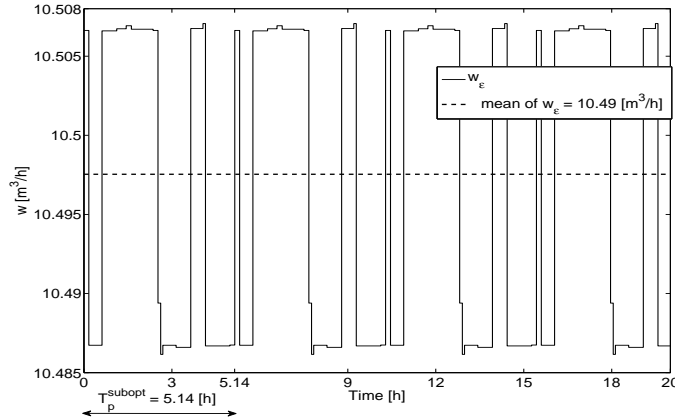

Fig. 5.3: Scheduled output flow rate of the storage tank with small variations

- Firstly, the maximal average plant productivity for the plant simulator example is found in $MOSEL$ [PW07] by setting up large bounds for $w^{min} = 4 \ [m^3/h]$ and $w^{max} = 18 \ [m^3/h]$.

- Then, the scheduling problem is solved again in $MOSEL$ by setting up small limits, $\epsilon = \pm 10^{-2}$ around w^m, i.e. $w^{min} = w^m - 10^{-2}$ and $w^{max} = w^m + 10^{-2}$. In this particular case it was found that $w^m_\epsilon = w^m = 10.49 \ [m^3/h]$, which means that even though the solution possibilities were restricted the optimum is found. Because the variations around w^m_ϵ (Figure 5.3) are very small its average value is applied to the simulator without risk of infeasible operation of the tank.

The obtained suboptimal schedule in terms of stand by times and averaged tank output flow rate is applied on the simulator and the simulation results are presented in Figures 5.4 and 5.5.
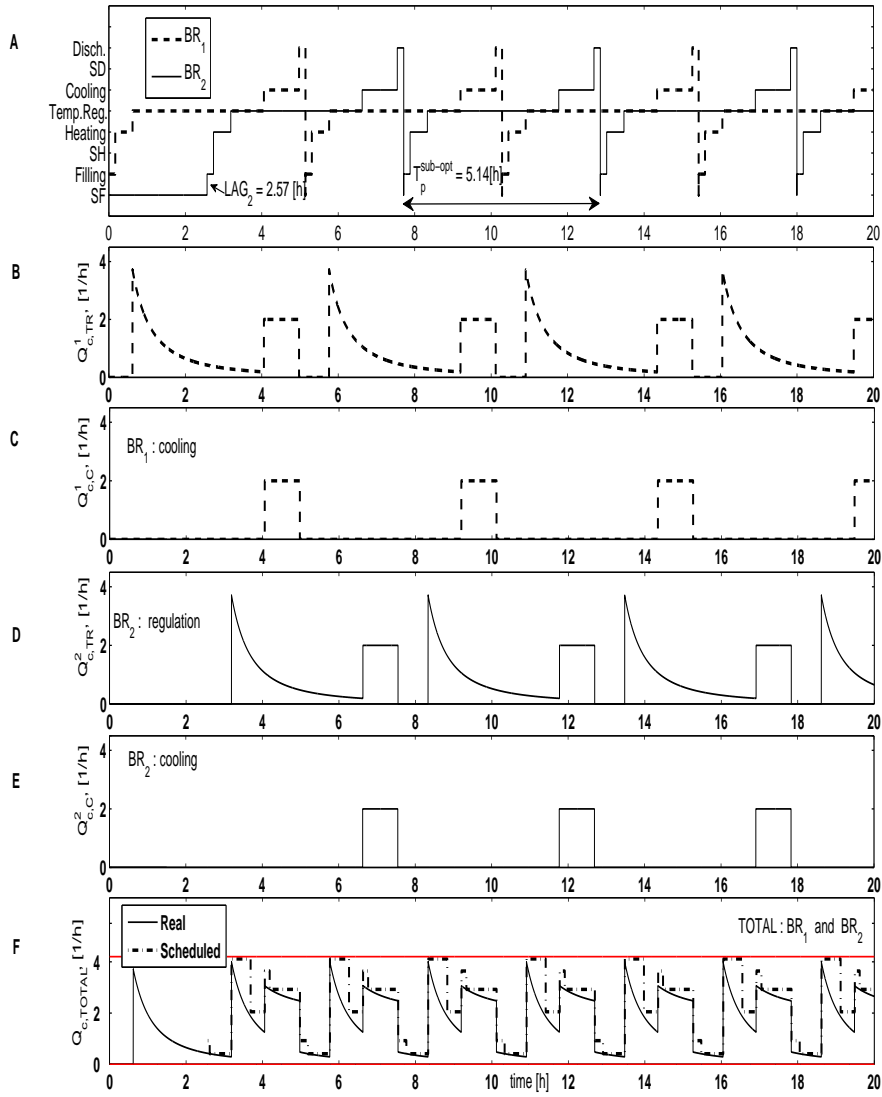

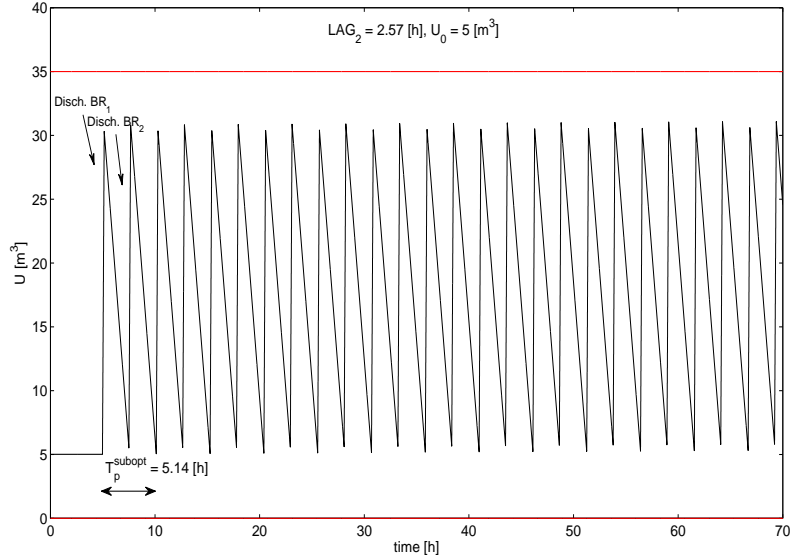Fig. 5.4: CASE 3: Suboptimal MILP periodic solution

Fig. 5.5: CASE 3: Suboptimal periodic volume profile

Scheduling

In Figure 5.4, A we give the chart of the plant schedule. As seen after the time lag of 2.57 $[h]$ the operation is periodic with zero-stand by times. The cycle length is $T_p^{subopt} = 5.14$ $[h]$. This period is suboptimal because it is larger than the optimal one, 4.74 $[h]$ (Figure 3.10 A) found in Chapter 3.

Cooling water sharing

The sub optimality comes also from the fact that the cold water used during the cooling phases is constant (Figure 5.4 C and E) which leads to under utilization of the available cooling water resources. For comparison in the optimal CASE 2 it is variable (see Figure 3.10 C and E). There is no conflict of cooling water sharing as seen in Figure 5.4, F. However it is observed that the total scheduled cooling water flow rate (given in dash-dotted line) has larger values than the really used one. This shows once again the sub optimality of the solution due to

the fact that its values are constant from one side and on the other hand they are bigger than the real ones, meaning the real available cooling water resource is not used effectively.

As seen in Figure 5.5, applying the flow rate $w^m = 10.49 \ [m^3/h]$ the tank volume profile (with initial volume of $U_0 = 5 \ [m^3]$) is periodic after the discharging of BR_1.

5.3 Other sub-optimal scheduling approaches

Within the framework of the European Excellence network HYCON, alternative approaches for designing schedules for our benchmark chemical plant have been discussed by other groups in [GGR07] and [RSdP06]. In this section, we report briefly on these contributions. In both contributions, as in the present thesis, the authors address the scheduling issue for cyclically operated plants with parallel reactors using common resources and a continuous output. In order to make the problem tractable, as above, several essential simplifications are introduced. These simplifications are however stronger than for the $MILP$ approach (see Section 5.2.1).

filling	0.166	$[h]$
heating	0.4522	$[h]$
reaction	3.441	$[h]$
cooling	0.919	$[h]$
discharging	0.166	$[h]$

Table 5.2: Fixed processing duration used in HMPC and TDEC

i. It is assumed that the successive phases have a fixed processing duration (known in advance) given in Table 5.2. The processing times are identical to those of Table 5.1 used in the $MILP$ approach. This will allow a quantitative comparison of the results. Remark however that here the reaction phase (with temperature regulation) is considered as being a single phase and is not decomposed in 4 subtasks as it was done for the $MILP$ case.

ii. The way of avoiding resource conflicts is very crude : it is imposed a priori that a limiting resource can never be used simultaneously by the two production lines. This means that any task which is resource consuming cannot occur at the same time on both reactors. This is a very restrictive condition which was not imposed in the $MILP$ approach since there it is allowed to have tasks simultaneously consuming the cooling water on both reactors.

iii. Last but not least, in order to further facilitate the problem, it is assumed that the cooling water is **not** a limiting resource for the temperature regulation during the reaction phase. This is a very critical assumption since the regulation phase is by far the longest phase of the cycle and since, as we have seen in the case-studies of Chapter 3, the main risk of resource conflict precisely arises when the reactions take place simultaneously in both reactors (or to a smaller extent when the reaction in one reactor is simultaneous to the cooling phase in the second reactor). By ignoring the constraint associated to the regulation phase, it is clear that the main difficulty in terms of conflicting resources is totally alleviated.

In [GGR07] the problem is formulated within a discrete event framework by modelling systems components as multirate timed automata. A periodic schedule is computed by using an off-line optimisation method with the goal of minimising the cycle duration while avoiding resource conflicts. With the data of Table 5.2 and under conditions i, ii, iii, it is clear that the $MILP$ optimal solution obtained in Section 4.2 is also an optimal solution of this timed discrete event (TDE) approach, i.e. with a productivity $w = 10.49$ [m³/h] and a cycle length T_p = 5.14 [h]. Unfortunately, condition iii also implies that many other equivalent solutions can be obtained, including unfeasible solutions that would give cold water conflicts when implemented on the simulator as soon as the limitation of cold water during the regulation phase is taken into account. It is the case for instance with the solution described by the Ganttchart in Figure 5.6. An additional interesting feature of this TDE approach is to incorporate easily in the problem some uncertainties regarding the durations of the process phases. Instead of assuming a given fixed time for each phase (Table 5.2), it is rather assumed that the duration of each phase lies inside some time interval (around the nominal values of Table 5.2). Then the scheduling

problem is treated as the problem of minimising the cycle length for the *worst-case* scenario.
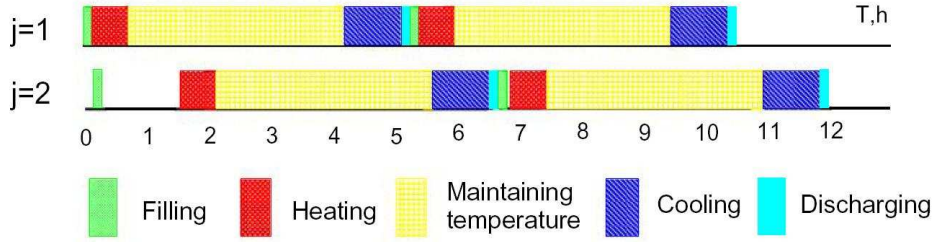

Fig. 5.6: Figure 13 from the paper [GGR06]: Reactors schedule when the heating time is imprecisely known.

In [RSdP06], the schedule is produced on-line by using a classical Model Based Predictive Control (MPC) scheme. The internal model of the plant is an hybrid simulation model similar to the one we have developed in Chapter 2. The objective function is formulated as

$$J = \int_0^{ph} \alpha_1 (V_{ST} - V_{STref})^2 + \alpha_2 (V_{ST} - V_{STmin})^2 +$$
$$+ \alpha_3 (V_{ST} - V_{STmax})^2 + \alpha_4 (1/w)^2 + \alpha_4 (T_{constraint})^2$$

where ph denotes the prediction horizon. The first three terms are intended to control the level of the storage tank. The fourth term is intended to maximize the productivity by penalizing too small values of the production rate w. The last term is intended to prevent the plant from simultaneous occurrences of the same phases in both reactors (condition ii above) : the variable $T_{constraint}$ is an overall measure of the overlapping times between similar phases in both reactors (see [RSdP06] for details). The decision variables include the stand by times Δ_{SF1}, Δ_{SH1}, ... and Δ_{SD2} and the product outflow rate w. At each time step, the nonlinear optimization is performed using Sequential Quadratic Programming (SQP). With the data of Table 5.2 and a prediction horizon of 3 production cycles, a simulation experiment of 25 hours is reported in [RSdP06]. The obtained solution is approximately periodic with average production rate is $w = 9.65$ [m^3/h], to be

compared to the optimal value of $w^{opt} = 11.39$ [m^3/h]. An important drawback of the method is to produce an outflow rate which is time varying with a huge overshoot of about 800% at each cycle, Figure 5.7.
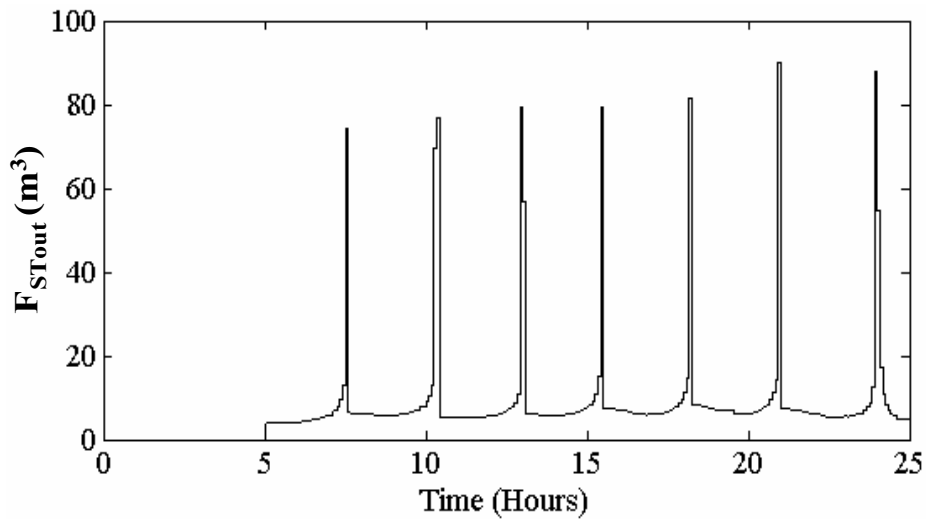

Fig. 5.7: Figure 7 from the paper [RSdP06]: Sub-optimal tank output flow rate $F_{STout} \triangleq w$ [m^3/h].

5.4 Conclusions

In this Chapter the optimal scheduling of the hybrid chemical plant has been formulated as an optimal control problem. Three strategies, one based on a cyclic *MILP* scheduling and others based on hybrid model predictive control and time discrete control, respectively, were also presented. In all of them the obtained solutions are suboptimal, based on the introduction of some additional assumptions simplifying the initially defined highly constraint optimization problem. Application of the periodic *MILP* scheduling solution on the plant simulator is given together with a comparison with the optimal solution obtained intuitively though simulations in Section 3.4. Next Chapter deals with

the consequence of the introduction of a constant disturbance during the optimally scheduled plant operation.

Chapter 6

Feedback control strategies for periodic schedules in presence of disturbances

In this Chapter we consider the optimally scheduled plant process under piecewise constant disturbances. As shall be seen the plant operation may be stopped either due to a conflict for the resources shared by the reactors or due to overflow/underflow of the tank. Consequently two separate feedback control strategies are proposed and analyzed, namely:

i. *the resources sharing conflict is solved by a strategy based on a model predictive control (MPC) approach and using the concept of batch synchronization*

ii. *a simple PI control is applied on the tank not only to stabilize the process but also to ensure a smooth material transfer to the downstream processing.*

The efficiency of both strategies is illustrated through a set of disturbance scenarios.

6.1 Introduction

In Chapters 3 and 5 we have considered the scheduling problem for productivity maximization of the benchmark plant, subject to resource and tank capacity limitations, on the basis of a **perfect** knowledge of the hybrid plant model. The model involves physical parameter values such as T_c (cold water temperature), T_h (hot steam temperature), F_{in} (reactant feed flow rate), Q_h (hot steam transfer rate) etc... Moreover the switching between the phases triggered by state events guards depends on on-line measurements of continuous state variables like V (reactor volume), T (reactor temperature) or C_A (reactant concentration).

It would obviously be unrealistic to assume that all these parameters and measurements are error free and exactly known. Our concern here is to analyze the plant behaviour under periodic schedules in the case where there are **constant (or piecewise constant)** errors on the parameters and measured values.

Under such piecewise constant disturbances, two types of problems may arise:

1) The occurrence of a step disturbance may induce a drift in the reactors hybrid trajectory. As a result:

i.) if the reactors are driven by a *sub-optimal schedule* the hybrid trajectory can either converge to a new sub-optimal schedule or a conflict for the resources arises (Subsection 6.2.1).

ii.) if the plant is driven by the *optimal schedule* and the disturbance is not very big, no conflict arises but the hybrid trajectory converges to a new sub-optimal schedule (Subsection 6.2.1);

2) As it has been seen Chapter 3, Section 3.4 the volume profile of the buffer tank is periodic (Figure 3.14) but naturally the occurrence of a disturbance (e.g. its input flow rate is smaller or bigger than the scheduled one) may lead to its overflow or under-filling.

Our objective in this chapter will be to propose and analyze control strategies in order to cope with these problems. In Section 6.2, we present a model based predictive control approach to avoid resource conflicts. In Section 6.3-6.4 we present a PI control approach to stabilize the buffer tank.

6.2 Model predictive control to avoid resource conflict

As a matter of illustration, let us consider the two-reactors operation of CASE 2 and refer to Figures 3.9 and 3.12. It is clear that if BR_1 starts its operation close to the total cooling water conflict zone, the occurrence of disturbances could lead to a conflict of cold water sharing. The same is valid for BR_2 if it starts working close to the minimal cooling water conflict zone.

A way to cope with disturbances is by computing a new production scheduling based on a selected criteria when the rescheduling has to be done. The use of $MILP$ scheduling formulations (as in Chapter 5) may however be time-consuming [SP99] and there is a need for finding formulations that are able to give fast solutions even for fairly large instances. A possibility, as shown in [PW07] is to design transient schedules that aim at bringing the system from some initial state (possibly not good with respect to productivity) to a new better state from which a periodic schedule with good productivity is computed.

Another way also discussed by [PW07] is to incorporate the non-linear dynamics (including the disturbances) in the formulation but the computing time may become excessive.

As it was also mentioned in Chapter 5, a simple but conservative solution may be to assume a priori that the duration of each phase lies inside a given, wide enough, time interval [GGR07].

In this Section, we are concerned with feedback control in order to avoid resource conflicts in the case of, possibly unknown, piecewise constant disturbances. Our solution is based on an adaptive model predictive approach.

We focus on the two-reactors plant operating under a T_p-periodic schedule. We assume that, during each phase, one or several constant parameters may undergo disturbances under the form of step variations. The proposed control strategy is based on the model predictive control paradigm and uses the concept of batch synchronization given in [Mel03]. The model which is used in this model predictive control (MPC) is the plant simulator which has been described in Chapter 2 and is therefore supposed to be run on-line.

The basic issues of the proposed control strategy are the conflict detection, the computation and the allocation of the stand by times on the corresponding reactor. These problems are addressed by the control strategy illustrated in Figures 6.1 - 6.2.

6.2.1 Adaptive control strategy

The control algorithm is stated under the following assumptions:

i. There is an ideal periodic schedule with zero (Figure 3.10) or non-zero (Figure 3.11) stand by times;

ii. The parameters F_{in}^{max}, Q_h^{max}, Q_c^{min}, Q_c^{max}, F_{disch}^{max}, T_h, T_c undergo piecewise constant disturbances. The time interval between two successive disturbance steps is larger than the period T_p (i.e. there is at most one disturbance step for each parameter within each cycle).
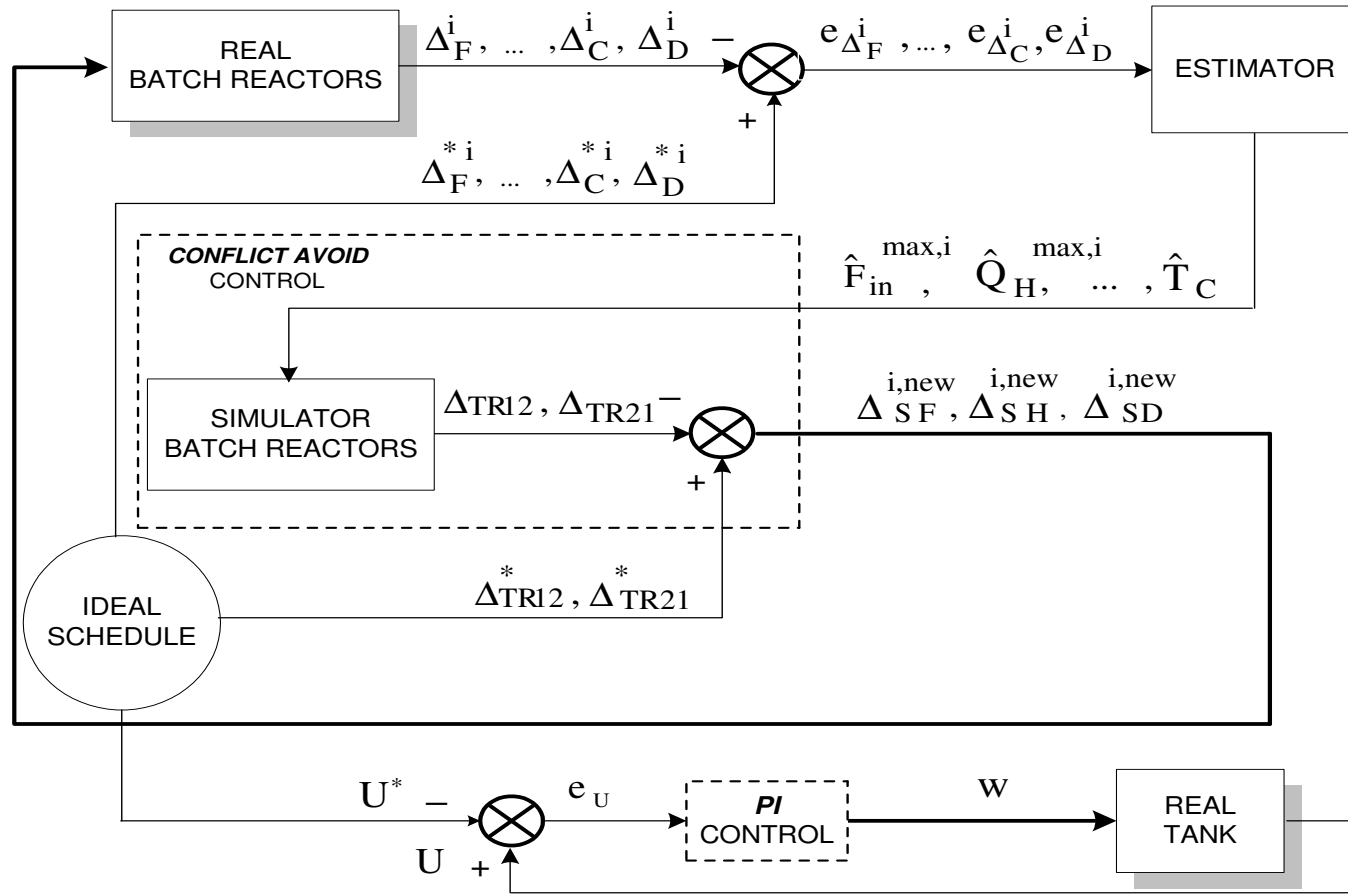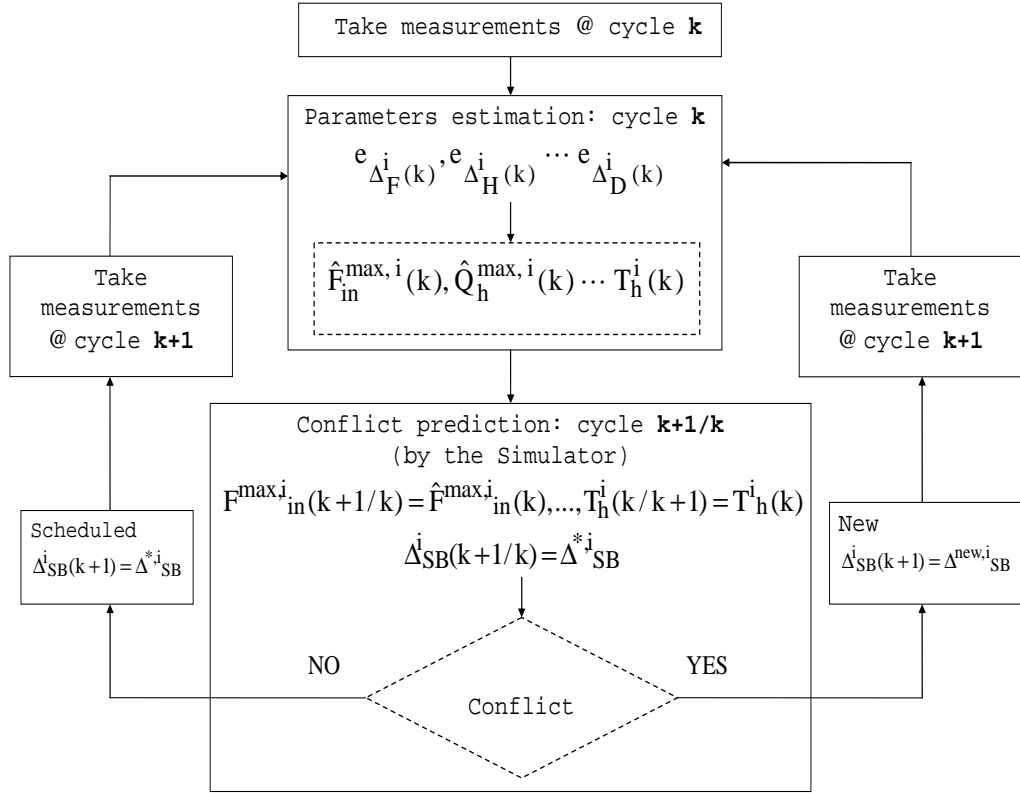
Fig. 6.1: Global control of the plant

Fig. 6.2: Feedback strategy to avoid a cold water conflict

iii. Only conflicts for cold water may arise because of the disturbances. The disturbances are not big enough to induce conflicts for raw material or hot water;

iv. The disturbances on Q_c^{max} and T_c are never big enough to prevent the temperature regulation to be effective.

Under these assumptions, the control algorithm given in Figure 6.2 (for $i \in \{1, 2\}$) is described as follows.

Step 1 Take measurements of the phases time duration (cycle k)

At the end of the phases: filling, heating, cooling and discharging in k^{th} cycle of each rector, their **real** time durations, $\Delta_F^i(k)$, $\Delta_H^i(k)$, ..., $\Delta_D^i(k)$ **are measured**.

Step 2 Parameters estimation (cycle k)

The measurements are compared with the **scheduled** time durations, Δ_F^*, Δ_H^*, ... and Δ_D^* and the errors are obtained i.e. $e_{\Delta_F^i}(k) = \Delta_F^* - \Delta_F^i(k)$, ... and $e_{\Delta_D^i}(k) = \Delta_D^* - \Delta_D^i(k)$. These errors are used to find **estimations** of the reactors parameters $\hat{F}_{in}^{max,i}(k)$, $\hat{Q}_h^{max,i}(k)$, ..., $\hat{T}_h^i(k)$, $\hat{T}_c^i(k)$.

As an estimator one can consider a table, obtained off-line by the simulator, relating the time errors with these parameters.

Step 3 Conflict prediction (cycle $k + 1/k$)

    i. The parameters values, **predicted** for cycle $k+1$, are set to be equal to the **estimated** ones i.e. : $F_{in}^{max,i}(k + 1/k) = \hat{F}_{in}^{max,i}(k)$, $Q_h^{max,i}(k + 1/k) = \hat{Q}_h^{max,i}(k)$, ..., $\hat{T}_c^i(k + 1/k) = \hat{T}_c^i(k)$.

    ii. To optimize the plant productivity the stand by times at cycle $k + 1$ are **predicted** to be equal to their scheduled values i.e. $\Delta_{SB}^i(k + 1/k) = \Delta_{SB}^{*,i}$.

    iii. Based on *i.* and *ii.* the simulator **predicts** for cycle $k + 1$ whether a cold water sharing conflict shall arise.

        a) **No conflict:** The scheduled stand by times to be used on the plant in cycle $k + 1$ are **not** changed.

        b) **A conflict: New** stand by times are computed for the cycle $k + 1$ (see **Step 4**).

Step 4 (a conflict at cycle $k+1$) Stand by times computing and allocation on the reactors (cycle $k+1/k$)

Consider Figure 6.3 where two successive cycles of the reactors operation, k and $k+1$ are shown. By Δ^*_{TR12} and Δ^*_{TR21} are denoted the scheduled values of the time distance between the regulation phases on BR_1 and BR_2 and vise-versa. In the presence of disturbances these time distances change and as a result a cooling water conflict may arise.
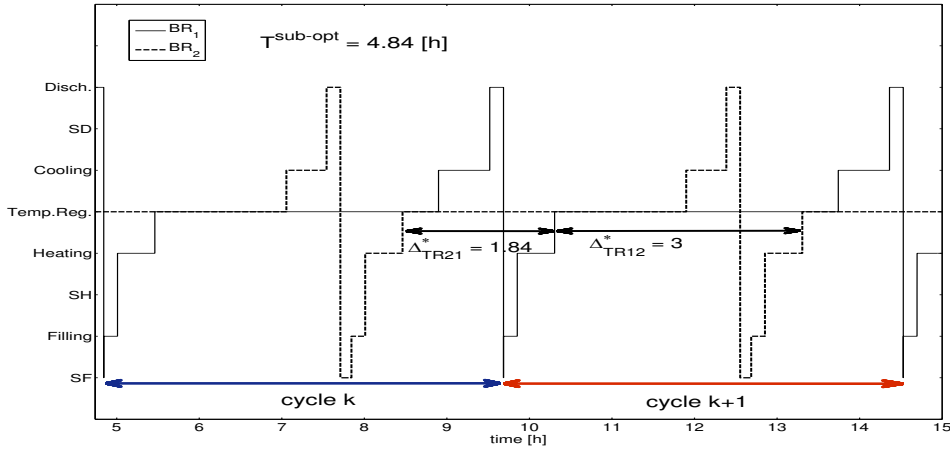

Fig. 6.3: Sub-optimal periodic schedule with no disturbances

For cycle $k+1$ the difference between the **predicted** $\Delta_{TR12}(k+1/k)$, $\Delta_{TR21}(k+1/k)$ and the **scheduled time separations** Δ^*_{TR12}, Δ^*_{TR21} is computed and it is allocated for $k+1$ cycle as a stand by time on the appropriate reactor. This is done as follows:

- if $\Delta^*_{TR12} - \Delta_{TR12}(k+1/k) < 0$ there is an **increase** of the real time distance with respect to the scheduled one between the reaction phases of BR_1 and BR_2. A natural way to avoid the conflict is, at cycle $k+1$ to add the difference $|\Delta^*_{TR12} - \Delta_{TR12}(k+1)|$ as a stand by time (for instance before filling) on BR_1. Note that in this way we are **controlling** the real time distance

$\Delta_{TR12}(k+1)$ to become equal to Δ^*_{TR12} and the conflict is avoided;

- if $\Delta^*_{TR12} - \Delta_{TR12}(k+1/k) > 0$ there is a **decrease** of the real time distance with respect to the scheduled one between the reaction phases of BR_1 and BR_2. To prevent a conflict at cycle $k+1$ this difference is added as a stand by time on BR_2;

- if $\Delta^*_{TR21} - \Delta_{TR21}(k+1/k) < 0$ there is an **increase** of the real time distance with respect to the scheduled one between the reaction phases of BR_2 and BR_1. To avoid a conflict at cycle $k+1$, the difference $|\Delta^*_{TR21} - \Delta_{TR21}(k+1/k)|$ has to be removed [2] from the stand by times of BR_2. Here, as was already discussed in Chapter 3, Section 3.3.3, the need of a sub-optimal robust schedule is evident.

- if $\Delta^*_{TR21} - \Delta_{TR21}(k+1/k) > 0$ we add, at cycle $k+1$, the absolute value of this difference as a stand by time on BR_1.

  Note that at the cycle $k+1$ the stand by time to be applied is computed by one of the four expressions. The stand by times can be added also if for some reasons it is needed to slow down the process production, while keeping at the same time the process periodic.

Step 5 Get new measurements at cycle $k+1$ and go to **Step** 2.

In this section, as a matter of example, we have focused on the case where only conflicts for the cold water may arise. But it is clear that the application of the proposed algorithm to avoid conflicts for other shared resources can be developed in a similar way, namely by taking into account the time separation between the phases where the conflict can arise. For more general plants having a large number of reactors the extension of the MPC should take into account the number of reactors that are simultaneously active during the production cycle and

---

[2] this case in not treated in the thesis

also the corresponding time separation between pairs of successively working reactors.

6.2.2 Simulation results

Let us consider the application of the control strategy on the plant-simulator under four different scenarii of an **unmeasured** step disturbance, namely:

Constant disturbances: During the 3th cycle of the reactors operation i.e. at $time \approx 13 \; [h]$:

Disturbance scenario 1: the hot steam transfer rate $Q_h^{max,2}$ *decreases* incidentally from 3 $[1/h]$ to 2 $[1/h]$ (i.e. with -33%). All the other parameters are unchanged with values as given in Table 3.3 and in Figure 3.2.

Disturbance scenario 2: only the parameter hot steam transfer rate $Q_h^{max,2}$ *increases* incidentally from 3 $[1/h]$ to 4 $[1/h]$ (i.e. with $+33\%$).

Note that due to the fact that the operations of both reactors are interconnected, through the computation of the cold water transfer rate during the cooling phase (Chapter 3, Section 3.3), the disturbance on BR_i induces a disturbance on BR_j, $j \in \{1,2\} \; i \neq j$.

Disturbance scenario 3: there is a step disturbance together on BR_1 and BR_2 such that the hot steam transfer rates $Q_h^{max,1}$ and $Q_h^{max,2}$ decrease from 3 $[1/h]$ to 2 $[1/h]$. The other parameters are unchanged.

Stochastic disturbance (*Disturbance scenario* 4): Finally the **disturbance** on $Q_h^{max,2}$ $[1/h]$ is **stochastic** having the form given in Figure 6.4, actually $Q_h^2(t)$ has a normal distribution with mean value 2 and a standard deviation of 0.5. There is no change on the other parameters.
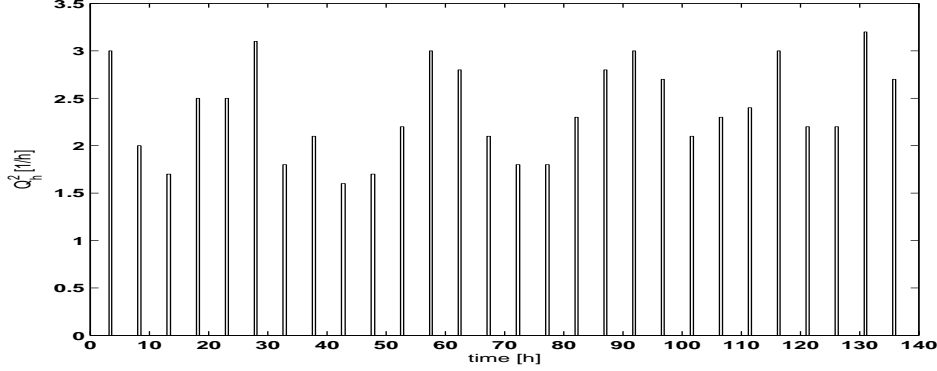
Fig. 6.4: Scenario 4: stochastic disturbance on Q_h^2

Sub-optimal periodic schedule

In this section, we illustrate the behaviour of the model predictive control strategy in a case where the ideal periodic schedule is sub-optimal.

Let BR_2 start its operation with a time lag of 3 $[h]$ with respect to BR_1. The stand by time before filling on BR_2 is $\Delta_{SF2} = 0.134$ $[h]$ and $T_p^{sub-opt} = 4.84$ $[h]$. The scheduled time distances can be seen in Figure 6.3 and they are $\Delta_{TR12}^* = 3$ $[h]$ and $\Delta_{TR21}^* = 1.84$ $[h]$. Referring to Figures 3.9 and 3.12 it is seen that the reactors operation is close to the minimal cold water conflict zone. Here we apply the above presented strategy to avoid such a conflict. Let us denote by k^{conf} the cycle during which a conflict arises.

- **Batch-reactors under *disturbance scenario* 1*:* As a matter of illustration consider the plant schedule given in Figure 6.5 which shows how a conflict is predicted and avoided over two successive cycles. Using the developed adaptive control strategy it is predicted that at cycle $k^{conf} = 4$ the available cooling water quantity which BR_1 needs to perform its cooling phase is smaller than the minimal required one (Figure 6.6) and a cold water conflict will arise. Referring to Figure 6.5 it is seen that at the conflict $time \approx 18$ $[h]$ the **predicted** time distance between the reaction phases of BR_1 and BR_2 is 3.16 $[h]$. Consequently
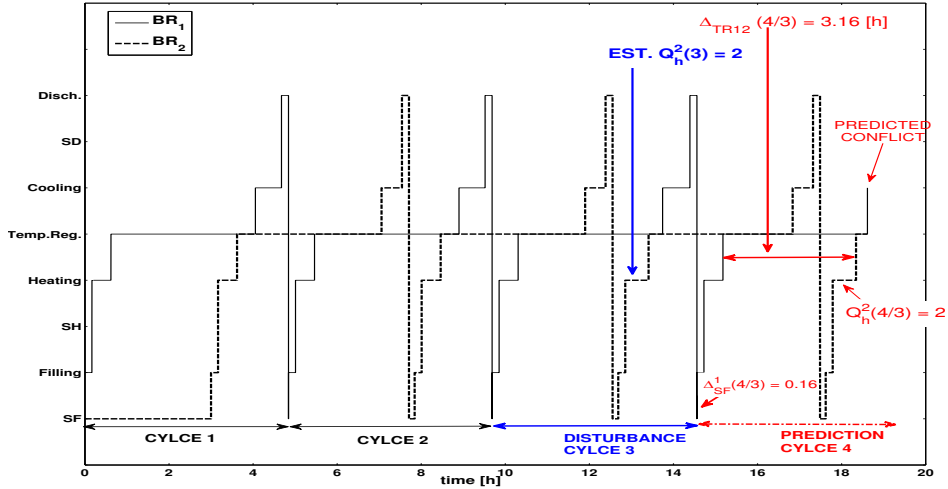
Fig. 6.5: Schedule: a conflict

the stand by time before filling of BR_1 during the 4th cycle must be set to $\Delta_{SF}^1(4) = |\Delta_{TR12}^* - \Delta_{TR12}(4/3)| = 0.16 [h]$.
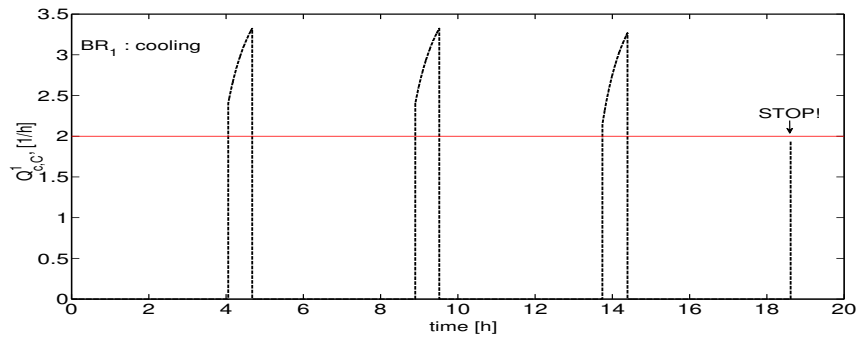
Fig. 6.6: Cold water profile: a conflcit

The complete MPC-controlled plant schedule is given in Figure 6.7 [3]. Note that by the $\Delta_{SF}^1(4) = 0.16$ $[h]$ introduction, the conflict occurring in 4th cycle is avoided. Moreover because the

---

[3] for better results illustration $final\ time = 52$ $[h]$; by the blue color we indicate that the disturbance is constant

disturbance is constant i.e. $Q_h^{max,2}(4/3) = \hat{Q}_h^{max,2}(4)$ the reactors operation is completely synchronized (i.e. as if there is **no** disturbance in cycle 4). As a result no conflict was predicted in cycle 5. It can be observed that the conflict appears periodically ($T_p^{new} = 9.90[h]$ bigger than $4.84[h]$) at each $k^{conf} + 2m$ cycle, $m \in Z_{>0}$. The periodic time evolution of the total cold water flow rate $Q_{c,TOTAL}(t) = Q_c^1(t) + Q_c^2(t)$ ($final\ time = 140\ [h]$) is shown in Figure 6.8.
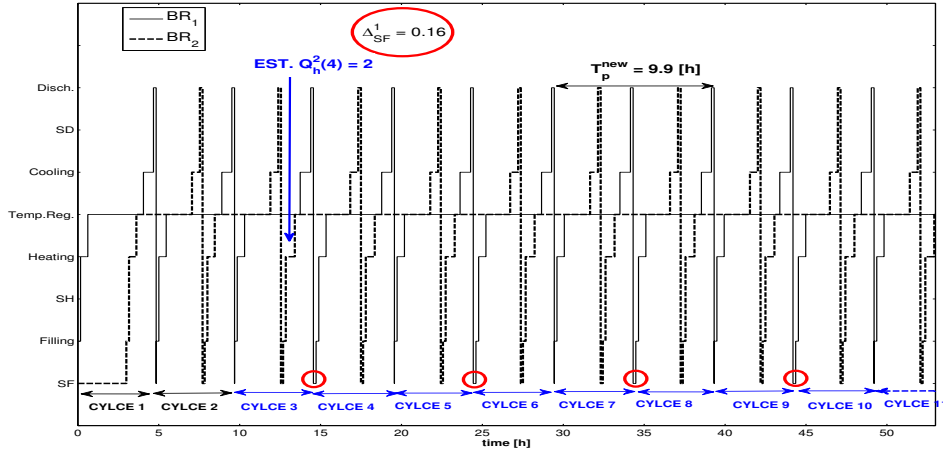
Fig. 6.7: Sub-optimal periodic schedule: scenario 1; just after the disturbance converge to: $T_p^{new} = 9.90[h]$

- **Batch-reactors under *disturbance scenario* 2*:* In this case **no** cold water conflict was detected. Essentially this is because the real time duration of the heating phase is now shorter ($\Delta_{SH}^2 = 0.391\ [h]$) than the scheduled one ($\hat{\Delta}_{SH}^{*,2} = 0.453\ [h]$) and in that way BR_2 is moving away from the conflict zone. Moreover because both reactors influence each other, as seen from the total cold water flow rate $Q_{c,TOTAL}(t) = Q_c^1(t) + Q_c^2(t)$ given in Figure 6.9, the hybrid plant trajectory **converges** to a **new** sub-optimal periodic operation with a period $4.80\ [h]$. Naturally it is smaller that the original one $4.84\ [h]$ because $\Delta_{SH}^2 < \Delta_{SH2}^{*,2}$.
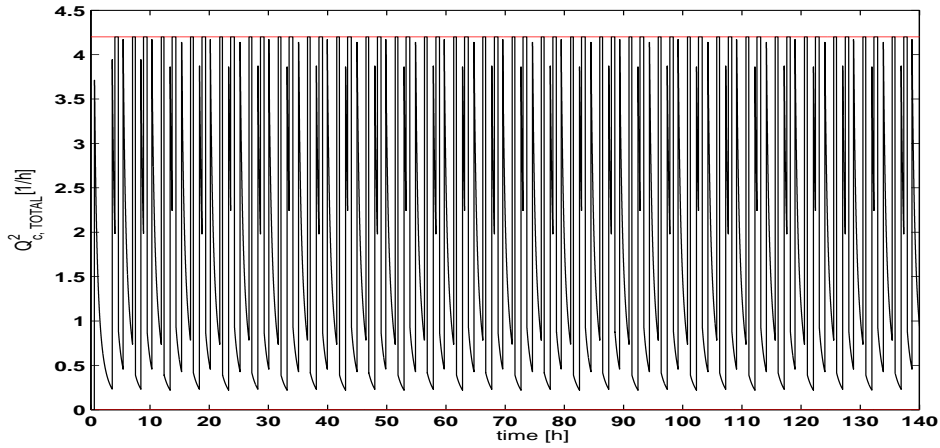
Fig. 6.8: Sub-optimal periodic cold water profile: scenario 1; just after the disturbance ($time \approx 13[h]$) converge to: $T_p^{new} = 9.90[h]$
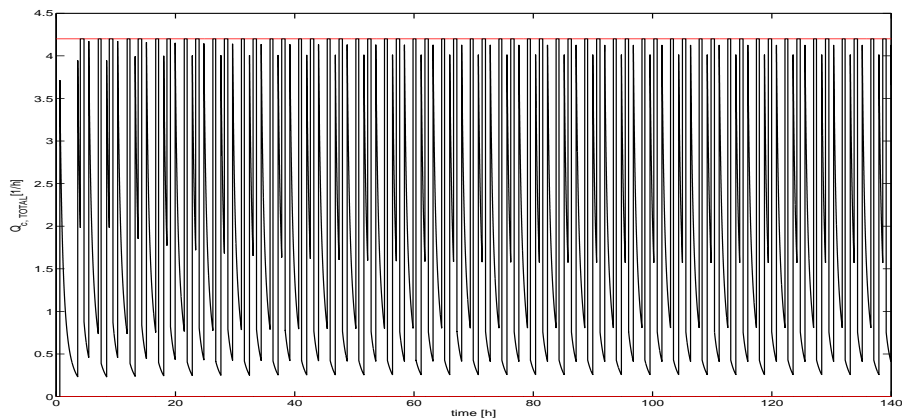
Fig. 6.9: Sub-optimal periodic cold water profile: scenario 2; $time \approx 60[h]$ converge to: $T_p^{new} = 4.80[h]$

- **Batch-reactors operation under the *disturbance scenario* 3*:** Since the perturbation is acting on both reactors simultaneously the scheduled time difference Δ_{TR12}^* and Δ_{TR21}^* are not changed. As a result **no** conflict arises. The plant operation is illustrated in Figure 6.10. Here the profile of the total cold water flow rate $Q_{c,TOTAL}(t) = Q_c^1(t) + Q_c^2(t)$ is given. Note that the plant operation is periodic right from the beginning and
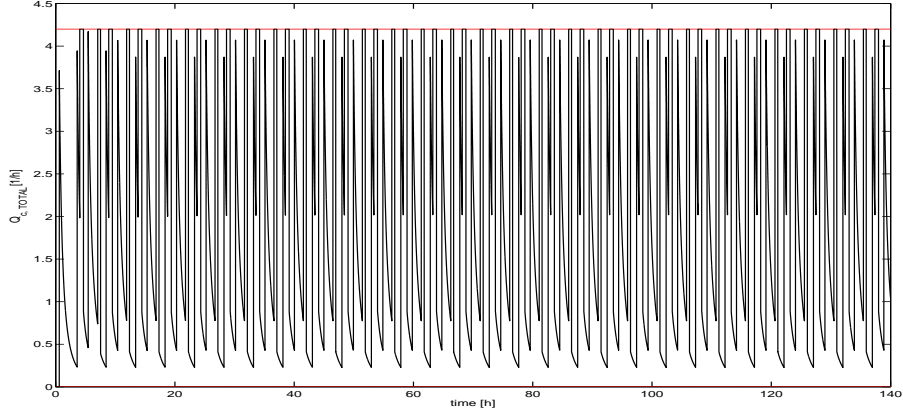
Fig. 6.10: Sub-optimal periodic cold water profile: scenario 3; just after the disturbance converge to: $T_p^{new} = 4.92[h]$

due to the disturbance its period has changed to $T_p^{new} = 4.92$ [h]. Here the new-period is **larger** than the original 4.84 [h] because $\Delta_{SH}^i > \Delta_{SH}^{*,i}$, $i \in \{1, 2\}$.

- **Batch-reactors under the *stochastic disturbance scenario* 4:** The hot steam transfer rate Q_h^2 is a stochastic disturbance input given in Figure 6.11 A. Figure 6.11 B represents the new stand by times (before filling) computed by the MPC algorithm and applied on BR_1 such as to avoid a cold water sharing conflict. The interpretation of Figure 6.11 B is as follows. At cycle 1 the value of the hot steam rate of BR_2 Q_h^2 $[h^{-1}]$ is equal to the scheduled one and consequently as seen in Figure 6.11 B the scheduled stand by time (before filling) of BR_1 (i.e. $\Delta_{SF1} = 0$ [h]) is not modified. At cycle 2 the hot steam changes from 3 $[h^{-1}]$ to 2 $[h^{-1}]$ and consequently by the MPC strategy it is found that a cold water conflict is avoided by adding a stand by time (before filling) on BR_1 of 0.15 [h]. At cycle 3 there is again a change at Q_h^2 and as a result the new stand by time for the next cycle is found to be 0.18 [h]. The interpretation of the remaining stand by times profile of BR_1 is made similarly. The total cooling water profile $Q_{c,TOTAL}(t) = Q_c^1(t) + Q_c^2(t)$ is

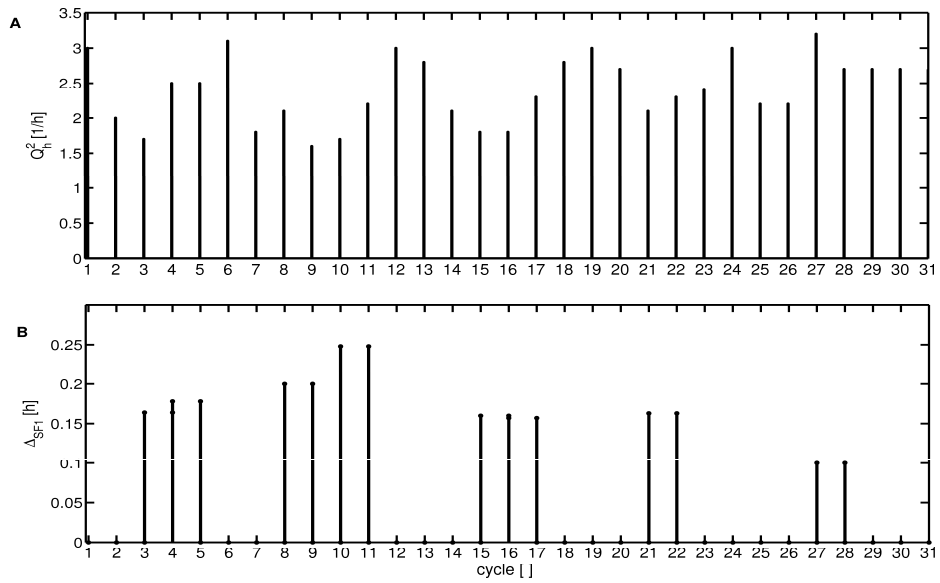depicted in 6.12. As expected **no** periodicity is observed.

Fig. 6.11: Scenario 4 - *A:* Hot steam profile of BR_2; *B:* stand by times (**control action**) before filling on BR_1
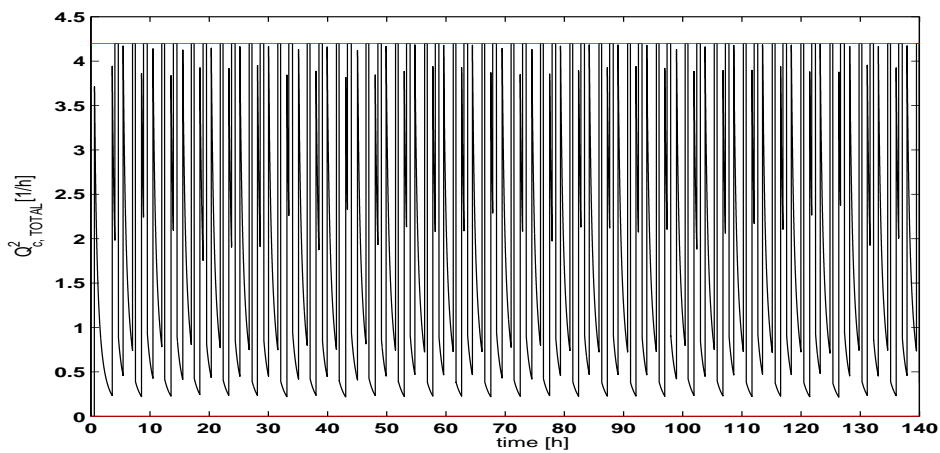

Fig. 6.12: Sub-optimal cold water profile (**no more periodic**): scenario 4

Optimal periodic schedule

Consider now the plant-simulator operation under the optimal periodic schedule as described in Subsection 3.3.2. Note that in this case the reactors operation is faraway from the minimal cold water conflict zones (Figures 3.9 and 3.12) and consequently a cold water conflict could arise only if the disturbance is big enough to cause an acceleration or a delay of the reactors operation such that one of the two borders 1.76 $[h]$ and 3.13 $[h]$, respectively to be reached. The plant operation subject to *disturbance scenarii* 1 and 2 is illustrated, through the profiles of the total cold water flow rate $Q_{c,TOTAL}(t) = Q_c^1(t) + Q_c^2(t)$, in Figures 6.13 and 6.14, respectively.

- In the *disturbances scenario* 1 it is know that $Q_H^2 < Q_H^{2,*}$ and as a result $\Delta_H^1 > \Delta_H^{*,1}$. Consequently at *time* $\approx 70\ [h]$ the hybrid plant trajectory **converges** to a **new** periodic operation with a period 4.80 $[h]$ which is **larger** than the optimal one 4.74 $[h]$.
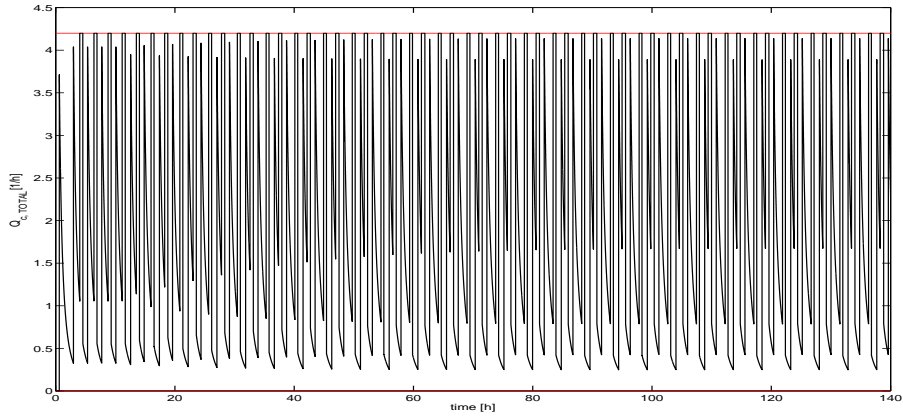
Fig. 6.13: Optimal cold water profile: scenario 1; $time \approx 70[h]$ converge to: $T_p^{new} = 4.80[h]$

- Similarly to the previous case the hybrid plant trajectory **converges** to a **new** periodic operation with a period **smaller** than

the optimal one 4.74 $[h]$ and equal to 4.71 $[h]$. It is reached after approximately 75 hours.
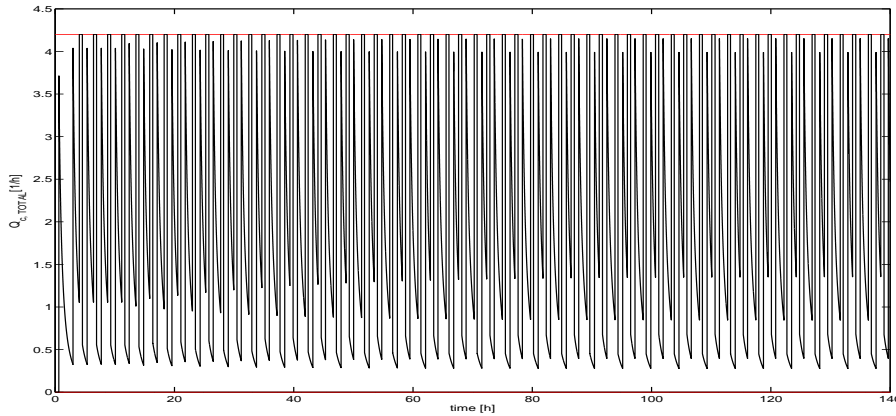

Fig. 6.14: Optimal cold water profile: scenario 2; $time \approx 75[h]$ converge to: $T_p^{new} = 4.72[h]$

6.3 PI feedback stabilisation of the buffer tank

In the previous section we have considered a plant with two reactors but we have ignored the presence of the storage tank.

Consider now the plant operating under a sub-optimal periodic schedule as given in Subsection 6.2.2 and assume that it is subject to *a disturbance scenario* 1. As seen in Figure 6.8 thanks to the used control strategy the conflict of cold water sharing is avoided. However the control is such that the disturbance is not rejected but propagates to the next plant unit, namely the storage tank. Actually the tank capacity limitations shall lead to the shut down of the plant operation. It is seen in Figure 6.15 that at $time \approx 3\ [h]$ the minimal tank capacity is reached.

Note that here due to the time evolution of the tank trajectory (Figure 3.14) a continuous control at a given level (i.e. a set point) is
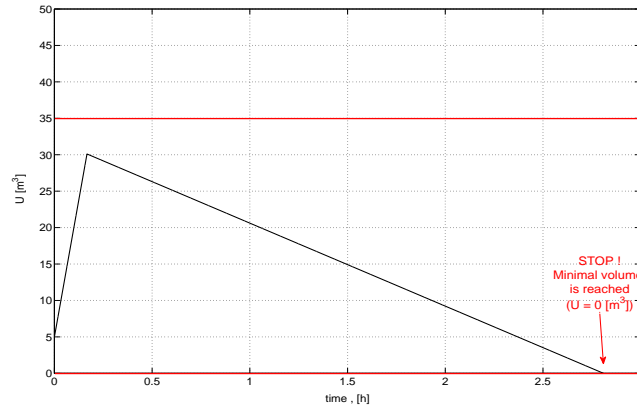
Fig. 6.15: Evolution of the volume $U(t)$ in the presence of a constant disturbance on the cold water flow

not possible. Moreover we can not design a controller to follow the scheduled tank profile (Figure 3.14) because we can not change the time when the inflow product enters the tank i.e. the time when the reactors are discharged in it. Consequently we can classify this type of problem, where a tight control of the tank level around a given set point is not considered important, as an averaging level control problem [FS03] [CL80] [CM89] [SO86]. Generally speaking the averaging level control has two competitive objectives: providing a smooth rate of change of the tank output flow rate while at the same time assuring that the minimal and the maximal tank volume bounds are not exceeded. Some of the works related to this kind of control problem are summarized as follows.

Luyben and co-workers have presented in [CL79] a way to tune the P and PI level controllers such that to reject an inflow rate step disturbance, based on the specifications for the maximum allowed variations *(MAV)* of the tank outflow rate and for a peak level height. They have also proposed in [CL80] an alternative control system combining the advantages of P and PI in order to avoid an overshoot of the tank outflow rate. Another approach is presented by McDonalds at all [MMT86] which is such that the smallest possible *MAV* of the tank outflow rate are achieved for a given maximum peak level height and a known step inflow disturbance. Note that the control law filters the

perturbation. A further extension of [MMT86] is made by Morari and co-workers [CM89] which suggest its model predictive control implementation. The proposed controller assures good disturbance filtering and rapid settling time. Another way to solve the averaging control problem is proposed by Sbarbaro et all in [SO86]. Here the problem is formulated using energy based approach. It is shown that the method can deal with multiple tank systems described by nonlinear dynamics and moreover it establishes the stability of the closed loop system.

Generally speaking a common point in all these control methods is that the tank inflow is continuous, which is not the case in this thesis.

A possible solution in this case is the use of a predictive inventory control, as proposed in a report provided by the *Solvay Group* [Mel03]. The aim is to ensure that each time when a reactor is discharged the volume in the tank at that moment is equal to some mean level. Moreover there are some constraints on the minimal and maximal tank output flow rate ensuring that the volume constraints are satisfied.

In contrast to [Mel03] the feedback control strategy that we shall use is based on the averaging control principle and our aim is to control a tank system having a discontinuous inflow and continuous outflow by acting on its output flow rate $w(t)$ in order to:

i. not only to stabilize the operation of the storage tank but also to ensure

ii. that the output flow rate variations have a small amplitude in order to avoid upsetting the operation of the downstream processes and at the same time to

iii. maintain the tank volume between some minimal U^{min} and maximal U^{max} bounds.

Moreover note that here the goal is not to reject the existing perturbation but rather to have small control variations in spite of large amplitude disturbances.

In the next subsection a periodic continuous time model of the hybrid periodic process performed in the storage tank based on Fourier series decomposition is given.

6.3.1 Fourier series continuous time model of the tank

As it has been seen up to now (Chapter 3), the plant operation is driven by T_p - periodic inputs i.e. flow and transfer rates. Consequently the hybrid storage tank process can be modelled not only by a hybrid automaton (Chapter 2, Subsection 2.1.2) but also as a continuous process subject to a periodic input signal:

$$\dot{U}(t) = F(t) - w(t) \tag{6.1}$$

For a plant having N reactors the elements of this equation are defined as follows:

i. $F(t) = \sum_{i=1}^{N} F_{disch}^{i}(t)$

   is the total piecewise constant output flow rate of all reactors and as a sum of T_p-periodic signals it is also T_p-periodic. For a cycle $k = 0, 1, 2...$ the discharging flow rate from i^{th} reactor $F_{disch}^{i}(t)$ is a piecewise constant signal having the form:

$$F_{disch}^{i}(t) = \begin{cases} F_{disch} & \text{if } t_{StrD}^{i} + kT_p \leq t < t_{StpD}^{i} + kT_p \\ \\ 0 & \text{otherwise} \end{cases}$$

   where t_{StrD}^{i} is the time when i^{th} reactor enters its discharging phase, t_{StpD}^{i} is the time when the discharging is stopped.

   Due to its periodicity the signal $F(t)$ can be decomposed as follows:

$$F(t) = F^m + \Delta F(t)$$

   where F^m is the mean constant value and $\Delta F(t)$ is the corresponding zero mean periodic component i.e.:

$$F^m = \frac{1}{T_p} \int_0^{T_p} F(\tau)d\tau \neq 0$$

   and

$$\frac{1}{T_p} \int_0^{T_p} \Delta F(\tau) d\tau = 0$$

ii. $w(t)$ is the output flow rate of the tank. As it was defined in Chapter 3, when the plant is driven by a periodic schedule, $w(t)$ is constant:

$$w(t) = w^m = F^m$$

Consequently the tank model 6.1 becomes simply:

$$\dot{U}(t) = \Delta F(t) \tag{6.2}$$

By using the fact that $F(t)$ is a T_p- periodic function, there exists a T_p periodic steady-state solution of the tank volume equation 6.2 $U(t) = U(t + T_p) = U^m + \Delta U(t)$ $[m^3]$ [Bur85], where U^m is the mean value and $\Delta U(t)$ is the zero mean periodic component. An easy way to analyze a periodic system is by presenting it in terms of Fourier series [HV03].

The zero mean T_p-periodic component $\Delta F_{disch,TOTAL}(t)$ of the total input flow rate of the tank in terms of Fourier series is expressed as follows:

$$\Delta F(t) = \sum_{n=1}^{\infty} a_n \cos(n\omega_p t) + \sum_{n=1}^{\infty} b_n \sin(n\omega_p t) \tag{6.3}$$

where a_n and b_n are Fourier series coefficients computed by equations (6.4) and (6.5), respectively; $\omega_p = \frac{2\pi}{T_p}$ $[rad/h]$ is the fundamental frequency of $F(t)$; $n\omega_p$ is the frequency of the nth sinusoid ($n = 1, 2, 3...$) and each sinusoid has a common period T_p. A sinusoid whose frequency is an integer multiple of the basic frequency is called an harmonic of the sinusoid at the basic frequency [HV03].

$$a_n = \frac{2}{T_p} \int_0^{T_p} \Delta F(t) \cos(n\omega_p t) dt \tag{6.4}$$

$$b_n = \frac{2}{T_p} \int_0^{T_p} \Delta F(t) \sin(n\omega_p t) dt \tag{6.5}$$

Consequently the Fourier series of the tank input flow rate is:

$$F(t) = F^m + \sum_{n=1}^{\infty} a_n \cos(n\omega_p t) + \sum_{n=1}^{\infty} b_n \sin(n\omega_p t) \qquad (6.6)$$

The magnitude spectrum is defined as the set of harmonic amplitudes:

$$A_n = \sqrt{a_n^2 + b_n^2} \quad n = 1, \ ... \ + \infty \qquad (6.7)$$

Consider now the T_p- periodic volume profile of the tank $U(t)$ $[m^3]$. Its Fourier series representations in trigonometric form is:

$$U(t) = U^m + \sum_{n=1}^{\infty} a_n^U \cos(n\omega_p t) + \sum_{n=1}^{\infty} b_n^U \sin(n\omega_p t) \qquad (6.8)$$

where the coefficients a_n^U and b_n^U are easily shown to be equal to

$$a_n^U = -\frac{b_n}{n\omega_p} \qquad (6.9)$$

$$b_n^U = \frac{a_n}{n\omega_p} \qquad (6.10)$$

while the magnitude spectrum is:

$$A_n^U = \sqrt{(\frac{b_n}{n\omega_p})^2 + (\frac{a_n}{n\omega_p})^2} = \frac{A_n}{n\omega_p} \qquad (6.11)$$

Hence the tank volume U $[m^3]$ equation (6.8), in terms of Fourier series has the form:

$$U(t) = U^m - \sum_{n=1}^{\infty} (\frac{b_n}{n\omega_p}) \cos(n\omega_p t) + \sum_{n=1}^{\infty} (\frac{a_n}{n\omega_p}) \sin(n\omega_p t) \qquad (6.12)$$

Example 1: no process disturbances

Consider the plant operating under the optimal schedule as given in Figure 3.10. The optimally scheduled input flow rate of the tank is a sum of two reactors output flow rates:

$$F(t) = \sum_{i=1}^{2} F_{disch}^{i}(t)$$

For a cycle $k = 0, 1, 2...$ the discharging flow rate of the first reactor $F_{disch}^{1}(t)$ has the form:

$$F_{disch}^{1}(t) = \begin{cases} 162 & \text{if } 4.58 + k4.74 \leq t < 4.74 + k4.74 \\ \\ 0 & \text{otherwise} \end{cases}$$

where 4.58 [h] and 4.74 [h] are the times when the first reactor starts and finishes discharging, respectively. For the second reactor the output flow rate $F_{disch}^{2}(t)$ is expressed similarly:

$$F_{disch}^{2}(t) = \begin{cases} 162 & \text{if } 6.95 + k4.74 \leq t < 7.11 + k4.74 \\ \\ 0 & \text{otherwise} \end{cases}$$

where 6.58 [h] and 7.11 [h] are the times when the second reactor starts and finishes discharging, respectively in the tank.

The magnitude spectrum of the tank input flow rate $F(t)$ computed trough equations (6.4)-(6.5) is given in Figure 6.16. In Figure 6.17 it is observed that the Fourier series approximation of the flow rate $F(t)$ for $n = 100$ harmonics is quite good.

The magnitude spectrum of the tank volume U [m^3], computed trough equation (6.24), is plotted in Figure 6.18 and in Figure 6.19 it is seen that its Fourier series approximation for $n = 100$ harmonics is also quite good.
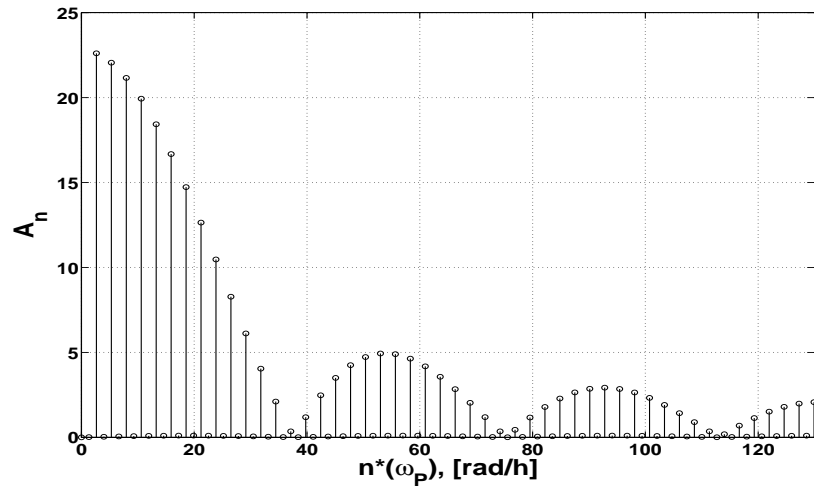
Fig. 6.16: Magnitude spectrum of $F(t)$
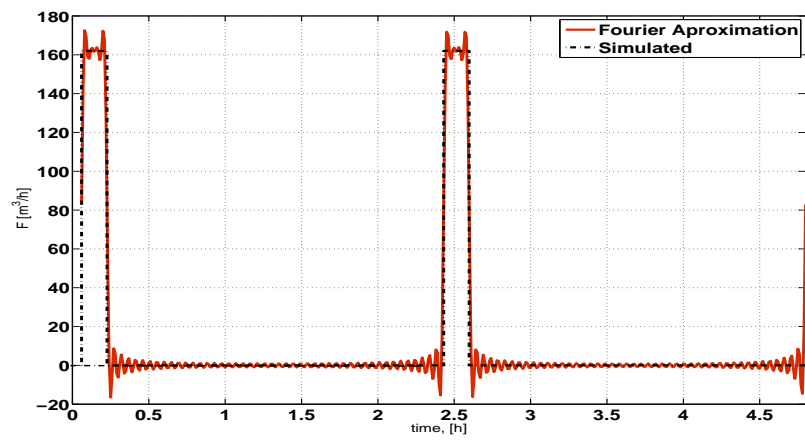
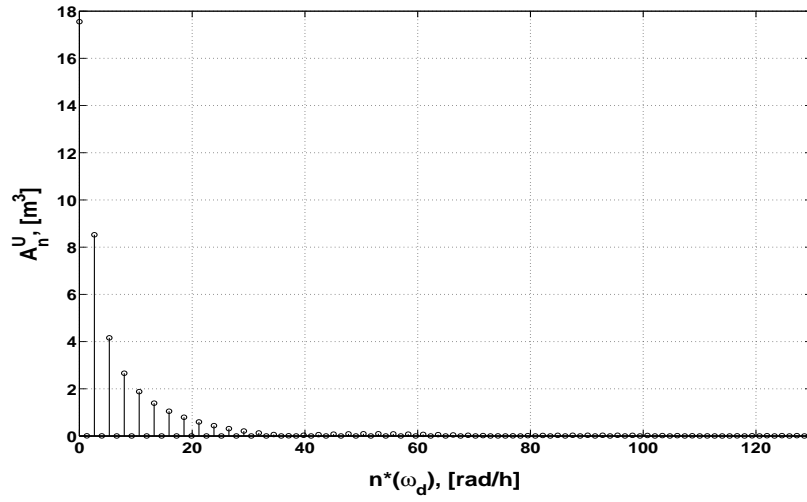Fig. 6.17: Fourier series approximation of $F(t)$

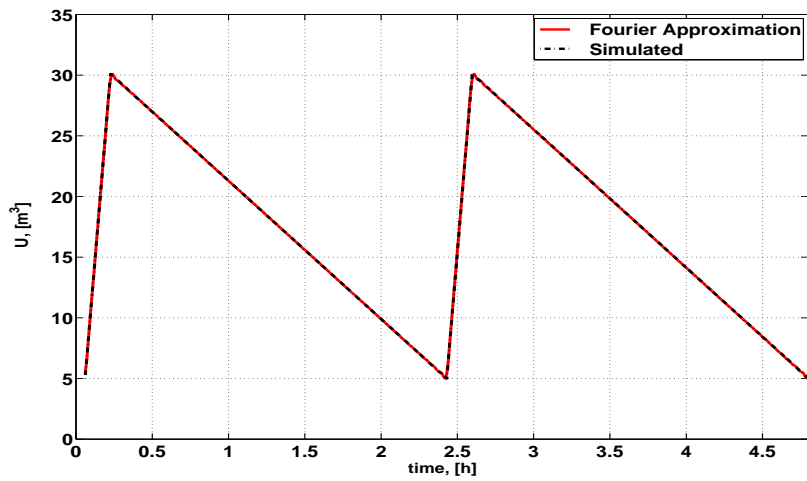Fig. 6.18: Magnitude spectrum of the tank volume $U(t)$

Fig. 6.19: Fourier series approximation of the tank volume $U(t)$

6.3.2 *PI* feedback control stabilization

The control objective has been defined at the beginning of Section 6.3. Here we examine how this control objective can be achieved by using a simple PI control strategy (see Figure 6.1) .

The control problem is formulated as follows. In order to stabilize the tank operation, we consider the problem of controlling its volume U by acting on the output tank flow rate $w(t)$. The PI controlled closed loop tank system is written as:

$$\dot{U}(t) = F(t) - \underbrace{\left(K_p U(t) + K_I \int_0^t \left(U(\sigma) - U^* \right) d\sigma \right)}_{w(t)} \quad (6.13)$$

K_p and K_I are the controller proportional and integral gains, respectively; U^* is a reference value for the tank content and $w(t)$ $[m^3/h]$ is the manipulated output flow rate of material leaving the tank. The design problem can be stated as that of selecting the PI controller gains K_p and K_I as well as the reference level U^* such that:

  i. the operation of the storage tank is stable;

 ii. and in the same time:

$$\min_{K_p, K_I, U^*} \sup_t \left| w(t) - \frac{1}{T_p} \int_t^{t+T_p} w(\tau) d\tau \right| \quad (6.14)$$

$$\text{subject to: } U^{min} \leq U(t) \leq U^{max} \quad (6.15)$$

Let us now consider separately the two goals *(i)* - Stability and *(ii)* - Constraints (6.14)-(6.15) of the PI controller.

i. Stabilization of the tank process

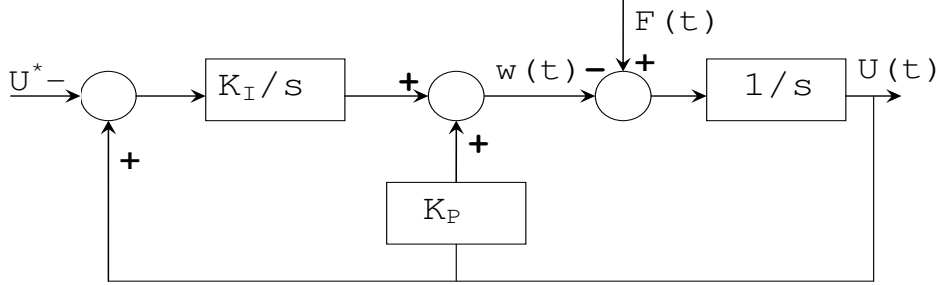Figure 6.20 is a block diagram of the tank system under PI control.

Fig. 6.20: Input-output model for the PI-controlled tank system

The transfer matrix of the system is:

$$\begin{bmatrix} U \\ w \end{bmatrix} = \begin{bmatrix} \dfrac{K_I}{s^2 + K_p s + K_I} & \dfrac{s}{s^2 + K_p s + K_I} \\[2ex] \dfrac{K_I s}{s^2 + K_p s + K_I} & \dfrac{K_p s + K_I}{s^2 + K_p s + K_I} \end{bmatrix} \begin{bmatrix} U^* \\ F_{disch,p} \end{bmatrix} \quad (6.16)$$

Hence, the closed loop system is stable if and only if the controller coefficients are strictly positive $K_p > 0$ and $K_I > 0$.

ii. Controller tuning under constraints (6.14)-(6.15)

Moreover the objective is to find the coefficients K_p, K_i and U^* as to satisfy *Constraints* (6.14)-(6.15). To achieve this we first consider the tank volume and output flow rate amplitudes as a function of K_p, K_i and U^* in the absence of disturbances. Then in Section 6.4 we give a methodology for PI controller tuning in the presence of disturbances.

6.3.3 Fourier series based amplitudes of the tank volume and output flow rate

By using the fact that $F(t)$ is a T_p-periodic function, there exists a T_p-periodic solution of (6.13) $U(t) = U(t + T_p) = U^m + \Delta U(t)$ $[m^3]$ and in consequence $w(t) = w(t + T_p) = w^m + \Delta w(t)$ $[m^3/h]$ [Bur85], where U^m and w^m are the corresponding mean values and $\Delta U(t)$ and $\Delta w(t)$ are the corresponding zero mean periodic components.

Note that here we focus only the periodic steady-state solutions and disregard the transient.

The Fourier series representation of $U(t)$ is:

$$U(t) = U^m + \sum_{n=1}^{\infty} a_n^{UPI} \cos(n\omega_p t) + \sum_{n=1}^{\infty} b_n^{UPI} \sin(n\omega_p t) \quad (6.17)$$

with the coefficients:

$$a_n^{UPI} = \frac{a_n K_p + (\frac{K_I}{n\omega_p} - n\omega_p)b_n}{K_p^2 + (\frac{K_I}{n\omega_p} - n\omega_p)^2} \quad (6.18)$$

$$b_n^{UPI} = \frac{b_n K_p - (\frac{K_I}{n\omega_p} - n\omega_p)a_n}{K_p^2 + (\frac{K_I}{n\omega_p} - n\omega_p)^2} \quad (6.19)$$

and the amplitude spectrum:

$$A_n^{UPI} = \quad\quad\quad\quad\quad\quad\quad\quad\quad\quad\quad\quad\quad\quad\quad\quad\quad\quad (6.20)$$
$$= \sqrt{\left(\frac{a_n K_p + (\frac{K_I}{n\omega_p} - n\omega_p)b_n}{K_p^2 + (\frac{K_I}{n\omega_p} - n\omega_p)^2}\right)^2 + \left(\frac{b_n K_p - (\frac{K_I}{n\omega_p} - n\omega_p)a_n}{K_p^2 + (\frac{K_I}{n\omega_p} - n\omega_p)^2}\right)^2}$$

Since the controller involves an integral action, we have:

$$U^m = U^*$$

meaning that the **mean value** of the *PI* controlled volume profile U^m **coincides** with the **reference value**, U^*.

The Fourier series representation of the manipulated output flow rate $w(t)$ is:

$$w(t) = w^m + \sum_{n=1}^{\infty} a_n^{wPI} \cos(n\omega_p t) + \sum_{n=1}^{\infty} b_n^{wPI} \sin(n\omega_p t)$$

with the coefficients:

$$a_n^{wPI} = a_n^{UPI} K_p - K_I \frac{b_n^{UPI}}{n\omega_p} \tag{6.21}$$

$$b_n^{wPI} = b_n^{UPI} K_p + K_I \frac{a_n^{UPI}}{n\omega_p} \tag{6.22}$$

and the spectrum:

$$A_n^{wPI} = \tag{6.23}$$

$$= \sqrt{(a_n^{UPI} K_p - K_I \frac{b_n^{UPI}}{n\omega_p})^2 + (b_n^{UPI} K_p + K_I \frac{a_n^{UPI}}{n\omega_p})^2}$$

Since the controller involves an integral action, we have

$$w^m = F^m$$

i.e. the mean value of the manipulated output flow rate of the tank is equal to the mean value of the input flow rate.

Note that the same expressions for the tank amplitude spectrums A_n^{UPI} (6.20) and w_n^{UPI} (6.23) are valid for the case when the operation, due to disturbances, has a period T_d (and in this case $\omega_d = \frac{2\pi}{T_d}$) and average discharge rate F^{md}. The influence of the control parameters K_p and K_I on the A_n^{wPI} and A_n^{UPI} are analysed in the following propositions.

Proposition 1 *The amplitude A_n^{wPI} of each harmonic n of the tank output flow rate tends to zero when the controller coefficients K_p, K_I tend to zero i.e.*

$$\lim_{K_p, K_I \to 0} A_n^{wPI}(K_p, K_I) = 0$$

Proof

Let $\beta = n\omega_p$ and $D(K_p, K_I) = K_p^2 + (\frac{K_I}{\beta} - \beta)^2$. We replace the volume Fourier series coefficients given by Equations (6.18) and (6.19) in the expression for the tank output flow rate amplitude Equation (6.23) as a result:

$$A_n^{wPI} = \sqrt{\frac{\left(K_p\beta\left(a_nK_p + (\frac{K_I}{\beta} - \beta)b_n\right) - K_I\left(b_nK_p + (\frac{K_I}{\beta} - \beta)a_n\right)\right)^2}{\beta^2 D^2(K_p, K_I)}} +$$

$$+\sqrt{\frac{\left(K_p\beta\left(b_nK_p + K_p(\frac{K_I}{\beta} - \beta)a_n\right) + K_I\left(a_nK_p + K_p(\frac{K_I}{\beta} - \beta)b_n\right)\right)^2}{\beta^2 D^2(K_p, K_I)}}$$

Developing the denominator $D(K_p, K_I)$ and simplifying the numerator we have

$$A_n^{wPI} = \sqrt{\frac{\alpha(K_p^4 + \frac{K_I^4}{\beta^4} - 2\frac{K_I^3}{\beta^2} + K_p^2 + K_I^2)}{\left(\phi(K_p, K_I) + \beta^4\right)}}$$

where $\alpha = a_n^2 + b_n^2$ and $\phi(K_p, K_I) = K_p^4(1 + \frac{1}{\beta^4}) + 2K_p^2(\frac{K_I}{\beta} - \beta)^2 - 4\frac{K_I^3}{\beta} + 6K_I^2 - 4K_I\beta$. Consequently:

$$\lim_{K_p, K_I \to 0} A_n^{wPI}(K_p, K_I) = \frac{0}{\beta^2} = 0$$

Proposition 2 *The amplitude A_n^{UPI} of each harmonic n of the PI controlled volume profile tends the corresponding open loop harmonic A_n^U, when the controller coefficients K_p, K_I tend to zero i.e.*

$$\lim_{K_p, K_I \to 0} A_n^{UPI}(K_p, K_I) = A_n^U$$

Proof

Referring to Equations (6.24) - (6.20) and developing $D(K_p, K_I) = (K_p^2 + \frac{K_I^2}{(n\omega_p)^2} - n\omega_p)^2$, it is evident that

$$\lim_{K_p, K_I \to 0} A_n^{UPI} = \sqrt{(\frac{b_n}{n\omega_p})^2 + (\frac{a_n}{n\omega_p})^2} = \frac{A_n}{n\omega_p} = A_n^U \qquad (6.24)$$

6.4 Tuning the PI controller for a performance trade-off

Recall that the PI-controlled **closed loop** tank has the following transfer functions:

with respect to the tank volume:

$$U(s) = \frac{K_I}{s^2 + K_p s + K_I} U^* + \underbrace{\frac{s}{s^2 + K_p s + K_I}}_{H(s)} F(s)$$

with respect to the output flow rate:

$$w(s) = \frac{K_I s}{s^2 + K_p s + K_I} U^* + \underbrace{\frac{(K_p s + K_I)}{s^2 + K_p s + K_I}}_{G(s)} F(s)$$

As we have seen in Section 6.3.1 the input signal F is a piecewise constant periodic signal represented by its Fourier series as

$$F(t) = F^m + \sum_{n=1}^{\infty} A_n \sin(n\omega_p t + \phi_n)$$

and the output signals $w(t)$ and $U(t)$ are

$$w(t) = w^m + \sum_{n=1}^{\infty} A_n^w \sin(n\omega_p t + \phi_n^w)$$

$$U(t) = U^m + \sum_{n=1}^{\infty} A_n^U \sin(n\omega_p t + \phi_n^U)$$

with $w^m = F^m$ and $U^m = U^*$.

$G(s)$ and $H(s)$ are second order transfer functions with a damping factor:

$$\zeta = \frac{K_p}{2\sqrt{K_I}}$$

A reasonable choice is to take $\zeta = 1$ (i.e. a double pole) which implies:

$$K_p = 2\sqrt{K_I}$$

Consequently we have:

$$H(s) = \frac{s}{(s + \sqrt{K_I})^2}$$

$$G(s) = \frac{2\sqrt{K_I}s + K_I}{(s + \sqrt{K_I})^2}$$

and the controller tuning reduces to the tuning of the parameter K_I.

The tuning has to achieve an acceptable trade-off between two conflicting objectives:

- Reduce as much as possible the amplitude of the output flow rate $w(t)$ (i.e. precisely the amplitude of the signal $w(t) - w^m$ or equivalently the set of harmonics amplitudes A_n^w).

- Guarantee a large enough security margin of the tank volume to avoid overflows or underflows.

A measure of the relative attenuation of the $w(t)$ amplitude is given by the norm of $G(s)$ evaluated at ω_p:

$$|G(j\omega_p)| = \frac{\sqrt{K_I}\sqrt{(K_I + 4\omega_p^2)}}{K_I + \omega_p^2}$$

Indeed, it is clear that the amplitude of the fundamental harmonic A_1^w of $w(t)$ will be attenuated be a factor $|G(j\omega_p)|$ with respect to

the amplitude A_1 of the fundamental harmonic of $F(t)$, and, necessarily the higher order harmonics will be still more attenuated because $|G(jn\omega_p)| < |G(j\omega_p)|$ for $n > 1$. In addition, since we want $|G(j\omega_p)|$ to be small, it is clear that $K_I << \omega_p$ and therefore that an acceptable approximation is:

$$|G(j\omega_p)| \cong \frac{2\sqrt{K_I}}{\omega_p} \triangleq \alpha \qquad (6.25)$$

On the other hand, the **tank volume security margin** is related to the tank behaviour in presence of disturbances. Let us consider parametric step disturbance as we have introduced in Section 3.3. We assume that the system has a steady-state periodic behaviour and that at some time instant t_0, a step disturbance occurs. The effect of this disturbance can be modeled by two different step modifications of the input signal $F(t)$:

- a step modification of the maximal flow rate $F^{max} \rightarrow F^{max} + \Delta F^{max}$ which also leads to modification of the mean flow rate i.e. $F^m \rightarrow F^m + \Delta F^m$

- a step modification of the period $\omega_p \rightarrow \omega_p + \Delta\omega_p$ which also leads to the modification of the mean flow rate i.e. $F^m \rightarrow F^m + \Delta F^m$

Let us assess the effect of the step ΔF^m on the signal $\Delta U^m = U^m - U^*$. In Laplace coordinate we have:

$$\Delta U^m(s) = H(s)\Delta F^m(s)$$

while in time coordinate we have

$$\Delta_U^m(t) = \Delta F^m(t - t_0) \exp^{-\sqrt{K_I}(t-t_0)} \quad t \geq t_0$$

(see illustration in Figure 6.21).

The extremal deviation occurs at time $t_m - t_0 = 1/\sqrt{K_I}$. Its value is:

$$\Delta_m \triangleq \Delta_U^m(t_m) = \frac{\Delta F^m}{e\sqrt{K_I}} \qquad (6.26)$$
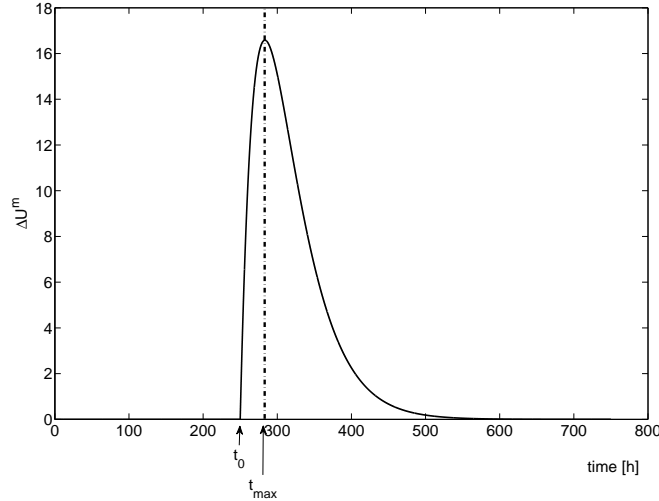
Fig. 6.21: Tank volume security margin

Hence, we can define Δ_m as the requested security margin of the tank volume. Finally, eliminating $\sqrt{K_I}$ between Equations (6.25) and (6.26), we get the following equation:

$$\boxed{\alpha(\frac{\Delta_m}{\Delta F^m}) = \frac{2}{e\omega_p}} \tag{6.27}$$

which is the **fundamental trade off relation** for the control tuning. This relation clearly shows the conflict between the output flow rate amplitude attenuation (represented by α) and the relative tank volume security margin (represented by $\frac{\Delta_m}{\Delta F^m}$).

This relation can be considered as defining a set of equivalent "Pareto-optimal" solutions (See Figure 6.22) where one performance criterion (e.g. α) can be improved only if the other performance criterion (e.g. $\frac{\Delta_m}{\Delta F^m}$) is degraded.

Another parameter of the PI controller which has to be set up is the reference values U^*. For safety reasons we assume that the minimal reactor volume is larger than zero $U^{min} > 0$ $[m^3]$. On the other hand knowing the values of the reactor security margin Δ_m as well as the
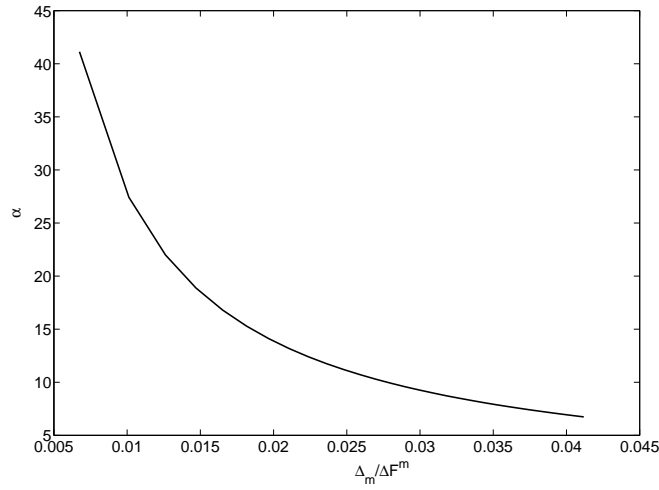
Fig. 6.22: "Pareto-optimal" solutions, $K_I \in \{0.8 * 10^{-4}, 0.3 * 10^{-2}\}$

variation of the tank volume profile in the absence of disturbances i.e. $\Delta_U^{sch} = U_{max}^{sch} - U_{min}^{sch}$ (See Figure 6.23) the volume reference U^* is:
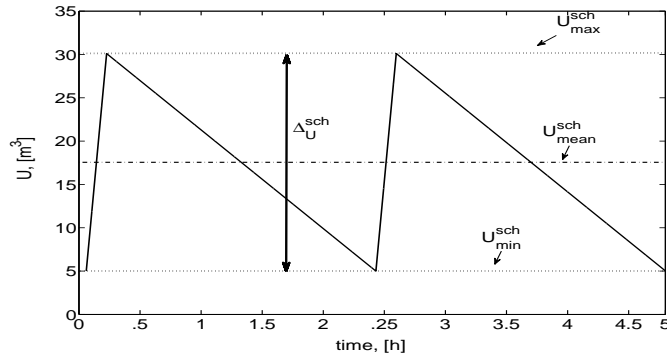
Fig. 6.23: Scheduled volume variation Δ_U^{sch}

$$U^* = U^{min} + \frac{\Delta_U^{sch}}{2} + \Delta_m \qquad (6.28)$$

As a result the maximal tank volume is

$$U^{max} = U^* + \frac{\Delta_U^{sch}}{2} + \Delta_m \tag{6.29}$$

We now illustrate this methodological analysis with a simulation study.

6.4.1 Simulation examples

Example 1 Consider a PI controlled storage tank such that:

i. input flow rate with *frequency* $\omega_p = 1.33$ $[rad/h]$, *amplitude* $F^{max} = 162$ $[m^3/h]$, *mean value* $F^m = 11.39$ $[m^3/h]$;

ii. the *output flow rate amplitude attenuation* is requested to be $\alpha = 4\%$;

iii. the *minimal tank volume* $U^{min} = 5$ $[m^3]$ and the *amplitude of the volume profile* (in the absence of disturbances) is $\Delta_U^{sch} = 25$ $[m^3]$;

iv. at time $t_0 \approx 140$ a step disturbance occurs on the maximal value of the discharging rate of each reactor F_{disch}^i such that it is changed from 162 $[m^3/h]$ to 142 $[m^3/h]$. As a result the characteristics of the total input flow rate of the tank $F(t)$ are changed as follows:

a) $\omega_p = 1.33$ $[rad/h]$, $F^{max,d} = 142$ $[m^3]$ and $F^{m,d} = 10$ $[m^3/h]$;

Determine:

i. the controller coefficient K_I;

ii. the relative tank volume security margin $\frac{\Delta_m}{\Delta F^m}$ and the reference value of the PI controller U^* (and respectively the size of the tank);

The problem is solved as follows:

Using Equation (6.25) it is easily found that $\sqrt{K_I} = 0.03$ and respectively $K_I = 0.0009$. Taking into account the existing disturbance $\Delta F^m = |F^m - F^{m,d}| = 1.39$ $[m^3/h]$ (see Figure 6.24 A) referring to

Equation (6.26) the tank volume security margin is $\Delta_m = 16.6 \; [m^3]$.

We know that $U^* = U_0 + \Delta_m + \frac{\Delta_U^{sch}}{2}$ respectively $U^* = 34 \; [m^3]$ and as a result by Equation (6.29) $U_{max} = 63.01 \; [m^3]$.

In order to evaluate the exact output flow rate amplitude we approximate the inflow rate with a *sine wave* with amplitude $F^{max,d}$ i.e. $F(t) \approx F^{max,d} \sin(\omega_p t)$. In Laplace transform:

$$F(s) = \frac{F^{max,d} \omega_p}{s^2 + \omega_p^2}$$

and its amplitude at $\omega = \omega_p$ is

$$|F(j\omega_p)| = \frac{F^{max,d}}{\sqrt{\omega_p^2 - 1}} = 58 \; [m^3/h]$$

Consequently using again Equation (6.25) it is found that:

$$|w(j\omega_p)| = \alpha |F(j\omega_p)| = 1.3 \; [m^3/h].$$

The controller coefficients $K_I = 0.0009$ and $U^* = 34 \; [m^3]$ are applied on the plant simulator and the simulation results are given in Figures 6.24-6.25. It is seen that the results coincide well with the theoretical expectations.

Let us now show that the developed methodological analysis is applicable also in a case of stochastic disturbances. Now we define the problem as follows.

Example 2 Let the above closed loop tank system having $U^{min} = 5$ $[m^3]$; $U_{max} = 63.01 \; [m^3]$ and a *PI* controller with $K_I = 0.0009$ (i.e $\alpha = 4\%$) is subject to:

i. a normally distributed stochastic disturbance on the maximal value of the tank input flow rate, appearing at time $t_0 \approx 140 \; [h]$. The mean value of the disturbance is equal to the ideal maximal input flow rate i.e. $F^m_{stoh} = F^{max} = 162 \; [m^3/h]$.

The aim is to determine the bound of the standard deviation of F^m_{stoh} $[m^3/h]$ i.e. $\sigma_{F^m_{stoh}} \; [m^3/h]$ such that the minimal and maximal volume
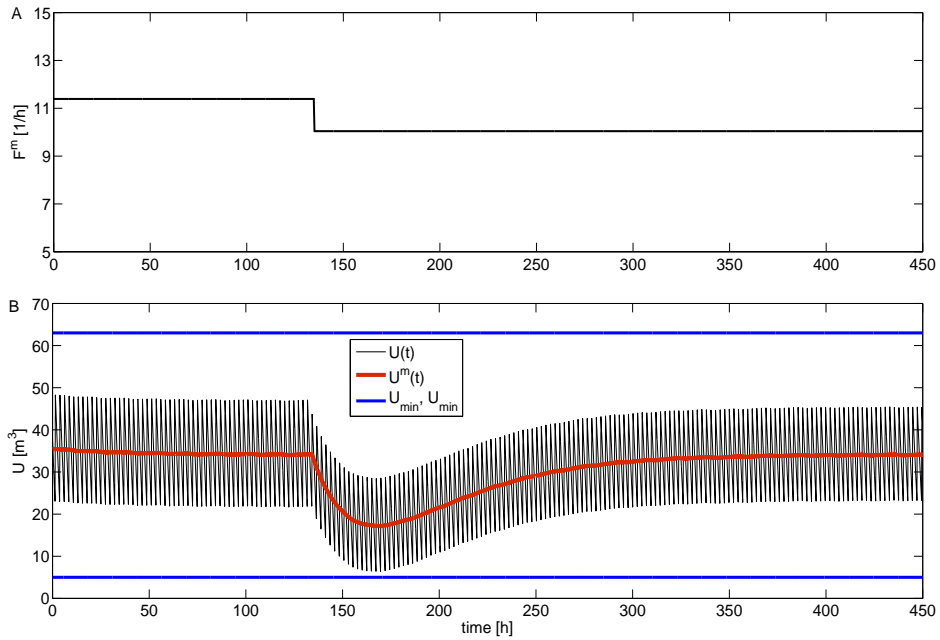
Fig. 6.24: Step disturbance of F^{max}: A - Mean input flow rate; B - PI controlled tank volume profile
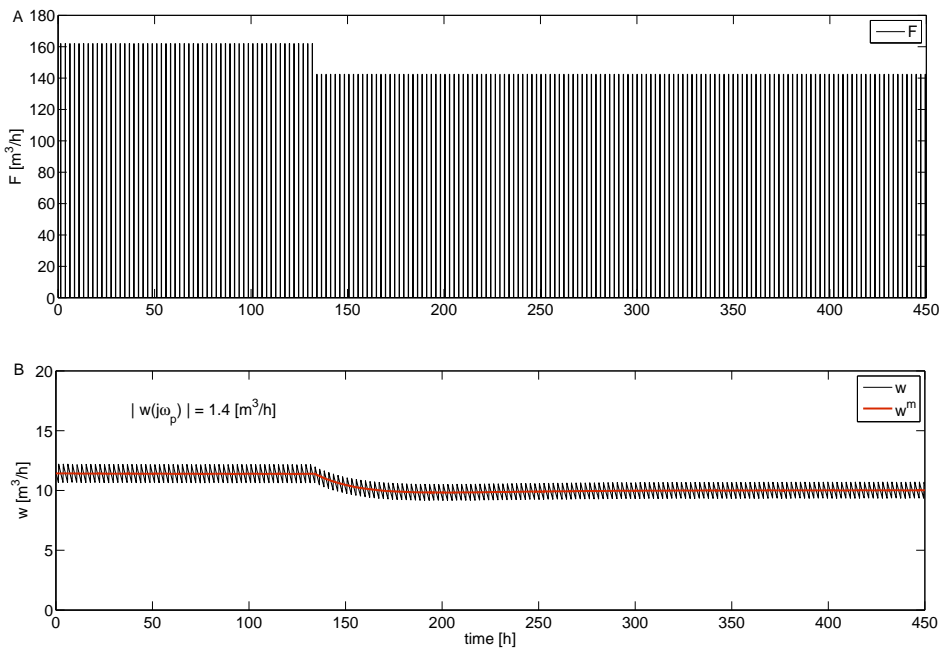
Fig. 6.25: Step disturbance of F^{max}: A - Tank input flow rate; B - PI controlled output flow rate
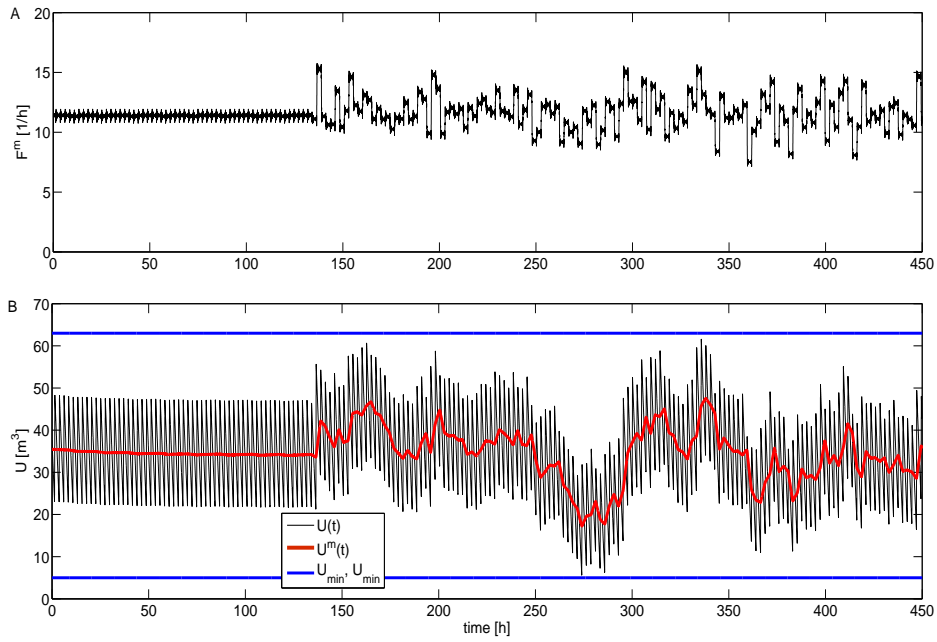
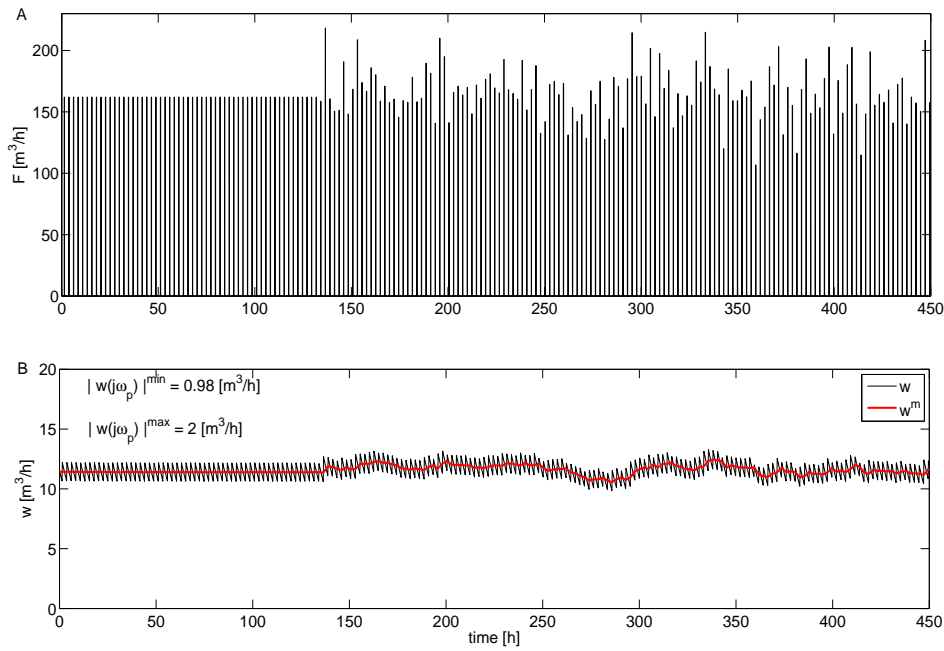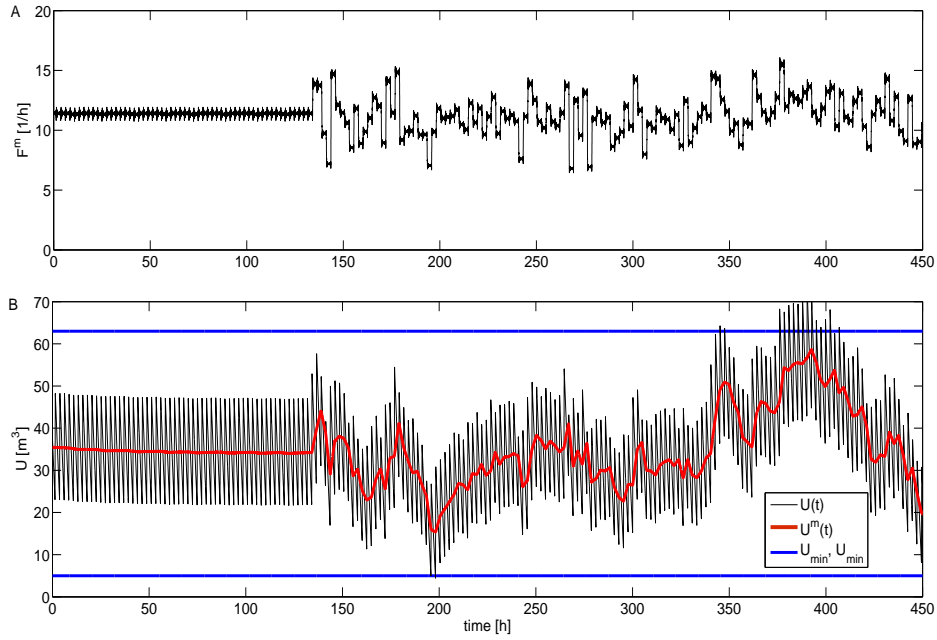Fig. 6.26: Stochastic disturbance on F^{max} (Δ_m satisfied): A - Mean input flow rate; B - PI controlled tank volume profile
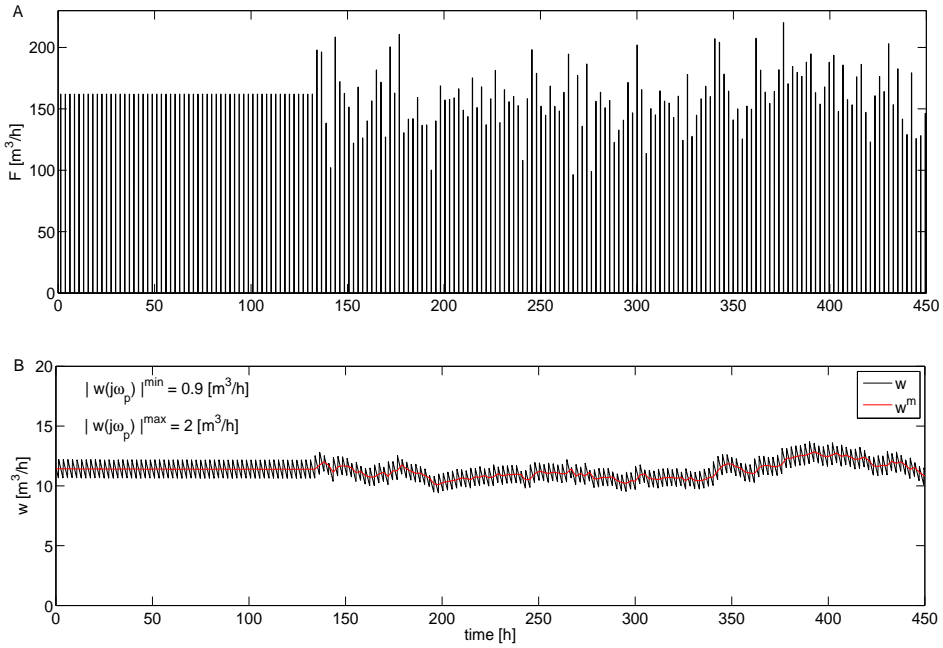

Fig. 6.27: Stochastic disturbance on F^{max} (Δ_m satisfied): A - Tank input flow rate; B - PI controlled output flow rate

Fig. 6.28: Stochastic disturbance on F^{max} (Δ_m **not** satisfied): A - Mean input flow rate; B - PI controlled tank volume profile

Fig. 6.29: Stochastic disturbance on F^{max} (Δ_m **not** satisfied): A - Tank input flow rate; B - PI controlled output flow rate

bounds must not be exceeded.

The problem is solved by performing a set of simulations on the plant simulator and the graphical results are given in Figures 6.26 - 6.29.

It is seen in Figure 6.26 B that if $\sigma_{F^m_{stoh}} = 20 \ [m^3/h]$ the PI controlled tank volume is in the desired bounds. The tank output flow rate is shown in Figure 6.27 B; $|w(j\omega_p)|^{min} = 0.98 \ [m^3/h]$ and $|w(j\omega_p)|^{max} = 2.0 \ [m^3/h]$ are its minimal and maximal amplitudes, corresponding to $F^{min}_{stoh} = 106 \ [m^3/h]$ and $F^{max}_{stoh} = 118 \ [m^3/h]$, respectively. Note that as desired the attenuation is of 2%.

For $\sigma_{F^m_{stoh}} = 26 \ [m^3/h]$ it is seen in Figure 6.28 B that the volume bounds are exceeded. Nevertheless as shown in Figure 6.29 B the desired the attenuation of 2% of the tank output flow rate is achieved. Naturally the minimal and the maximal flow rate amplitudes are smaller and respectively bigger than when a standard deviation of 20 $[m^3/h]$ is used. Here $|w(j\omega_p)|^{min} = 0.88 \ [m^3/h]$ and $|w(j\omega_p)|^{max} = 2.03 \ [m^3/h]$, corresponding to $F^{min}_{stoh} = 96 \ [m^3/h]$ and $F^{max}_{stoh} = 120 \ [m^3/h]$, respectively.

Example 3 Consider a PI controlled storage tank having:

i. input flow rate with *frequency* $\omega_p = 1.33 \ [rad/h]$ and *mean value* $F^m = 11.39 \ [m^3/h]$;

ii. the *output flow rate amplitude attenuation* is selected to be $\alpha = 4\%$;

iii. the *minimal tank volume* $U^{min} = 5 \ [m^3]$ and the *amplitude* of the volume profile is $\Delta_U = 25 \ [m^3]$;

iv. at time $t_0 \approx 140$ a step disturbance occurs on both reactors simultaneously such that

a) their heating temperature decreases incidentally from $T_h = 380$ $[K]$ to $T_h = 345 \ [K]$ (i.e. with -9%). Due to this perturbation the plant period is changed from 4.74 $[h]$ with $\omega_p = 1.33 \ [rad/h]$ to $T_p = 5.36 \ [1/h]$ with $\omega_p = 1.172 \ [rad/h]$ and consequently

the tank input flow rate has the same period with a mean value of $F^{m,d} = 10.1 \; [m^3/h]$ (See Figures 6.30 A - 6.31 A).

Determine:

i. the controller coefficient K_I;

ii. the relative tank volume security margin $\frac{\Delta_m}{\Delta F^m}$ and the reference value of the PI controller U^* (and respectively the size of the reactor);

The problem is solved similarly to Example 1.

Using Equation (6.25) it is easily found that $\sqrt{K_I} = 0.014$ and respectively $K_I = 0.0002$. Taking into account the existing disturbance $\Delta F^m = |F^m - F^{m,d}| = 1.29 \; [m^3/h]$ (see Figure 6.30 A) referring to Equation (6.26) the tank volume security margin is $\Delta_m = 18.17 \; [m^3]$. By using (6.28) and (6.29) it was found that: $U^* = 37.5 \; [m^3]$ and $U^{max} = 68.67 \; [m^3]$. The tank volume profile and its output flow rate are given in Figures 6.30 B-6.31 B.

6.5 Conclusions

In this Chapter we have analyzed the plant behaviour in the presence of constant or (piecewise constant) errors of the plant parameters and measured values. These errors can induce a resource conflict as well as a buffer tank overflow or wash-out. Consequently two control strategies are proposed and analyzed: a one based on a model predictive control approach and a simple PI control, respectively. The application of the former shows that in the case of a constant disturbance the resource conflict is avoided and the plant trajectory converges to a new periodic solution with a period larger than the one before the disturbance. The conflict is also avoided in the case of a stochastic disturbance but the operation is no more periodic. In accordance with the stability results obtained in **Chapter** 3 when the plant is driven by the optimal schedule no conflict is detected by the MPC but the hybrid trajectory converges to a new sub-optimal schedule. The simulation results from the application of the PI control of the tank, in
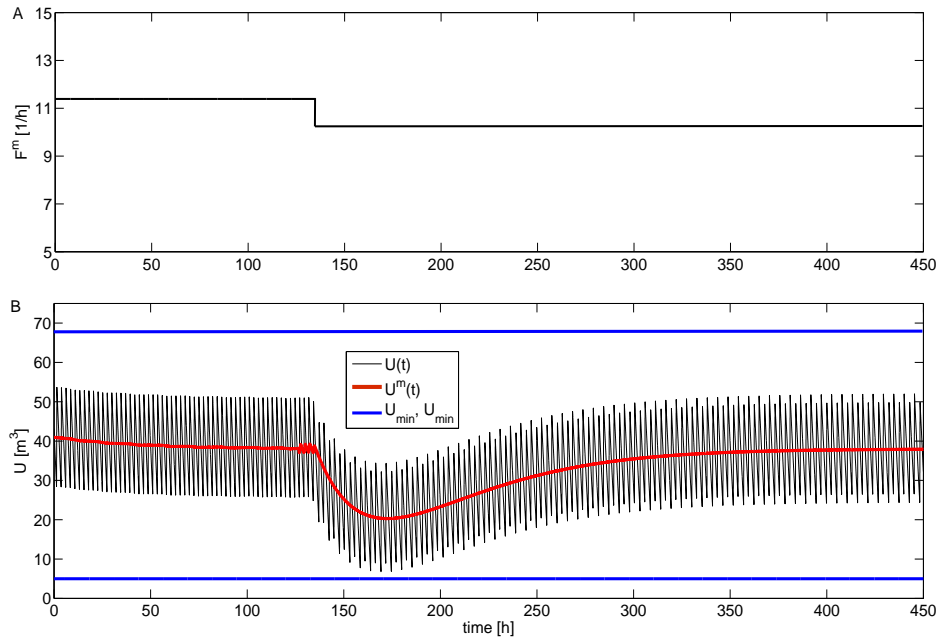
Fig. 6.30: Step disturbance on the period T_p: A: Mean input flow rate; B: PI controlled tank volume profile
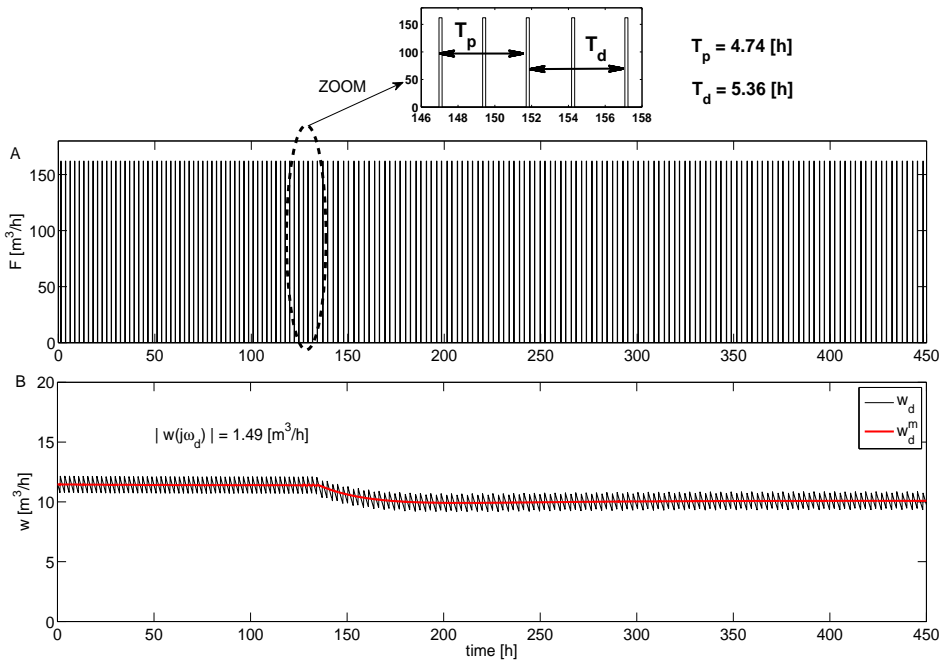

Fig. 6.31: Step disturbance on period T_p: A: Tank input flow rate; B: PI controlled output flow rate

case of step and stochastic disturbances clearly show that thanks to the developped methodology the desired trade-off namely, to reduce as much as possible the amplitude of the tank output flow rate and to assure a large enough security margin of the tank volume to avoid overflows or wash-outs is achieved.

Chapter 7

Conclusions

In this thesis, we have studied the problems of the: simulation modelling; design of off-line periodic schedules through simulation and the feedback control of periodic schedules in the presence of disturbances for "hybrid" chemical plants.

Simulation modelling. In **Chapter** 2 the processes performed in each reactor and the buffer tank are separately modeled by a hybrid automaton and the overall model is obtained as a combination of all hybrid automata models. According to the hybrid automaton formalism, for each unit all operation phases are defined and to each phase is associated a set of continuous differential equations (mass and energy balances). The phases sequence and the transition conditions between them which are driven by external or internal events are also specified. The main advantage of this separate modeling is that it avoids the enumeration over all elements of the discrete set of phases, the set of continuous-time and discrete-time dynamics, needed to model the plant behaviour at any time. A *Matlab-Simulink-Stateflow* environment is used for the development of a numerical simulator of the plant.

Design of off-line periodic schedules. Through a set of three cases studies in **Chapter** 3 it is shown that the *Simulink-Stateflow* simulator is a very useful tool for the design of periodic schedules such that resource sharing is achieved.

As a first step, by the simulator and the developed heuristic rule a set of schedules is discovered such that the overall plant behaviour

is always converging to the same periodic trajectory which appears to be an attracting limit cycle of the hybrid chemical plant. In the special case where the plant operation is initialised on the limit cycle, the operation is periodic right from the beginning. By optimal schedule we mean that the reactors operate at the maximal possible flow/transfer rates and that their stand by times are zero, as a result the highest possible productivity is achieved. As presented in Chapter 5 the optimal schedule gives better productivity results than the ones obtained by some other sub-optimal scheduling approaches. However for more general plants with a large number of batch reactors, the optimal control problem is clearly a highly nonlinear optimization problem which is extremely complicated. It is probably hopeless to try to design computer algorithms able to exactly solve this problem with a reasonable computational burden and within a reasonable time.

Furthermore the periodic plant operation can be made more flexible by adding stand-by times on the reactors to slow down the production rate for some reasons. Another advantage of the additional stand by times is that in the case of disturbance or model inaccuracies, they can be adjusted by the MPC based control algorithm, as defined in Chapter 6, to avoid resource conflict.

The stability analysis of the obtained by the heuristic rule optimal schedule, made in Chapter 4, shows that it is stable. During the modeling and the stability analysis we have considered two specific "reset maps" but more general functions $x^+ = h_{ij}(x^-)$ could be considered as well. Essentially $h_{ij} : \Re^n \to \Re^n$ is a diffeomorphism and x^+, x^- refer to the values of the state just after, and just prior to, the event respectively [His05].

Feedback control. The last issue, studied in **Chapter** 6 of the thesis, is the on-line scheduling of the plant in the presence of constant (or piecewise constant) disturbances on the plant parameters. We consider the plant operating under a periodic schedule. It was shown that two problems may arise, namely: the resource conflict and the tank over/under filing. For their solution which two independent control strategies are proposed: model based predictive

control (MPC) and a classical *Proportional - Integral* (PI) control, respectively.

The application of the former is used to avoid a conflict for the available quantity of cold water arising in the next reactor cycle. Through the simulations it is shown that in the case of a constant disturbance the conflict is avoided and the plant trajectory converges to a new sub-optimal periodic solution. The conflict is also avoided in the case of a stochastic disturbance but the operation is **no longer** periodic. In accordance with the stability results obtained in **Chapter** 3 when the plant is driven by the optimal schedule no conflict is detected by the MPC but the hybrid trajectory converges to a new sub-optimal schedule.

For the solution of the second problem the use of the classical continuous time PI control is possible because the plant operation is driven by periodic flow/transfer rates and as a result the hybrid storage tank process can be modelled not only by a hybrid automaton (**Chapter** 2), but also as a continuous process subject to periodic input/output signals. A Fourier series continuous time model of the tank is developed in **Chapter** 6.

The aim of the PI control not only to stabilize the buffer tank operation but also to achieve a performance trade-off. The obtained relation:

$$\boxed{\alpha(\frac{\Delta_m}{\Delta F^m}) = \frac{2}{e\omega_p}}$$

is called a **fundamental trade off relation** for the control tuning. Actually it can be considered as defining a set of equivalent "Pareto-optimal" solutions (See Figure (7.1)) where one performance criterion (e.g. the relative attenuation of the tank output flow rate amplitude, α) can be improved only if the other performance criterion (e.g. the relative tank volume security margin $\frac{\Delta_m}{\Delta F^m}$)) is degraded.
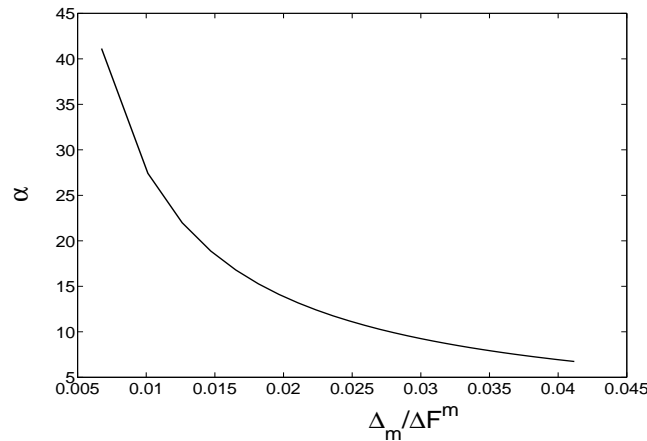
Fig. 7.1: "Pareto-optimal" solutions

The simulation results in case of step and stochastic disturbances clearly show that the desired trade-off namely, to reduce as much as possible the amplitude of the tank output flow rate and to assure a large enough security margin of the tank volume to avoid overflows or wash-outs is achieved.

The problem of the on-line scheduling of "hybrid" chemical plants having a lot of parallel production lines and shared limited resources is far to be solved.

In practice the chemical plants have more than two parallel working reactors, consequently a future extension of the proposed MPC such as to consider more reactors could be a challenging issue.

As we have seen through the simulations, by means of the proposed MPC strategy, the plant trajectory converges to a new periodic schedule. An interesting question would be to extend the limit cycle stability analysis of **Chapter** 4 to the case of the closed loop plant under MPC.

As was defined the drawback of the developed MPC approach is that it is used to solve a resource conflict arising in the next cycle of the reactor processes. Naturally an interesting investigation could be its developpment in order to avoid a conflict appearing in the current cy-

cle.

A future direction can be the combination of the developed MPC based feedback control with an optimization scheduling based for instance on $MILP$ approach. The main issue here could be the definition of a criteria stating that a new periodic production schedule is computed as soon as some performance criteria is degraded. Some results in this direction are already given in [SWB$^+$05b].

Chapter A

Appendix 1

A.1 Plant simulator

The plant simulator presented briefly in Chapter 3 is given here in details. A compete guide of the used *Simulink* and *Stateflow* graphical components and functions can be found in [Inc96] [Mat02].

Recall that the main *Simulink* model of the plant simulator shown in Figure (A.1) has four basic modules, namely:

  i. 2 subsystems: *Batch Reactor* 1 and *Batch Reactor* 2 to simulate the HAM of each batch reactor;

 ii. a subsystem: *Storage Tank* to simulate the HAM of the tank;

iii. 2 subsystems: $Qc1\_cool(t)$ and $Qc2\_cool(t)$, to calculate the cold water transfer rate, during the cooling phase of each reactor (See Section 3.3);

 iv. 2 subsystems: *w* and *w : PI - control*, the former is use to set output flow rate of the tank to its scheduled value and the latter to compute it based on a PI control law.
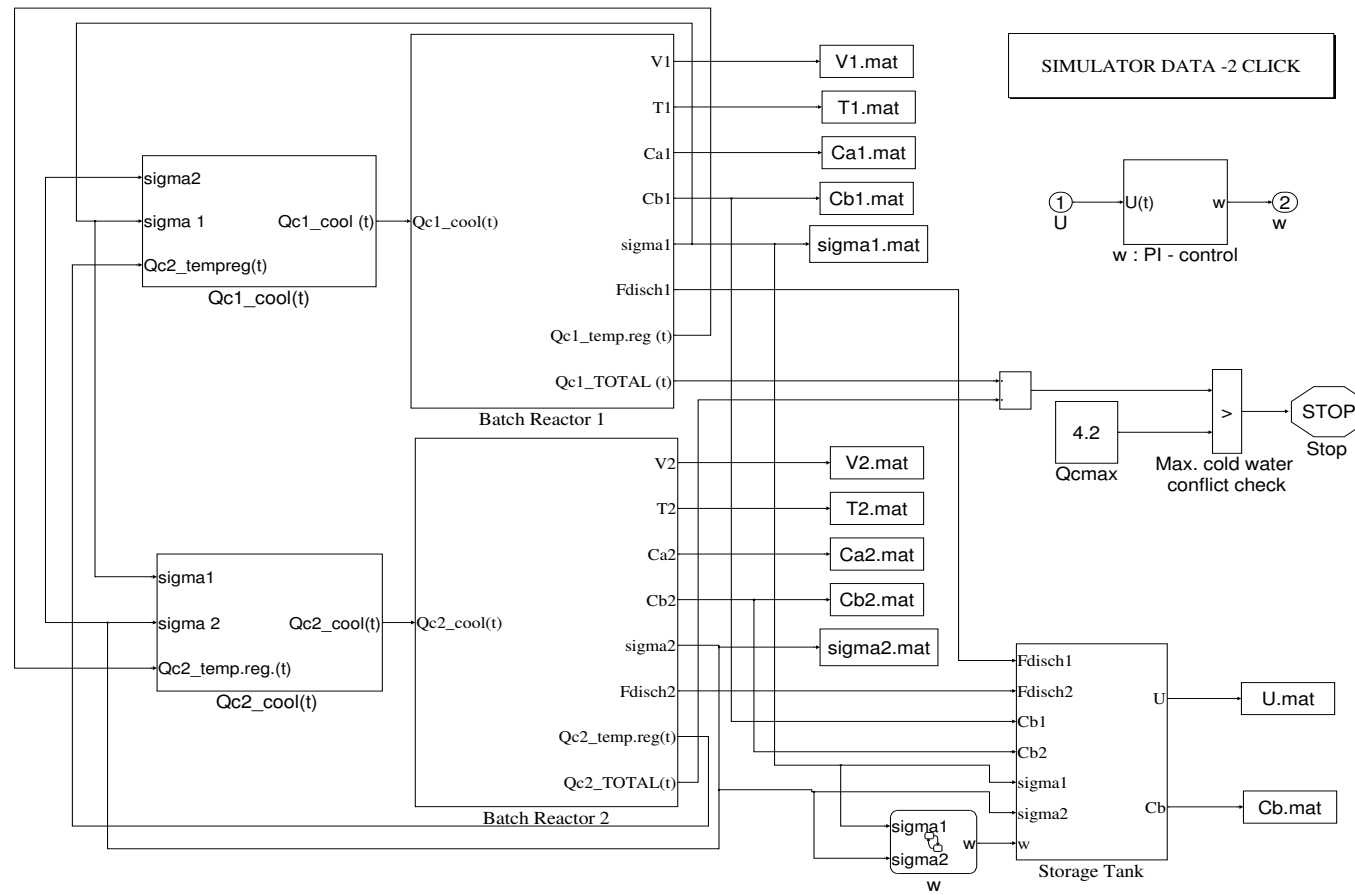
Fig. A.1: Plant simulator

Moreover:

  i. the block "SIMULATOR DATA - 2 CLICK" is used to load the plant parameters given in Tables (3.1) - (3.3), via a *Matlab* code in the *Matlab* work space;

 ii. the blocks "NAME.mat" are used to save the time evolutions of the reactors and the tank continuous and discrete state variables.

The various building modules of the simulator are described in more details hereafter.

A.2 Batch reactor one subsystem

The *Simulik-Stateflow* model of BR_1 is depicted in Figure (2.5) of Chapter 2, Section 2.2.1. This model is obtained after a double click on the *Batch Reactor* 1 block of Figure (A.1). The model of BR^2 is identical (Subsection A.5.1). The BR_1 model has of two mutually connected subsystems: a *Stateflow* and a *Simulink* diagrams.

The *Stateflow* diagram of BR_1 is presented in Chapter 2, Figure (2.6). Recall that the *Simulink* blocks used to model the continuous dynamics of the BR_1 HAM during each phase has the form shown in Figure (A.2). The sub-systems give the time evolution of the state variables: *V1, Ca1, Cb1, T1* as well as the one of the cooling water used during the BR_1 reaction phase *Qc1_temp.reg.(t)*.

The content of the first block of the model i.e. the `Volume   mass balance` block has been already presented in Chapter 2, Figure (2.8).

The *Simulink* blocks presented in Figure (A.3) are obtained after a double click on the *Simulink* sub-system `Reactant A mass balance` and are used to model the Equations (A.1). The the input variables `k3` ; `Carest` and `Cain` are coming from *Stateflow* digram given in Figure (2.6). Based on the active phase the variable `k3` makes active one of the Equations (A.1). It accepts value 1 during the phases **Heating, Temp.Reg. and Cooling** and 0 otherwise (meaning that there is no change in the reactant A dynamics e.g. $C_A^1 = C_{A,in}$). The variables `Carest` and `Cain` are used to **reset** the initial conditions for the
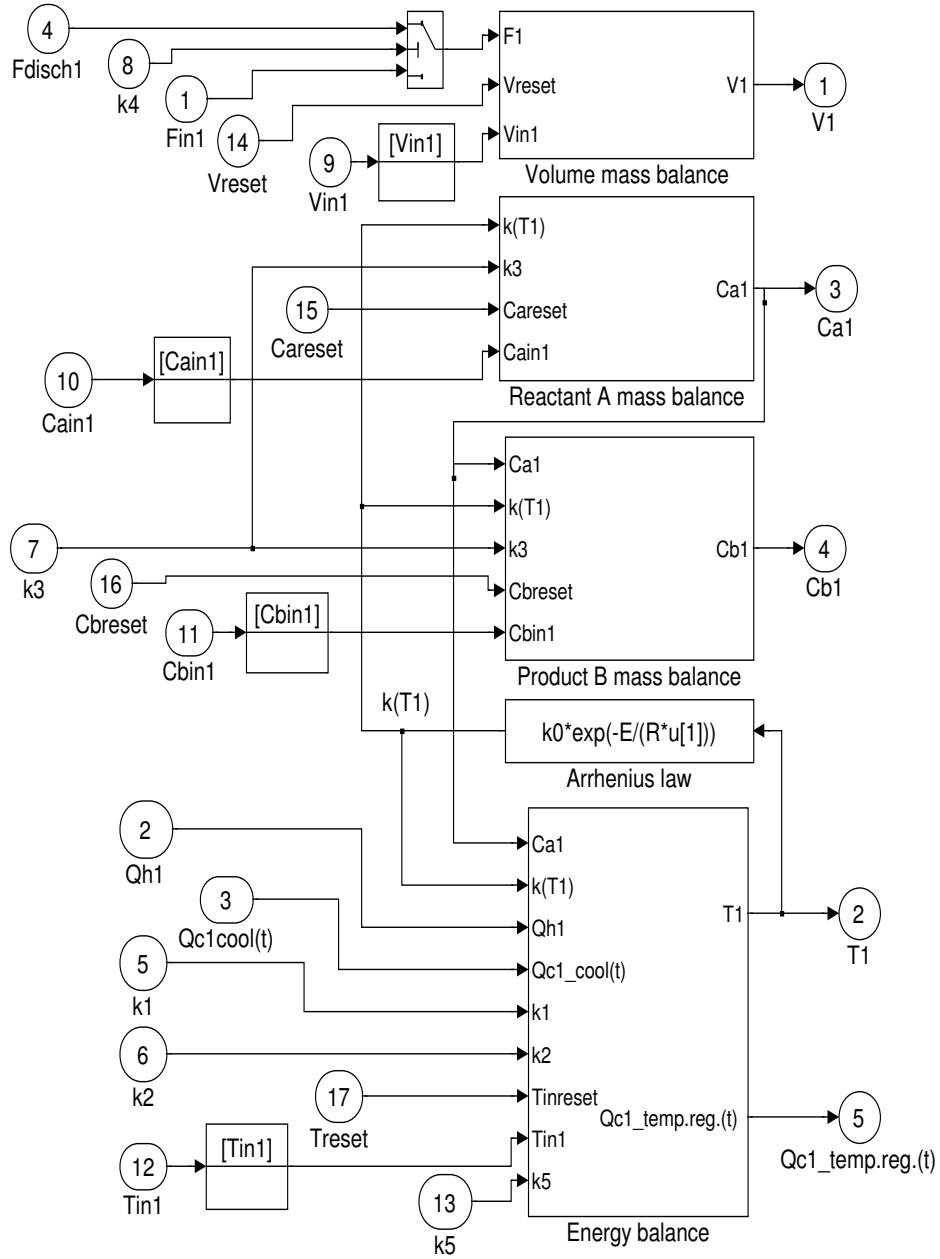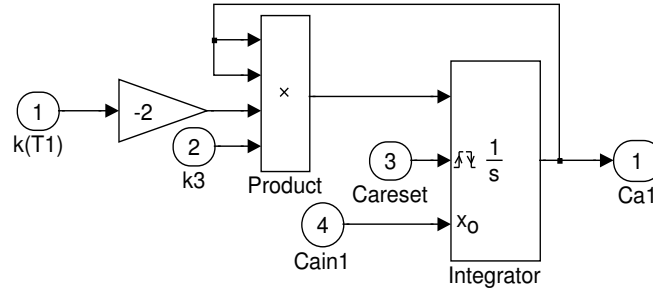
Fig. A.2: BR_1 Simulink model

Fig. A.3: BR_1 Simulink model of the reactant A mass balance Equations (A.1)

phases **Stand by Filling** and **Filling** (See Chaper 2, Section 2.2.1). The input signal $k(T1)$ models the dependence of the reaction rate on the temperature by an *Arrhenius law* i.e. $k(T^i) = k_0 exp^{-\frac{E}{RT^i}}$ (see the 4th block in Figure (A.2)). The output of the model is the reactant concentration Ca1.

$$
\begin{aligned}
\textbf{Stand by Filling:} \quad & C_A^i = 0 & \text{(A.1)} \\
\textbf{Filling, Stand by Heating:} \quad & C_A^i = C_{A,in} \\
\textbf{Heating, Temp.Reg. and Cooling:} \quad & \frac{dC_A^i}{dt} = -2k(T^i)(C_A^i)^2 \\
\textbf{Stand by Discharging, Discharging:} \quad & C_A^i = C_{A,tr}
\end{aligned}
$$

The *Simulink* diagram given in Figure (A.4) is used to model the product B mass balance equations (A.2). Similarly to the reactant A model it is also obtained after a double click on the *Simulink* subsystem Product B mass balance (Figure (A.2)) and it has the same inputs except for the variables Cbrest and Cbin which has the same purpose as for the reactant A. The model output is the product concentration Cb1. The continuous dynamics equations here are:
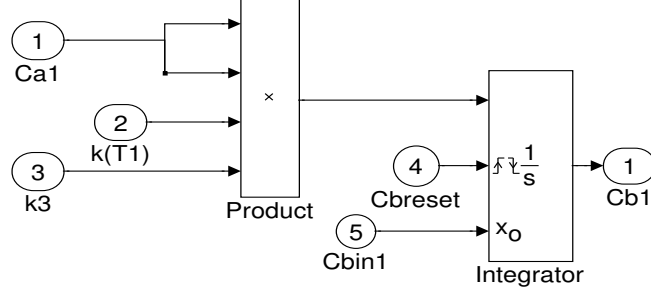
Fig. A.4: BR_1 Simulink model of the product B mass balance Equations (A.2)

$$\begin{aligned}
\textbf{Stand by Filling:}\quad & C_B^i = 0 & \text{(A.2)}\\
\textbf{Filling, Stand by Heating:}\quad & C_B^i = 0 \\
\textbf{Heating, Temp.Reg. and Cooling:}\quad & \frac{dC_B^i}{dt} = k(T^i)(C_A^i)^2 \\
\textbf{Stand by Discharging, Discharging:}\quad & C_B^i = C_{B,tr}
\end{aligned}$$

The contents of the *Simulink* `Energy balance` sub-system (Figure (A.2)) used to compute the temperature T^1 time evolution (Equations (A.3)) is given in Figure (A.5). It is composed of two sub-systems, the upper one models the energy balance during the **heating phase** (see Figure (A.6)) and the lower one the energy balance during the **temperature regulation and cooling phases** (see Figure (A.7)).

The inputs `k1`, `k2`, `Trest` and `Tin1` are coming from BR_1 *Stateflow* diagram (Figure (2.6)). Depending on the BR_1 phase, the variable $k1$ accepts values $\{1, 2, 3\}$ and $k2$ is 0 or 1. For instance if $k1 = 2$ and $k2 = 1$ then BR_1 is in the **heating phase**, consequently the $dT1/dt$ signal coming from the **heating** sub-system passes through the `Multiport Switch` block and then it is integrated; if $k1 = 1$ and $k2 = 0$ then BR_1 is in one of the stand by phases (e.g. $T^1 = T_a$, Equations (A.3)) or in the filling or discharging phase, consequently there is no change in T^1 dynamics. The variables `Trest` and `Tain reset` the T^1 initial conditions for the phases **Stand by Filling** and **Filling** (See Chaper 2, Section 2.2.1). The input variable `Qh1` comes also from the BR_1 *Stateflow* diagram (Figure (2.6)) and is used to set
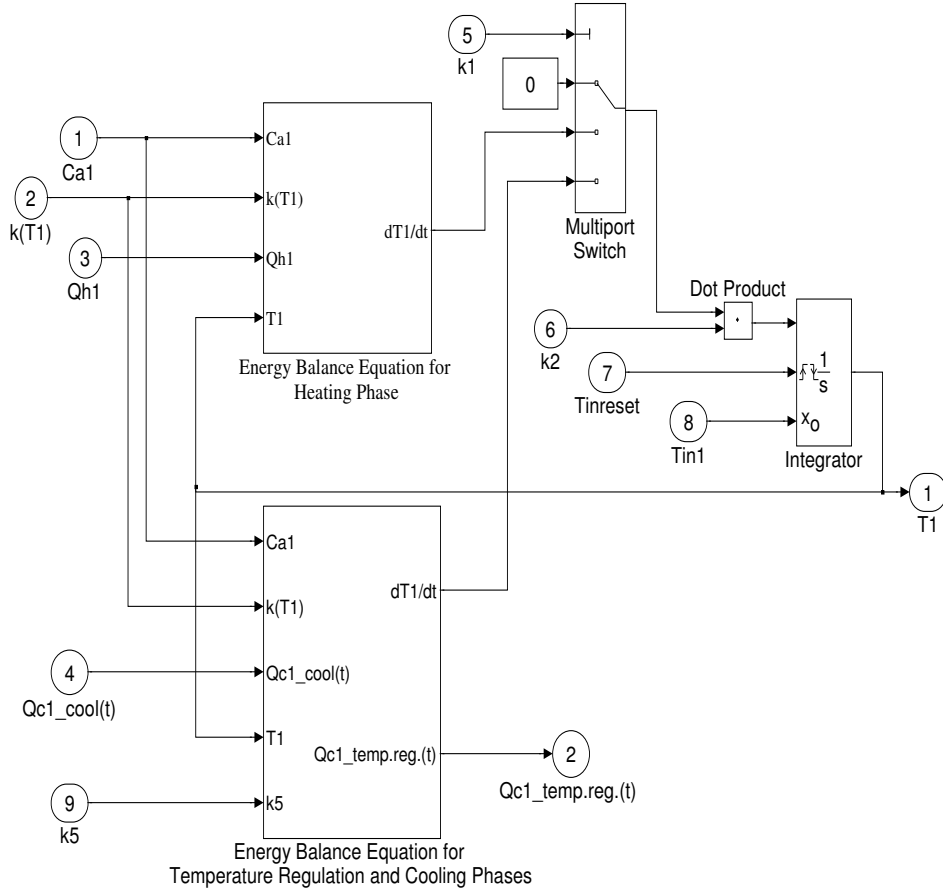
Fig. A.5: BR_1 Simulink model to compute the energy balance Equations (A.3)

the value of the hot steam flow rate to Q_h^{max} (or some other value) during the phase **heating** and to zero during all other phases. The last *Stateflow* input is k5 and it is used to compute the cold water profile of BR_1 needed during the reaction phase in which case $k5 = 2$ and it is 1 otherwise (See Figure (A.7)).

The inputs k(T1) (defined above) and Qc1_cool(t) (Figure (A.8)) are coming **outside** BR_1 *Stateflow diagram*. The outputs of the model are the temperature T1 and the cold water used during the reaction phase Qc1_temp.reg.(t).

$$\textbf{Stand by Filling:}\quad T^i = T_a \qquad \text{(A.3)}$$

$$\textbf{Filling, Stand by Heating:}\quad T^i = T_{in}$$

$$\textbf{Heating (see Figure (A.6)):}$$

$$\frac{dT^i}{dt} = -\rho k(T^i)(C_A^i)^2 + Q_h^i(T_h - T^i)$$

$$\textbf{Temp.Reg.:}\quad T^i = T_{max}$$

$$\textbf{Cooling see Figure (A.7)):}$$

$$\frac{dT^1}{dt} = -\rho k(T^i)(C_A^i)^2 + Q_h^i(T_h - T^i)$$

$$\textbf{Stand by Discharging, Discharging:}\quad T^i = T_{min}$$
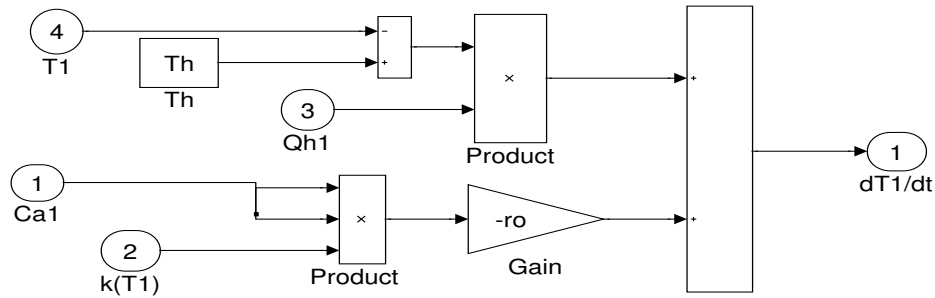
Fig. A.6: BR_1 Simulink model to compute the energy balance during the heating phase (Equations (A.3))

A.3 Cooling water subsystem for reactor one

The *Simuling* model of the algorithm for cooling water computing, given in Section 3.3, is shown in Figure (A.8). It is obtained after a double click on the block $Qc1$ *cool*(t) (Figure (A.1)). It has three main modules: two *Stateflow* subsystems *cold water sharing* and *Min. cold water conflict check* and a `Multiport Switch` block. The three model inputs are `sigma1` , `sigma2` (denoting the reactors phases) and $Qc2$
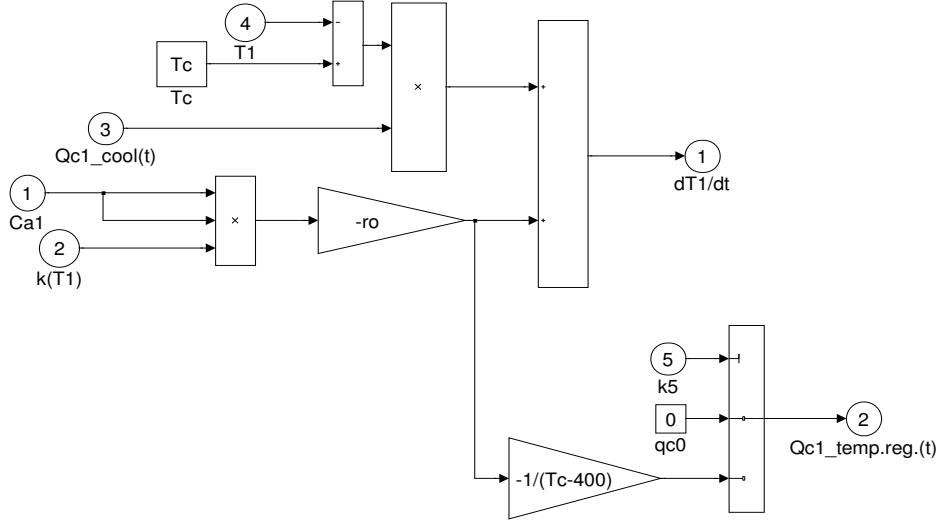
Fig. A.7: BR_1 Simulink model to compute the energy balance during the reaction and cooling phases (Equations (A.3))

temp.reg. (i.e. the cooling water time profile of BR_2 during the regulation phase, see Figure (A.23)). The output of the model is the cold water used during the BR_1 cooling phase `Qc1_cool(t)`.

Consider the *Stateflow* subsystem *cold water sharing* given in Figure (A.10). The state variable of the system is `cw1` and it accepts values $\{1, 2, 3, 4\}$ for the corresponding phases: $Qc0$ (BR_1 is not in the cooling phase); $Qcmax$ (BR_1 is alone in cooling); $Qcmaxdemi$ (BR^1 and BR_2 are together in the cooling phase); and finally $Qcmax\ TR2$ denoting that BR_1 is in the cooling while at the same time BR_2 is in the regulation phase, respectively. These values are used to switch the `Multiport Switch` block (Figure (A.8)) between the values 0, Q_c^{max}, $Q_c^{max}/2$ and $Q_{c,cooling}^1 = Q_c^{max} - Q_{c,temp.reg.}^2$, respectively. For instance if the state $Qcmax$ is active then $cw1 = 2$ and the `Multiport Switch` block passes the signal $Q_c^{max} = 4.2[h]$. On the other hand the phases transitions are performed depending on the working phase of both reactors. For instance the transition from the discrete state $Qc0$ to $Qcmax$ is done when BR_1 goes to cooling phase while at the same time BR_2 is neither at the cooling nor at the reaction phase. In state flow code

this is expressed as follows: [sigma1==6&sigma2~=5&sigma2~=6].

The *Stateflow* subsystem *Min. cold water conflict check* given in Figure (A.9) is used to determine the moment when the minimum cooling water condition is reached. As seen it has two discrete states *noconflict*; *minQcconflict* and a state variable *stp* accepting values 0 and 1, respectively. Initially the system is in state *noconflict* (this is indicated by the single arrow connected over this state) and $stp = 0$. As soon a minimal cooling water conflict is detected i.e. $Q^1(t) \leq Q_c^{min}$ (or in *Stateflow* code : [(sigma1==6)&Qc1<=2]) the transition to the state *minQcconflict* is taken and the state variable accepts values one i.e. $stp = 1$. The variable *stp* is connected with the *Simulink* Stop (Figure (A.8)) block and when $stp = 1$ this block is activated and the simulations stopped.
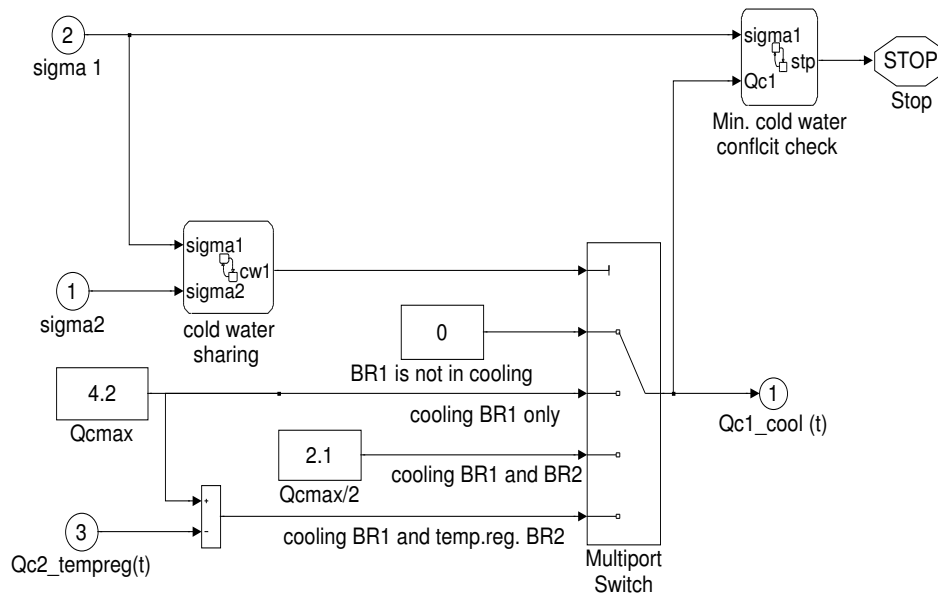
Fig. A.8: BR_1 Simulink model to compute the cold water during the cooling phase, see Section 3.3

noconflict

entry:
stp = 0;

[sigma1==6&Qc1<2]

minQcconflict

entry:
stp= 1;
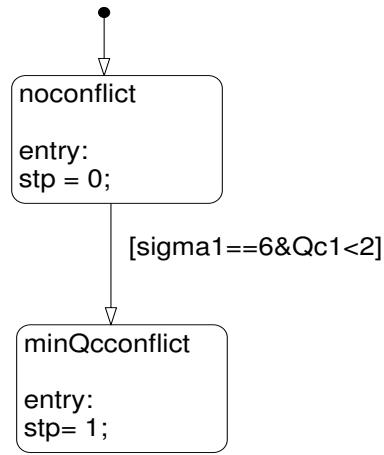
Fig. A.9: BR_1 Stateflow diagram to stop the simulation if a minimum cold water bound is reached, see Section 3.3
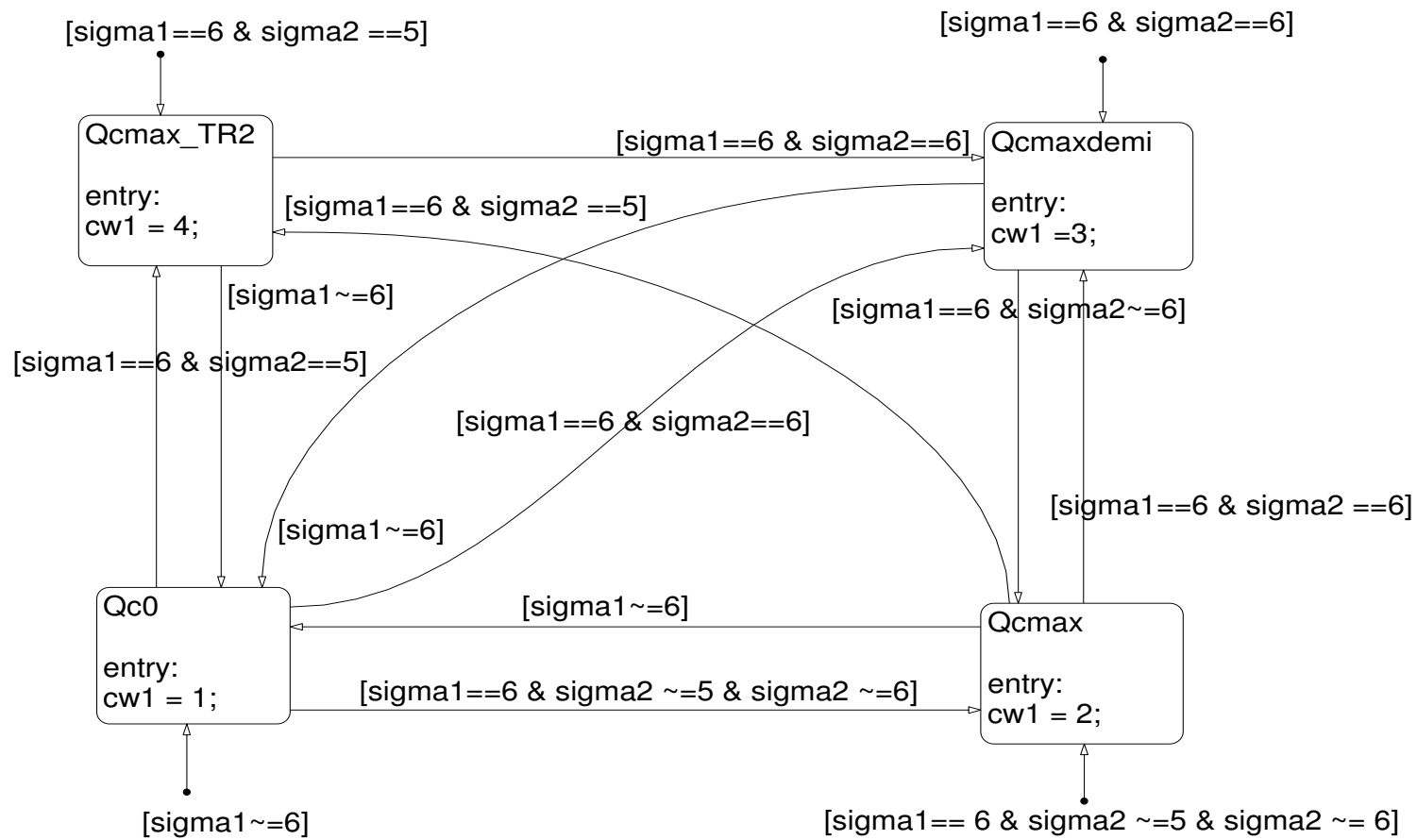
Fig. A.10: Stateflow diagram to set the values for the BR_1 cold water during the cooling phase, see Section 3.3

A.4 Tank subsystem
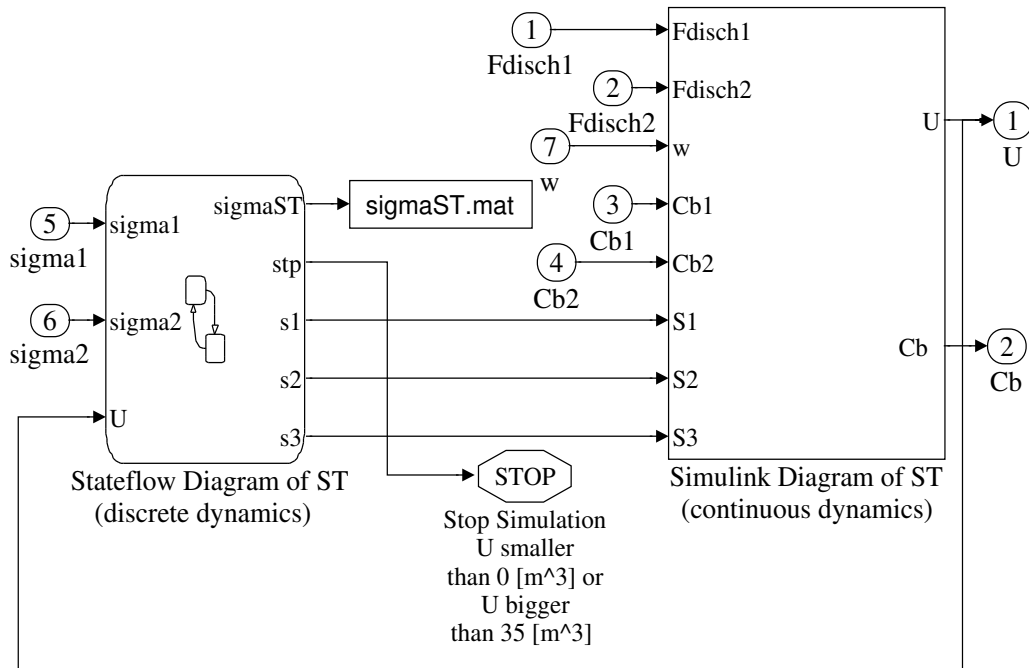
Fig. A.11: Simulink-Stateflow diagram of the storage tank

The *Simulik-Stateflow* model of tank is depicted in Figure (A.11). This model is obtained after a double click on the *Storage Tank* block of Figure (A.1). The *Stateflow* diagram was previously given in Figure (2.9) and the *Simulink* block to model the continuous dynamics equations is depicted in Figure (A.12). The inputs $S1$, $S2$, $S3$ are coming from its *Stateflow* diagram and are used to activate one of the three pairs of tank continuous dynamics equations given by Equation (A.4)).
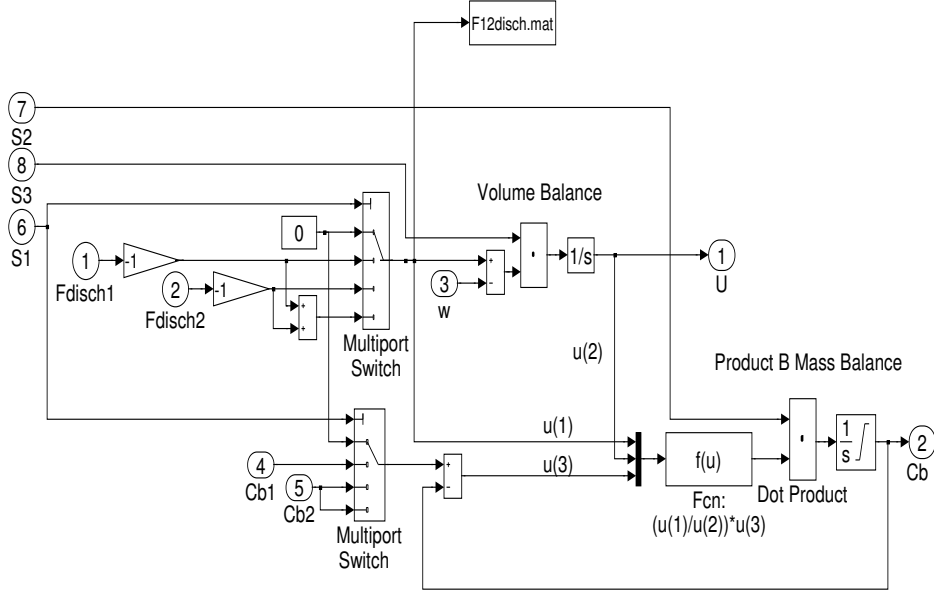
Fig. A.12: Simulink model of the storage tank

$$\textbf{Discharging:} \quad \frac{dU}{dt} = -w \qquad \text{(A.4)}$$

$$\frac{dC_b U}{dt} = 0$$

$$\textbf{Filling from } BR^i \quad \frac{dU}{dt} = F_{disch}^i - w$$

$$\textbf{and discharging:} \qquad \frac{dC_b U}{dt} = F_{disch}^i C_b^i - w$$

$$\textbf{Filling from } BR^1 \quad \frac{dU}{dt} = \sum_{i=1}^{2} F_{disch}^i - w$$

$$\textbf{and } BR^2 \textbf{ and discharging:} \qquad \frac{dC_b U}{dt} = \sum_{i=1}^{2} F_{disch}^i C_b^i - w$$

The tank output flow rate w is defined by the *Stateflow* diagram depicted in Figure (A.13). As seen it has two states off and *on*. Initially the system is in state off (this is indicated by the single arrow connected on left on the state) respectively the rate is zero and it becomes

equal to $w = F^m$ (i.e. the state *on*) as soon as one of the reactors stars discharging which is expressed as `[(sigma1==8)|sigma2==8]` .

On the other hand in Figure (A.14) is shown the *Simulink* realization of Equation (6.13), when the tank output flow rate evolution is governed by a PI control law as given by Equation (6.13).
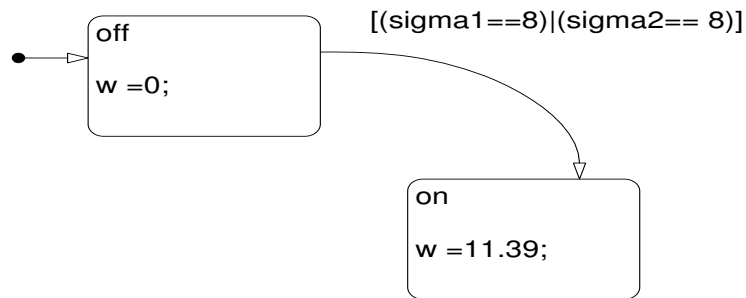
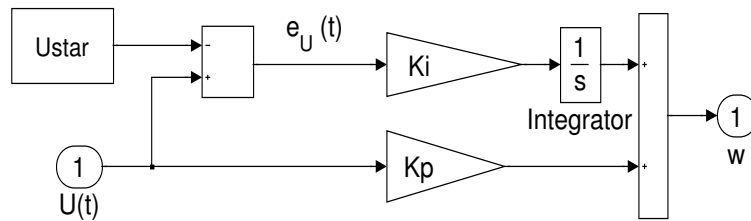Fig. A.13: Simulink model of the scheduled output flow rate of the tank

Fig. A.14: Simulink model of the PI controlled output flow rate of the tank, Equation (6.13)

A.5 Batch reactor two

A.5.1 Batch reactor two subsystem
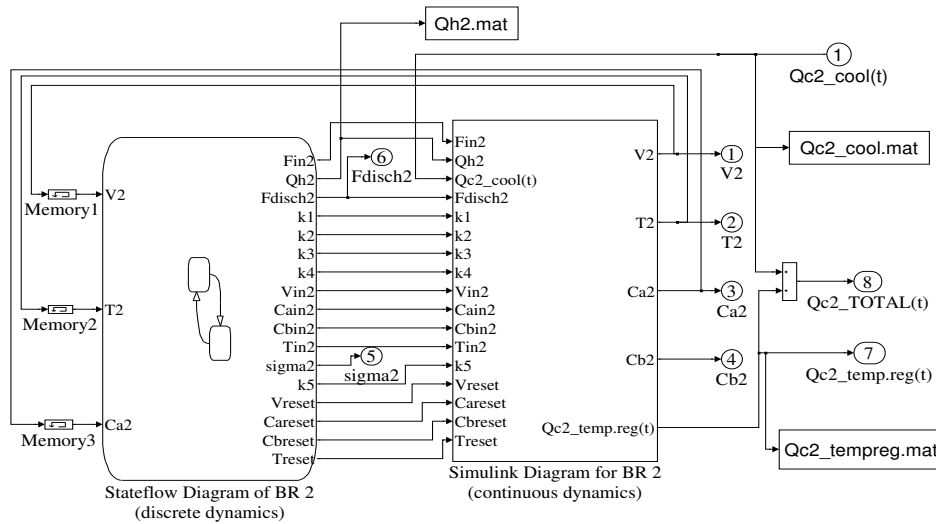
Fig. A.15: BR_2 Simulink-Stateflow diagram

Note that the only difference of the *Stateflow* diagram of BR_2 given in Figure (A.16) with respect to the one of BR_1 (See Figure (2.6)) is the presence of an additional *stand by state before filling* ($SF2aux$) used to introduce (as was described in Chapter 3, Section 3.3) through the transition condition `[after(lag/st,wakeup)]` the initial time lag of BR_2.
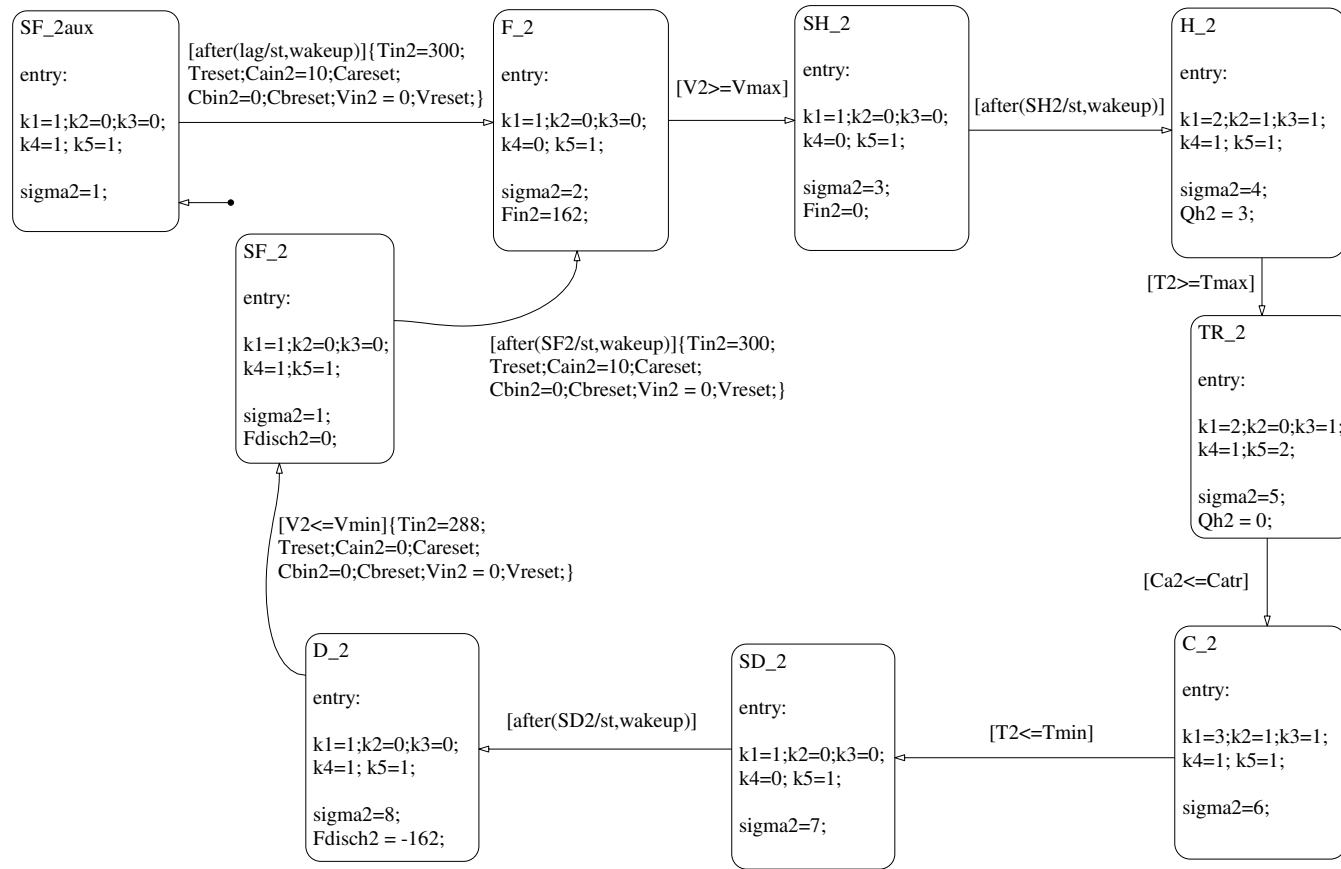
Fig. A.16: BR_2 Stateflow diagram
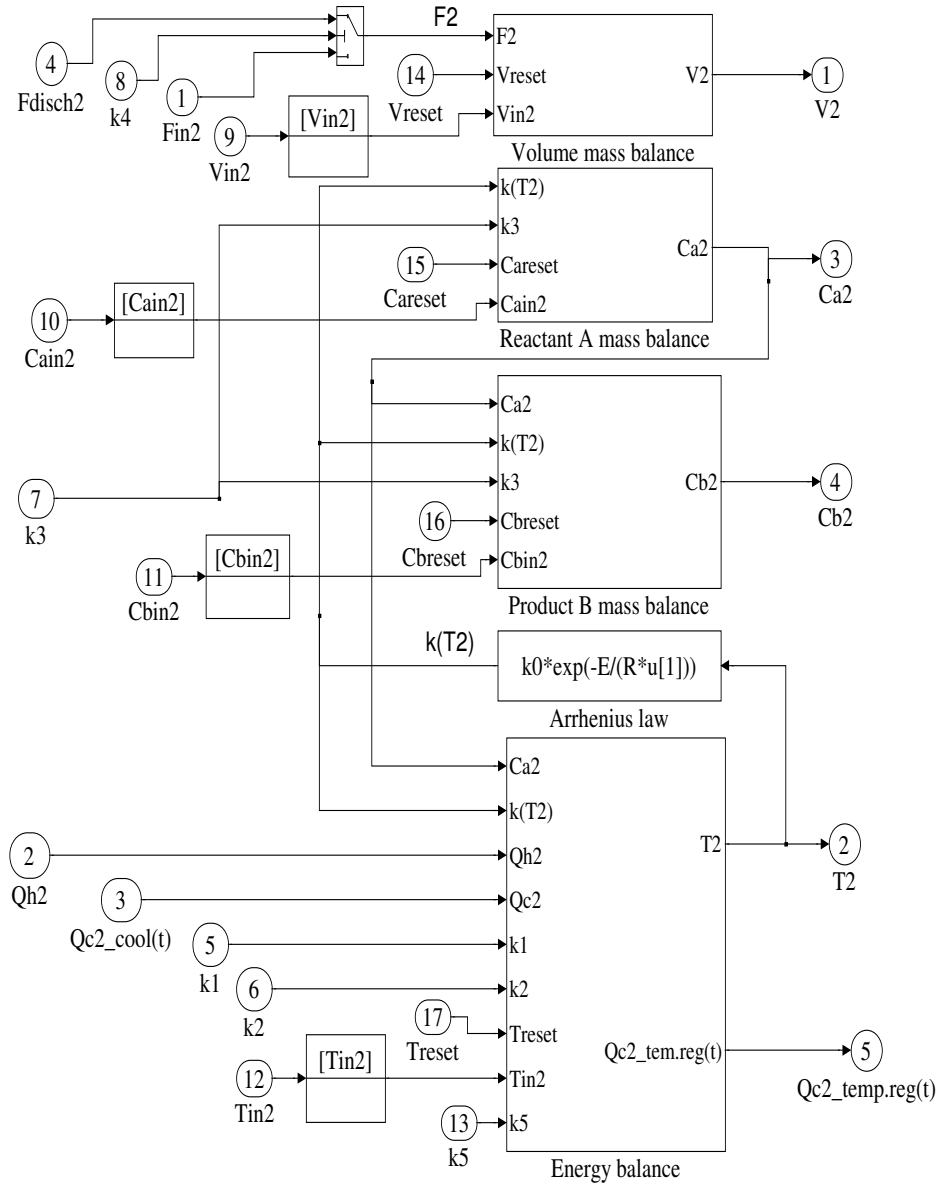
Fig. A.17: BR_2 Simulink model
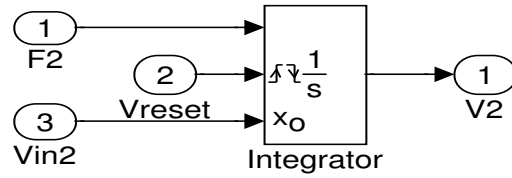
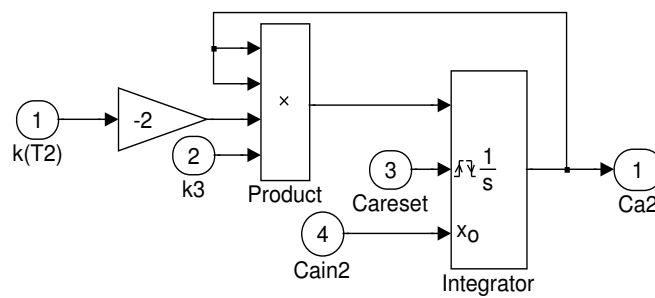Fig. A.18: BR_2 Simulink model of the reactant A mass balance Equations (A.1)

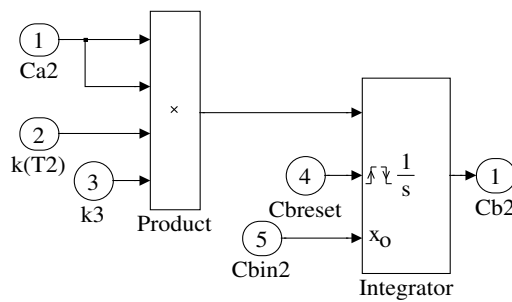Fig. A.19: BR_2 Simulink model of the product B mass balance Equations (A.2)

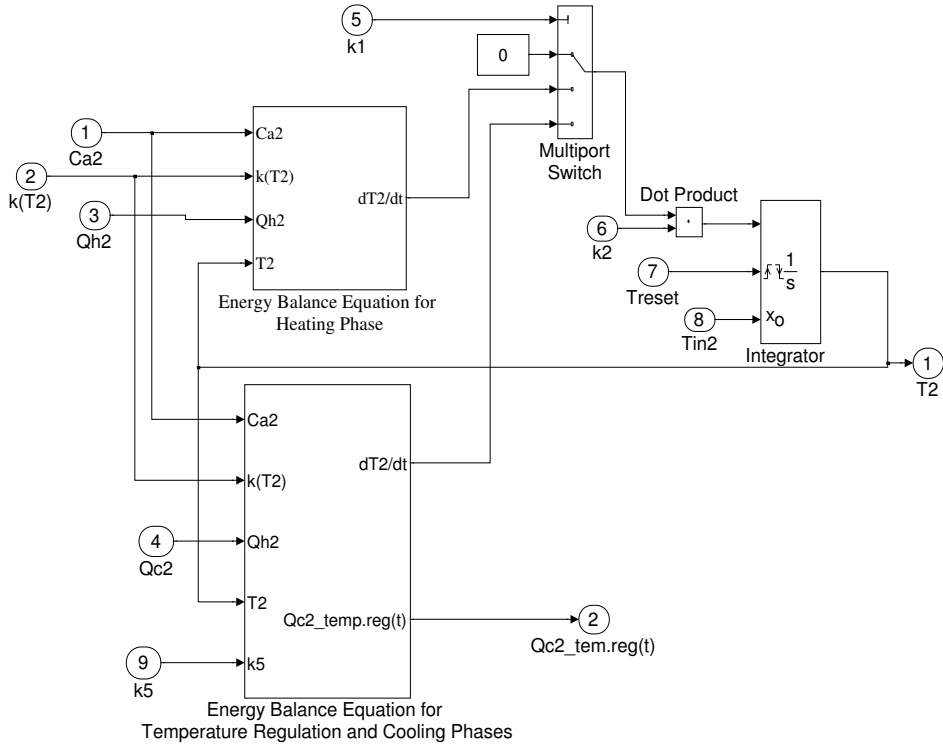Fig. A.20: BR_2 Simulink model to compute the product B mass balance

Fig. A.21: BR_2 Simulink model to compute the energy balance Equations (A.3)
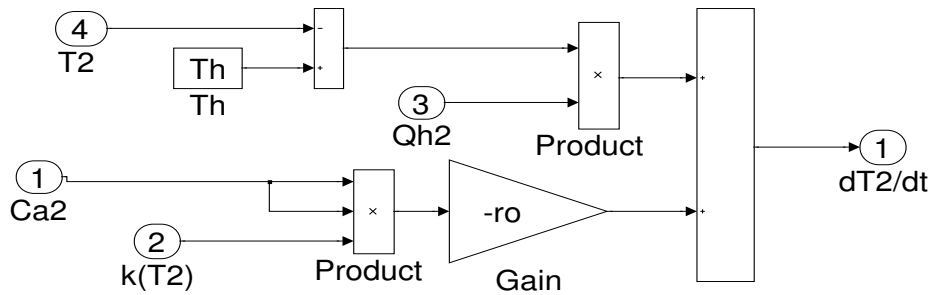

Fig. A.22: BR_2 Simulink model to compute the energy balance during the heating phase (Equations (A.3))
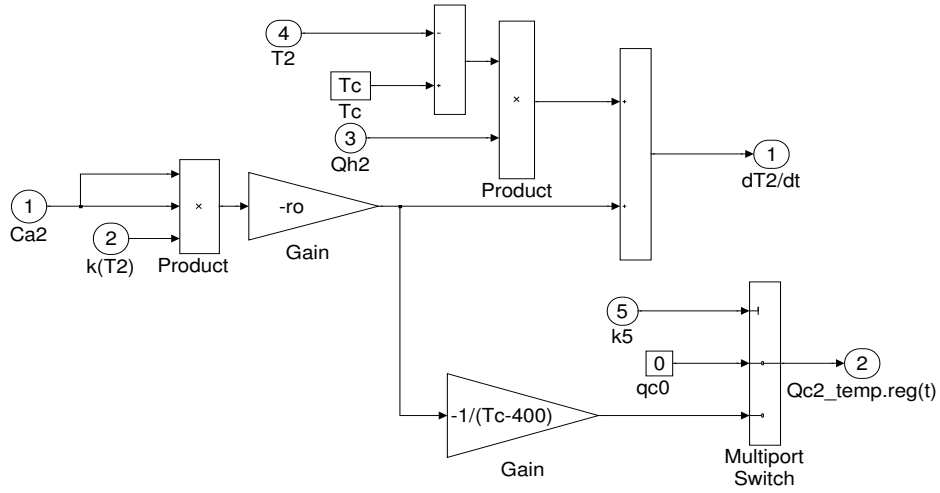
Fig. A.23: BR_2 Simulink model to compute the energy balance during the reaction and cooling phases (Equations (A.3))

A.5.2 Cooling water subsystem for reactor two
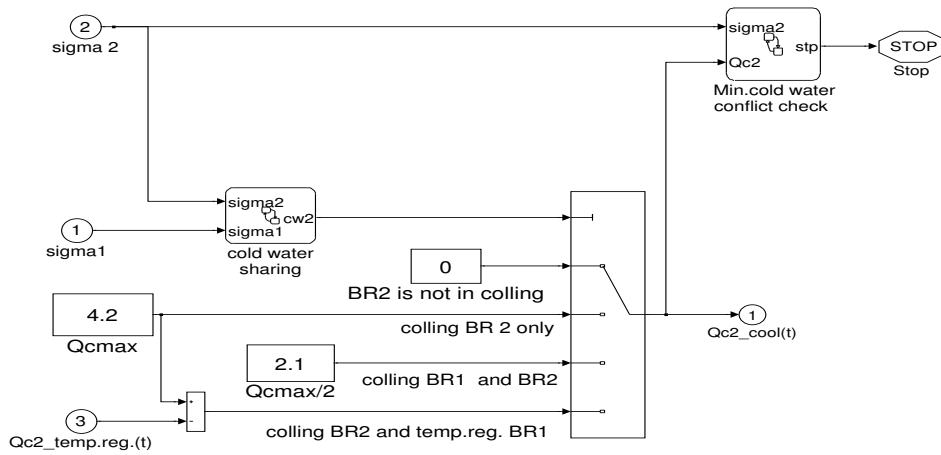

Fig. A.24: BR_2 Simulink model to compute the cold water during the cooling phase, see Section 3.3
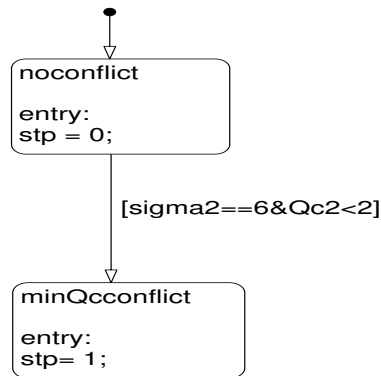

Fig. A.25: BR_2 Stateflow diagram to stop the simulation if a minimum cold water bound is reached, see Section 3.3
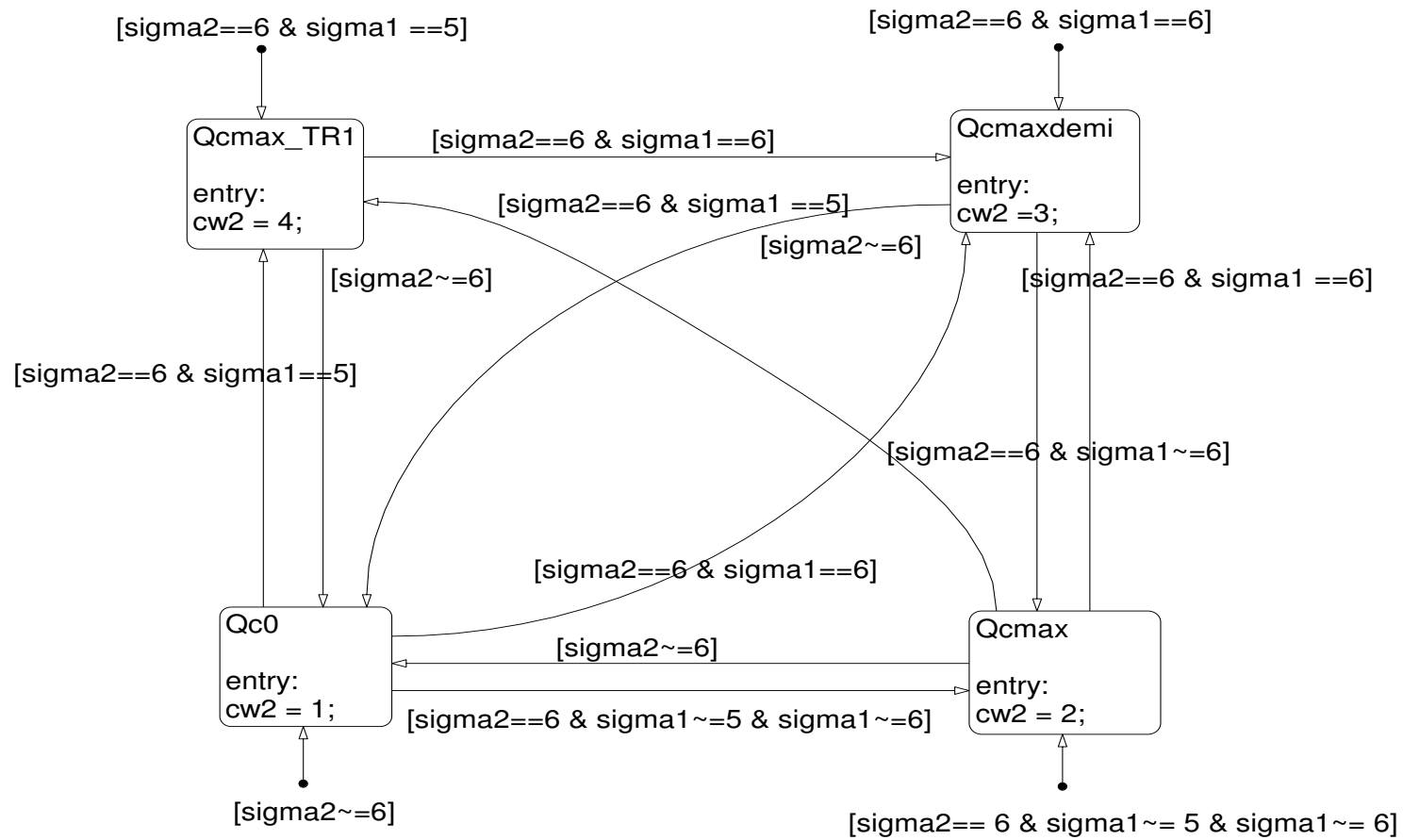
Fig. A.26: Stateflow diagram to set the values for the BR_2 cold water during the cooling phase, see Section 3.3

References

Bur85.   T.A. Burton. Stability and periodic solutions of ordinary and functional differential equations, volume 178 of Mathematics in Science and Engineering. Academic Press, Inc., Orlando, Fla, USA, 1985.

CL79.   T. S. Cheung and W. Luyben. Liquid-level control in single tanks and cascade of tanks with proportional only and proportional-integral feedback controllers. Industrial Engineering Chemical Foundation, 18(1):15–21, 1979.

CL80.   T. S. Cheung and W. Luyben. Nonlinear and nonconventional liquid level controllers. Industrial Engineering Chemical Foundation, 19(1):93–97, 1980.

CM89.   P. J. Campo and M. Morari. Model predictive optimal averaging level control. AiChE J. (4), 35:579–591, 1989.

FS03.   A. Faanes and S. Skogestad. Buffer tank design for acceptable control performance. Industrial and Engineering Chemistry Research, 42:2198–2208, 2003.

GGR06.   D. Gromov, S. Geist, and J. Raisch. Time discrete event control of a parallel production line with continuous output. ADHS 2nd IFAC Conference on Analysis and Design of Hybrid Systems, pages 90–99, Alghero, Italy, 2006.

GGR07.   D. Gromov, S. Geist, and J. Raisch. Time discrete event control of a parallel production line with continuous output. Discrete Event Dynamics Systems, Springer Netherlands, 18(2), August 2007.

Gir03.   A. Girard. Computation and stability analysis of limit cycles in piecewise linear hybrid systems. In 1st IFAC Conference on Analysis and Design of Hybrid Systems, pages 181–186, Saint-Malo, France, June 2003.

Har87.   D. Harel. Statecharts: A visual formalism for complex systems. Sci. Comput. Programming, 8:231–274, 1987.

His00.   I.A. Hiskens. Trajectory sensitivity analysis of hybrid systems. IEEE Transactions on circuits and systems-part I: fundamental theory and applications, 47:204–220, February 2000.

His01.   I. A. Hiskens. Stability of limit cycles in hybrid systems. In Proceedings of the 34th Hawaii International Conference on Systems Sciences, Maui, HI, January 2001.

His02.   I. A. Hiskens. Analysis of limit cycle stability in a tap-changing transformer. In Proceedings of the IEEE International Symposium on Circuits and Systems, pages V–693 – V–695, Scottsdale, AZ, May 2002.

His05.   I.A. Hiskens. Non-uniqueness in reverse time of hybrid system trajectories. Lecture Notes in Computer Science, 3414:339–353, 2005.

HV03.   S. F. Haykin and B. Van Veen. Signals and Systems. John Wiley and Sons, Inc., 111 River Street, Hoboken, NJ 07030, second edition, 2003.

Inc96.   Mathworks Inc. The Student Edition of SIMULINK, Dynamic System Simulation Software for Technical Education. Prentice Hall, Englewood Cliffs, NJ 07632, 1996.

Kha96.   H. Khalil. Nonlinear systems. Prentice Hall, Upper Saddle River, NJ 07458, second edition, 1996.

Mat02.   The MathWorks. Stateflow and stateflow coder - user's guide. 2002.

Mel03.   S. Melas. Pvc line predictive inventory control: a production rate optimization for a hybrid system. Solvay-Group report, pages 1–34, 2003.

MMT86.   K. McDonald, T. McAvoy, and A. Tits. Optimal averaging level control. AiChE J. (1), 32:75–86, 1986.

PC89.   T.S. Parker and L.O. Chua. Practical Numerical Algorithms for Chaotic Systems. Springer-Verlag New York, Inc., New York, NY, USA, 1989.

PW07.   Y. Pochet and F. Warichet. A tighter continuous time formulation for cyclic scheduling of a mixed plant. Computer and Chemical Engineering (Accepted for publication), 2007.

RL00.   M. Rubensson and B. Lennartsson. Stability of limit cycles in hybrid systems using discrete-time lyapunov techniques. In Proc. 39 th IEEE Conf. on Decision and Control, pages 1397–1402, Sydney, 2000.

RLP98.   M. Rubensson, B. Lennartsson, and S. Pettersson. Convergence to limit cycles in hybrid systems - an example. In Preprints of 8th International Federation of Automatic Control Symposium on Large Scale Systems: Theory and Applications, pages 704–709, PRio Patras, Greece, July 1998.

RSdP06.   M. Rodriguez, D. Sarabia, and C. de Prada. Hybrid predictive control of a simulated chemical plant. In International Scientific and Technical Encyclopedia, pages 90–99, Paris, France, July 2006. CTS - HYCON.

Sim03.   I. Simeonova. Development and implementation of an hybrid dynamical model for a chemical plant with parallel production lines and shared resources. DEA Thesis, Université catholique de Louvain, Belgium, 2003.

SO86.   D. Sbarbaro and R. Ortega. Averaging level control: An approach based on mass balance. Journal of Process Control, 17:621–629, 1986.

SP99.   G. Schilling and C.C. Pantelides. Optimal periodic scheduling of multipurpose plants. Computers and Chemical Engineering, Elsevier, 1999.

SW03.   B. De Schutter and W.M.H.Heemels. Modelling and control of hybrid systems. In Lecture Notes of the DISC Summer School, Koningshof, Veldhoven, The Netherlands, June 2003.

SWB+05a. I. Simeonova, F. Warichet, G. Bastin, D. Dochain, and Y. Pochet. Hybrid automaton for an hybrid industrial process. Internal Report for the HYCON WP 4b, 2005.

SWB+05b. I. Simeonova, F. Warichet, G. Bastin, D. Dochain, and Y. Pochet. On - line scheduling of hybrid chemical plants with parallel production lines and shared resources: a feedback control implementation. CD-Rom Proceedings 17th IMACS World Congress, Paris, France, 2005.

SWB+06a. I. Simeonova, F. Warichet, G. Bastin, D. Dochain, and Y. Pochet. Feedback stabilisation of the periodic operation of an hybrid chemical plant. In International Scientific and Technical Encyclopedia, pages 90–99, Paris, France, July 2006. CTS - HYCON.

SWB+06b. I. Simeonova, F. Warichet, G. Bastin, D. Dochain, and Y. Pochet. Feedback stabilisation of the operation of an hybrid chemical plan. ADHS 2nd IFAC Conference on Analysis and Design of Hybrid Systems, Alghero, Italy, 2006.

Tes07.   B. Tesche. European chemicals industry in a globalized context: Challenges and strategies. In <u>CEO SOLVAY GmbH</u>, Drezden, Germany, May 2007.

Tho07.   R. Thommeret. Solvay indupa will produce bioethanol-based vinyl in brasil and considers state-of-the-art power generation in argentina. <u>Press Release</u>, 2007.

War07.   F. Warichet. Scheduling of mixed batch-continuous production lines. <u>Ph.D. thesis, UCL, Belgium</u>, 2007.

Wil03.   J.C. Willems. Lecture notes in hybrid systems. In <u>Graduate School on Systems and Control</u>, Louvain, Belgium, March 2003.